SPALLATION NEUTRON SOURCE FOR AN ACCELERATOR DRIVEN SUBCRITICAL REACTOR

Asiya Rummana

International Institute for Accelerator Applications

University of Huddersfield

A thesis submitted to the University of Huddersfield
in partial fulfilment of the requirements for the degree of

Doctor of Philosophy

June 2019

Copyright

Declaration

I herewith declare that I have four papers published as the proceedings of conferences and it is indicated where the material from these publications has been reproduced in this thesis.

Abstract

The progressive improvement in the operating performance of existing nuclear reactors has brightened the outlook for nuclear power around the globe. In order to use less carbon based power, the use of nuclear reactors provides an attractive solution. However, questions are raised by people on the safety and long term radioactive waste disposal in conventional nuclear reactor. Also a need for uranium enrichment replacement arises due to security and proliferation issues. Accelerator driven sub critical reactors (ADSR) are the subject of international research and development due to their enhanced safety and the potential to deal with nuclear waste. To sustain fission, an ADSR utilizes the neutron produced by spallation which has become an established technique for the production of high intensity neutron flux. Development of MYRRHA (Multipurpose hYbrid Research Reactor for High-tech Applications) is one of the promising designs in this area.

The focus of this thesis is to examine the potential of MYRRHA, with thorium fuel, as an actinide burner using the GEANT4 simulation toolkit. It compares the neutron fluxes and spectra in the reactor for thorium based fuel with those for a standard uranium-plutonium mixture. The fluxes and spectra that would be useful for transmutation studies are examined at designated locations of the reactor: the fuel cells, In-Pile Section (IPS) regions and isotope production cells. From this, the feasibility of the thorium mixture is demonstrated and the burn up rates are calculated. Fuel evolution studies are performed by solving the Bateman equations.

The Geant4 simulation toolkit is used for the investigations and the results are compared to MCNPX predictions. Before implementing the detailed geometry of MYRRHA in Geant4, a simple model is studied to predict the numbers and properties of spallation neutrons produced by proton beams on simple lead targets for proton energies between 100 and 1400 MeV. This is relevant for ADSR systems and other neutron sources. The results agree well with the limited experimental data for the spallation neutron yields. Results of MCNPX and Geant4 are compared and show good agreement between the two programs for the overall numbers, energy spectra, spatial and radial distributions. A parametrized form is presented which can be used for neutronics studies in reactor cores.

The use of thorium as an alternative to uranium fuel has advantages due to its proliferation resistance, abundance in nature and nuclear waste manage-

ment. Only small quantities of plutonium and minor actinides are generated in the thorium fuel cycle, which reduces the long term radiotoxicity of the spent fuel. However, few detailed numerical studies have been performed on this. Geant4 modeling of a reactor is not supported by the default toolkit as this does not provide data for isotopes having atomic number Z >92. The JEFF 3.1 library was installed to import the data for transuranic elements and changes were needed to the program.
The results reveal that MYRRHA can be utilized as a prototype for industrial transmutation system as it can convert a measurable amount of minor actinide waste into short lived products. Specifically, the amount of americium produced is much smaller than the amount incinerated, if thorium fuel is used.

Acknowledgements

First and foremost, I am most grateful to Allah Almighty who gave me the strength throughout the journey of my research, so that I could stay focused on my work with consistent hard work. Being a remote student, there were many times when things seemed unmanageable, but my faith in Him kept me going and helped me meet my own deadlines that I set for myself, way earlier than the actual ones. While doing the project work, whenever I felt low, I sought Almighty's help through prayers and found myself filled with renewed enthusiasm and dedication towards my work. I express my gratitude to my parents who encouraged me to join research and helped me at every step by providing continuous moral support.

It is my pleasure to acknowledge the overall direction, guidance and support of my supervisor Professor Roger John Barlow. He polished my skills through continuous encouragement. He always offered his help in learning new technologies. I am indebted to him for his approachability, even with distance being the issue and with his busy schedule as a director of IIAA. He understood my limitation of being distant and was always there to help me. He managed to schedule regular video meetings (almost weekly) through which he took the pain to teach me as if he was teaching me in person. His kind words, gentle advices and appreciation for good work are few of his attributes that helped me remain on the track. I would have never completed my research work several months ahead of the schedule without his timely guidance and feedbacks. I am delighted to say that he is an exceptionally good supervisor.

I am grateful to Professor Jakob Van Den Berg, Professor Thomas Edgecock, Professor Sue Kilcoyne and my co-supervisor Professor Rebecca Seviour for providing useful feedback on my research work.

Sincere thanks to ISOHIM and IAEA support to attend 4^{th} International workshop on ADSRs and thorium. My thanks are also extended to Edouard Malambou and Stankovskiy A for providing data for MYRRHA geometry and material compositions that were used in the simulation study.

Special thanks goes to my husband who helped me by providing helpful discussions. Writing the thesis was the toughest time for me due to adverse family circumstances. He did everything to make the environment favorable. He has been a great friend, always motivating and supporting me.

I would like to extend my thanks to Ibra College of Technology where I work till present. I am extremely thankful to my colleague Mr Andrei Francis Marcos De Guzman who helped me in handling software related issues. Enormous thanks to my friend Dr Saman Shafi for her loving support during my PhD journey.

Finally, my deepest thanks goes to my daughter Fatima Saad and son Syed Misbah for their innocent love which boosted me every day to stay dynamic.

To my parents, my husband and my children (Fatima and Misbah - who bear with me during the whole period of my research)

Contents

List of Figures

List of Tables

LIST OF TABLES

1

Introduction

The primary energy demand of the world is predicted to double by 2050 [1]. The limitation on the use of fossil fuels is due to their depletion with time, increase in their prices and further due to the global environmental policy to ensure reduction in the emissions of greenhouse gases. Renewable energy, alone can not be sufficient to meet the world's energy demand. So, both nuclear as well as renewable energy are the prime avenues. Particularly, the nuclear technology can be used as a replacement for fossil fuels due to its very small CO_2 and other greenhouse gas emissions. However, the main concerns in nuclear technology are the safety problem, proliferation issues and the disposal of the long lived highly toxic radioactive waste. New reactor designs with enhanced safety features and ability to burn the nuclear waste are vital for the adoption of nuclear power technology.

1.1 Thorium fuelled accelerator driven subcritical reactor (ADSR)

The analysis of the nuclear power market emphasizes the growing need for further expansion to deploy a new type of thorium fueled nuclear system called an ADSR which is gaining worldwide attention as an alternative to uranium enrichment. ADSR offers three main advantages [2]:

1. Safety: Since enriched uranium is not used, they are subcritical i.e. they constantly need some energy to burn their fuel. The most evident feature of the ADSR is that by switching off the proton accelerator, the fission processes instantly shut down. So, the reactor core is unable to sustain the chain reaction in the absence of an external supply of neutrons.

2. Burning actinide and radioactive waste: Thorium fueled ADSR can use the fission products as fuel, relieving the world from their long term dangerous storage. This will be discussed in detail in 1.3.

3. Energy production: Thorium being more abundant on earth than uranium and due to the capability of thorium based ADSR to utilize the fission product, the energy hence produced can meet the increasing power demand of the world in the long run (24000 years, an estimate [3]).

An ADSR system is composed of an accelerator, spallation target and sub-critical reactor core. In a subcritical state, the neutrons needed for fission are initially provided by the target system. The neutrons are generated by spallation process in which high energy protons bombard the spallation target which should have high neutron production efficiency [4]. Spallation neutrons induce fission which makes more neutrons. The output of the sub-critical reactor can be simply controlled by changing the beam current. The output power P is related to neutron source intensity S by the expression:

$$P \propto \frac{S}{1 - K_{\text{eff}}} \tag{1.1}$$

where K_{eff} is the effective multiplication factor of subcritical fuel system that can be adjusted through the control rod.

1.2 Nuclear waste

As a well-known fact, nuclear energy production is accompanied by radioactive waste generation. Based on the characteristics of nuclear waste, they can be placed under three broad categories [3]:

1. Transuranic nuclei: Plutonium, neptunium, americium and curium are highly radiotoxic due to the dominance of α decay and very long life.

2. Long-lived fission fragments (LLFF): They decay by undergoing β emission and the life times are larger than 1000 years.

3. Activation products: These are medium-lived fission fragments with very high activity at discharge and they demand around 300 years of safe storage time.

Radioactive waste are generated by different kinds of facilities and in a wide range of radionuclide concentrations. They are generated in a variety of physical and chemical

forms. Due to these differences the options for waste management also vary. Several schemes are there for the classification of radioactive waste based on their physical, chemical and radioactive properties. This classification is relevant to particular facilities in which the waste is managed. As per the IAEA report [5], six categories of waste are used as a basis for the classification scheme: exempt waste (EW), very short lived waste (VSLW), very low level waste (VLLW), low level waste (LLW), intermediate level waste (ILW) and high level waste (HLW). Out of these six categories, HLW are most important. These are the waste which contains large amount of long lived radionuclides and whose level of activity concentration is high enough to generate significant heat by the radioactive decay. Such waste needs to be considered for disposal in deep, stable geological formations usually several hundred meters or more below the surface.

Commercial light water reactors (LWR) produce power but they have a major drawback: the production of HLW that contains transuranic elements. These elements are actinides: plutonium (Pu), neptunium (Np), americium (Am) and curium (Cm) which are generated by a combination of successive neutron capture and radioactive decays in a fission reactor. Although they are only few percent of the spent fuel, they are the most problematic part of the nuclear waste as they impose a long term environmental burden of their geological storage. They are highly radio toxic and their half - lives are up to millions of years. If the spent nuclear fuel is not reprocessed it must be treated as HLW, and the cost and risk of storing this nuclear waste for a long time can not be neglected [6].

1.3 Thorium ADSR for waste transmutation

ADSR with thorium fuel has gained large scale interest worldwide in the past two decades for energy production and waste transmutation. Furukawa [7], Bowman [8] and Rubbia [9] have been the pioneers in this area [3]. Although ADSR are capable of burning any type of fuel, the choice of thorium provides the benefit of low radiotoxicity and proliferation resistance [10].

For the disposal of high activity nuclear waste, either the spent fuel can be sent for direct disposal (open cycle) or it can be reprocessed to extract transuranic and fission products (closed fuel cycle). The extracted species can then be transmuted into less radiotoxic or short-lived products. Figure 1.1 depicts the two approaches of spent fuel disposal. Transmutation (basically suited for fission product) is the transformation of radioactive nucleus into a stable one through neutron capture. On the other hand, incineration (suitable for transuranic elements) leads to nuclear fission of the species

on neutron capture. Energy and neutron production takes place with incineration.

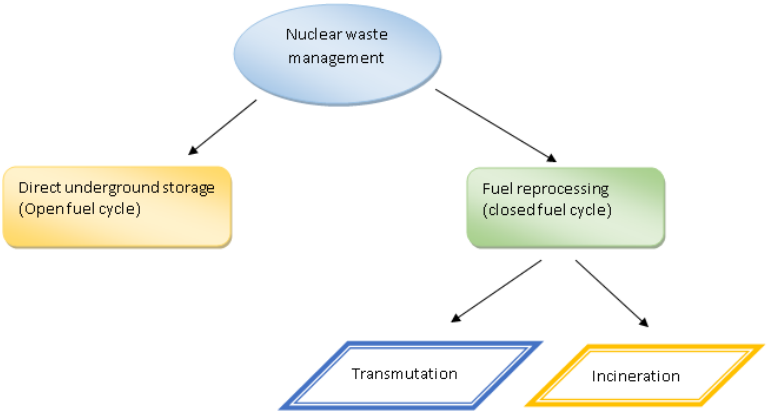

Figure 1.1: Nuclear waste management scenarios

In the commercial nuclear reactors relying on uranium-plutonium fuel cycle, ^{235}U is the primary fissile nucleus which provides fission neutrons needed for the power output as well as to maintain the criticality of the reactor. In uranium fuel cycle, for the first 500 years the radiotoxicity of the spent fuel is dominated by fission products. After this time, the fission products mostly decay and the radiotoxicity is dominated by transuranic elements particularly plutonium for about 100,000 years. The recycling of plutonium as MOX (Mixed oxide - PuO_2 and UO_2) can significantly reduce the overall radiotoxicity. The PUREX (Plutonium Uranium Reduction EXtraction) process is used to reprocess the spent uranium fuel. However, plutonium remains inaccessible in a once-through fuel cycle whereas in reprocessing separated plutonium oxide is produced which poses proliferation risk, and hence, needs stringent physical protection measures.

The radiotoxicity between 500 years to 100,000 years of plutonium and minor actinide inventories can be reduced by the usage of the thorium fuel cycle as lesser transuranic wastes are produced in the thorium-based fuel cycle which is easier to implement through the use of sub-critical reactors due to its improved neutron economy [3].

A comparison of open fuel cycle, uranium-plutonium cycle and thorium-uranium cycle is shown in Figure 1.2 [3]. Multi-reprocessing with 0.1% losses for U and Pu elements and 1% for minor actinides are assumed. As clear from the figure, significant reduction in radiotoxicity is observed for closed fuel cycles. In comparison to the uranium-plutonium cycle, the thorium-uranium cycle reduces the radiotoxicity by about two orders of magnitude in the first thousand years.

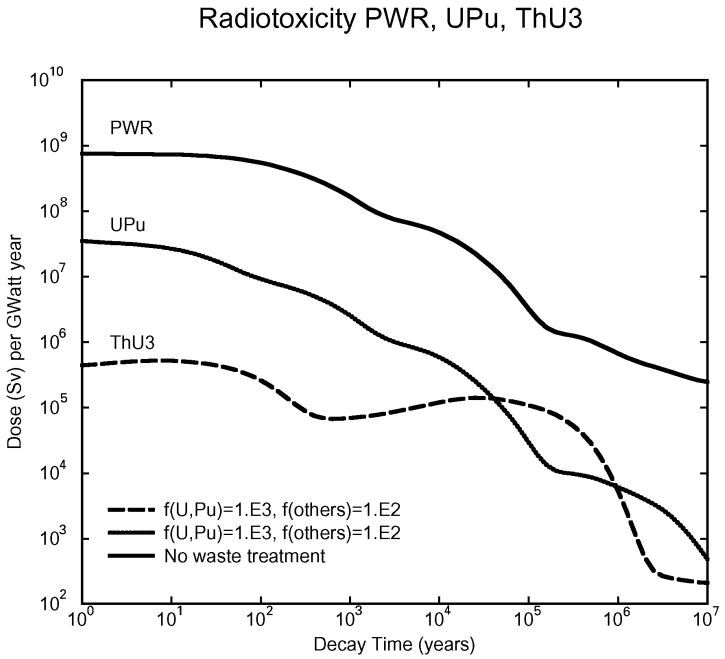

Figure 1.2: Comparison of radiotoxicities by open fuel cycle, uranium-plutonium cycle and thorium-uranium cycle. Reproduced from [3]

1.4 Thorium as a replacement for uranium

The thorium fuel cycle has gained sustained interest in recent years and several research activities worldwide are focused either on thorium fuel cycle or on the system that uses thorium as a fertile seed rather than ^{238}U. In the pioneering years of nuclear energy (mid-1950s to mid-1970s), there was worldwide growing interest particularly in developing countries with large thorium deposits and limited uranium resources. This enthusiasm decreased among developing countries (India was exception) due to the discovery of uranium deposits. Nevertheless, in recent years, the benefits of using thorium fuel have led to renewed interest in thorium in several developed countries [10].

Shippingport PWR demonstrated the use of the thorium fuel cycle as a first attempt in 1950s. The operation continued in 1970s with high enriched uranium (HEU) as a driver fuel and thorium as fertile target. The USA and Germany followed further R&D on thorium fuels till mid-1980s. A two-part fuel assembly was developed by LightBridge in which seed neutrons were provided by light enriched uranium (LEU) driver sub assembly to breed ^{233}U in an outer thorium sub assembly. India, having large thorium resources, has maintained sustained R&D in the thorium fuel cycle for

many decades [11].

Natural thorium (^{232}Th) is fertile, it does not contain any fissile material, unlike natural uranium which contains 0.7% fissile ^{235}U. It cannot be enriched in itself to produce materials of weapon's grade. Hence, it poses lower proliferation risk. Thorium is combined with ^{235}U or ^{239}Pu (fissile isotopes) in nuclear reactors for conversion to the fissile ^{233}U. In this way, its use can lead to the enlargement of the fissile material resources. Fertile to fissile thorium chain in the Figure 1.3 is analogue of the familiar Uranium chain as shown in the Figure 1.4.

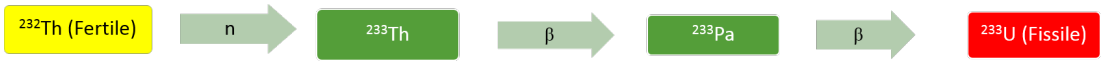

Figure 1.3: Thorium chain

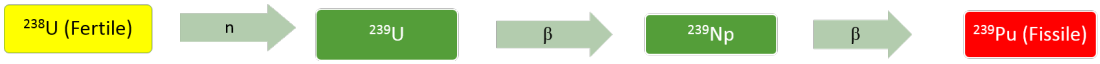

Figure 1.4: Uranium chain

There have been suggestions that initial loading of ^{235}U or ^{239}Pu can be avoided and ^{233}U can be generated in thorium filled ADSR by the spallation neutrons only. However, it is impractical as the time taken is excessively long for ^{233}U to build up to the point of useful fission energy production [11].

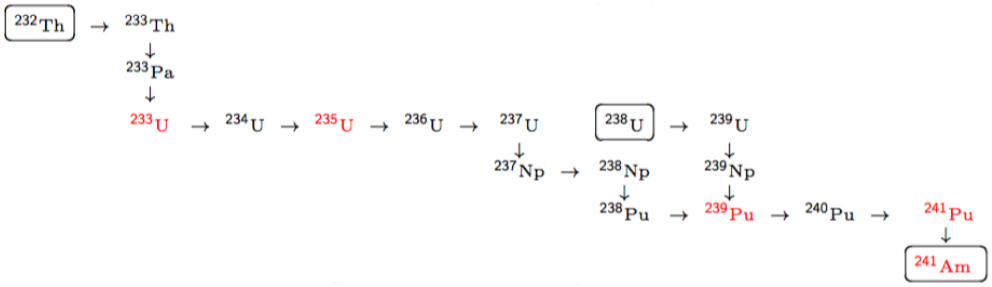

Figure 1.5: Minor actinides paths from ^{232}Th and ^{238}U. Reproduced from [12]

Fewer transuranic wastes are produced in the thorium-based fuel cycle which is easier to implement through the use of sub-critical reactors due to its improved neutron economy [3]. Figure 1.5 illustrates the path to minor actinides from ^{238}U and ^{232}Th for the purpose of comparing its production. The isotopes are moved one column to the right on absorbing a neutron while they move one row down following β decay.

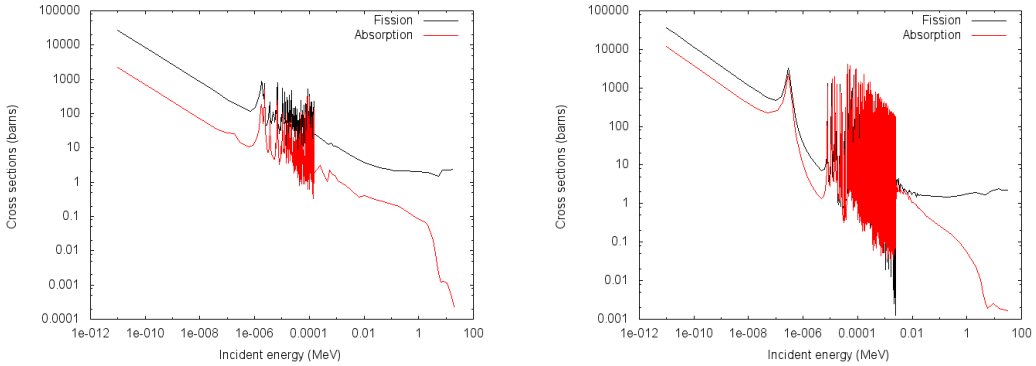

(a) ^{233}U **(b)** ^{239}Pu

Figure 1.6: Fission and absorption cross sections for ^{233}U and ^{239}Pu

^{232}Th captures a neutron and becomes ^{233}Th. ^{233}Th decays to ^{233}Pa by β emission. Protactinium decays to ^{233}U unless it absorbs a neutron which diverts the process to a different direction. ^{233}U has excellent fission probability (90%) and is the principal fissile isotope in the thorium fuel cycle whereas ^{239}Pu is the main fissile isotope in uranium fuel cycle. It is clear from Figure 1.5 that the path to minor actinide production from ^{232}Th is much longer than the path from ^{238}U. In addition, the probability of neutron capture by ^{233}U is less by a factor of 10 than its fission probability. These facts contribute to much smaller minor actinide production in the thorium fuel cycle as compared to the uranium fuel cycle.

Figure 1.6 shows the absorption and fission cross sections for ^{233}U and ^{239}Pu, plotted using the data from JEFF3.1N library [13]. The neutron energy ranges from thermal up to fast neutrons and these cross sections are large. It can be seen from the figure that the fission cross section of ^{233}U is $\sim$ 10 times more than the absorption cross section while for ^{239}Pu this factor is only 2-3.

For all the above reasons, it is a good idea to use thorium as an alternative to uranium fuel in an ADSR because of its properties:proliferation resistance, abundance in nature and nuclear waste management. Reactor MYRRHA operating in sub-critical mode with thorium fuel is considered to be the subject of the present study for nuclear waste management.

1.5 Motivation and research aims

Thorium power as an alternative to uranium has long been recognized and thorium-based fuels are already in use by several reactors [14]. Numerous factors like prolifer-

ation resistance, abundance in nature and nuclear waste management are the benefits of using thorium as an alternative to uranium fuel.

Rather than designing a new thorium filled reactor for the present investigations, design of reactor MYRRHA is taken into consideration as it is developed in more detail than any other system and the refinement continues till the system is constructed. Reactor MYRRHA with thorium fuel has not been studied earlier. GEANT4 is a widely used simulation program and it is interesting to use it for the first time to simulate the reactor MYRRHA.

Two broad research questions were identified. The first question was useful in getting acquainted with the program, the concepts of flux and energy before the more complicated geometry and processes of the main topic. It provided the basis for the neutronics in the reactor studies and the second question was more important and much more work of the research was focused on it.

1. What are the numbers, spatial distribution and energy spectra of neutrons produced by proton on lead cylindrical target, as predicted by GEANT4? Can we trust them (compare MCNPX and Data)? What do they tell us about the spallation process? Can we parameterise the results for use in the reactor simulations?

2. Can we use thorium ADSR to burn actinides using the MYRRHA design? Will thorium filled ADSR be better than uranium ADSR (i.e. will it generate fewer actinides, as one would naively expect)?

Taking the identified research questions into account, the aims of this work are formulated as follows:

- To investigate the neutron distribution and energy spectra for spallation targets.
- To implement the geometry of MYRRHA in GEANT4.
- To investigate the neutron distribution and energy spectra in the MYRRHA reactor.
- To verify the potential of MYRRHA (with thorium fuel) as an actinide burner using the GEANT4 simulation toolkit.

1.6 Thesis structure

The entire thesis is organized into 8 chapters:

Chapter 1: It provides an overview of the ADSR, the problem of the management of nuclear waste and utilization of thorium fuelled ADSR for minor actinide incineration.

Chapter 2: The chapter covers the relevant background information in order to provide the reader with an insight for the discussion in subsequent chapters. It reports literature on ADSR, thorium based fuel cycle as a replacement to uranium fuel cycle and minor actinides.

Chapter 3: The features of GEANT4 program are presented and Monte Carlo is discussed in detail.

Chapter 4: The neutronics of the spallation target using GEANT4 is predicted and benchmarked against the MCNPX results and the experimental data.

Chapter 5: Geometry of the reactor MYRRHA as received from [15] is implemented into GEANT4 code.

Chapter 6: Neutron fluxes and spectra at different locations of the reactor are investigated and compared with MCNPX predictions.

Chapter 7: Fuel evolution studies are performed for the uranium and the thorium chains and minor actinide incineration scenarios are examined.

Chapter 8: Conclusions of the thesis are highlighted with a suggestion for possible future extensions.

2

Theoretical Background

Neutrons are gentle probes that can deeply penetrate into materials without causing damage. Neutron scattering has become a powerful tool for scientific research as it provides information on crystallographic structure, atomic and molecular dynamics and magnetic properties. Neutrons are generally produced by fission in research reactors for neutron flux, by spallation in which a high energy proton beam impacts a heavy metal target to spall or chip the neutrons from the target [16], or by nuclear fusion reactions.

In a nuclear fission process, splitting of a nucleus takes place in which two or three neutrons and about 200 MeV of energy are released. The released neutrons further split another nucleus creating a chain reaction. Following processes are possible by the neutrons released from a fission reaction:

Process 1: These neutrons further induce fission.

Process 2: They get absorbed in the reactor without inducing fission. This leads to the production of actinides (Figure 2.3).

Process 3: They leak out from the reactor.

To sustain the chain reaction, the quantities of fissile materials are arranged in such a way that there remains a balance between the neutron production (process 1) and the neutron loss (process 2 or 3). When this condition of balance is achieved, the reactor is called a "critical reactor" [17].

In ADSR, the core is subcritical i.e. for each generation of neutrons, less than one secondary neutron initiates a nuclear fission. The sub criticality is achieved by limiting the amount of fissile material in the core. An external neutron source is needed to sustain the chain reaction.

For nuclear fusion reactors, two fusion reactions are particularly popular:

1. Deuterium tritium reactions (D-T reaction)
2. ^{3}He and deuterium reaction.

D-T reaction is most promising and is one of the interesting field of nuclear research. Neutron is produced in this reaction and around 17.6 MeV energy is released. However, very high energy is required to overcome the coulomb barrier and hence a critical temperature is required below which a reaction cannot be sustained. Energy can also be supplied by a high voltage source, as in commercial D-T Fusors. However, the numbers of neutrons that can be made in this way is very small, too low to be useful.

In spallation reaction there are three main stages. In the first stage that is intra nuclear cascade (INC) the proton interacts with the nucleons of the target and highly energetic particles are produced [18]. These high energy particles further interact with the other target nucleons leading to the production of more excited nuclei and hence neutrons in a nuclear cascade. In the latter stage the excited target nucleus de-excites by the evaporation of large number of low energy neutrons and other particles. The excited nuclei also undergo fission for many target materials. The fission fragments will de-excite by evaporation. The low energetic (typically 1 MeV) evaporation neutrons travel through the target and those escaping from it provides the neutron source [19].

High atomic number, high density and high/low melting point in solid/liquid are the desirable properties of a spallation target. The ideal candidates for effective spallation are Tungsten or Tantalum for solid targets and Lead or a Lead/Bismuth mixture for liquid targets.

2.1 Spallation neutron facilities

Over the past two decades increased interest is evoked in the nuclear community for spallation neutron sources (SNS). High current proton accelerator and heavy spallation target material are the main features of SNS. Famous SNS facilities worldwide are:

1. ISIS (UK)
2. SINQ (Switzerland)
3. SNS (USA)
4. JSNS (Japan)
5. ESS (Europe)

6. CSNS (China)

Table 2.1 shows the main features of these spallation neutron sources across the world [20]. Apart from reference [20], beam energy for ESS is taken from [21].

Facility	Location	Power (MW)	Beam energy (GeV)
SNS	ORNL, USA	1.4	1
ESS	Lund, Sweden	5	2.5
ISIS	RAL, UK	0.16	0.8
SINQ	PSI, Switzerland	0.9	0.59
JSNS	J-PARC, Japan	0.6	3
CSNS	IHEP, China	0.1	1.6

Table 2.1: Features of different spallation neutron sources across the world

2.2 ADSR systems and MYRRHA

A subcritical reactor coupled with a high intensity proton beam through a spallation neutron source is employed in the ADSR concept. ADSRs are gaining importance due to their capability to transmute nuclear waste, efficient fuel usage, safety and thorium utilization under the three stage power programme. ADSR remains sub-critical while producing power. In critical reactors around the globe, the number of neutrons produced is balanced by the number of neutrons lost through leakage and absorption by different materials inside the reactor. Due to this balance, a constant reactor power is maintained at any particular level. Fewer neutrons are produced than the ones lost by leakage and absorption in a subcritical reactor. So an external neutron supply is needed to maintain a constant reactor power. This external supply is provided by spallation in which neutrons are produced from the interaction of a high intensity proton beam with a heavy target. Nobel laureate physicist, Carlo Rubbia, conceived such reactors for the purpose of power generation, but later this concept caught worldwide attention for an equal role of burning nuclear waste [22].

Partitioning and transmutation in association with the accelerator driven systems and in combination with the geological disposal can provide an acceptable solution for the nuclear waste management problem [23]. ADSRs have a remarkable feature of being capable of adjusting sub-criticality levels. This capability converts an ADSR to a safe and reliable design ensuring that the effective multiplication factor, K_{eff} is not equal

to or more than one in any case. So they can tolerate higher minor actinide loadings than other systems. ADSR can burn both their own minor actinides as well as those produced by light-water reactors (LWR).

Various experiments have been performed around the globe in the field of ADSR development. These include [6]:

- MUSE program: MUSE - 4 program was performed at Cadarache Research Centre, CEA, France, to study the behavior of accelerator driven systems (ADS). MASURCA reactor facility was coupled with GENEPI accelerator and studies were performed on the development of new technologies to monitor parameters related to the reactor safety [24].
- GUINEVERE: The feasibility study of an accelerator driven system for nuclear waste transmutation was performed under the GUINEVERE (Generator of Uninterrupted Intense NEutrons at the lead Venus REactor) program. The fast reactor Venus-F of SCK.CEN in Mol (Belgium) was coupled to an external source of neutrons produced by GENEPI-3C accelerator [25].
- Yalina: It is a sub-critical assembly at Radiation Physics and Chemistry Problems Institute of the National Academy of Sciences of Belarus at Minsk-Sosny, Belarus. The purpose of the facility was to investigate the neutronics properties of ADS and the properties of nuclear reactions, particularly transmutation reactions [26].
- HYPER: HYbrid Power Extraction Reactor (HYPER) is the accelerator driven sub-critical system designed by Korea Atomic Energy Research Institute (KAERI). It is designed for the transmutation of transuranic elements and fission products [27].

Worlds first experiment on ADSR took place in March 2009 at Kyoto University Research Reactor Institute [28]. The purpose of this research was to evaluate ADSR as an energy producing device. For this experiment, Kyoto University Critical Assembly (KUCA) was utilized as the subcritical reactor. To drive the ADSR, FFAG synchrotron was used as an accelerator that realizes high beam current and high energy. A proton beam of 110 MeV energy from the accelerator was directed into the tungsten target in the subcritical fuel system of KUCA. Helium detectors were placed near the reactor core to measure the neutron counting rate as a function of time. The assembly of KUCA reactor and the KURRI-FFAG accelerator complex is shown in Figure 2.1. The basic parameters of KURRI- ADSR experiment are presented in Table 2.2.

In this experiment, the number of neutrons as a function of time was recorded and plotted for different K_{eff}. Two components are observed: the fast component that

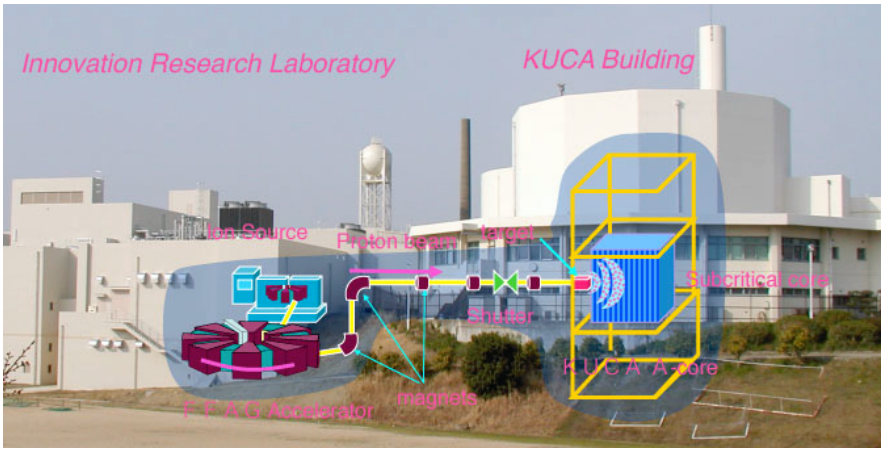

Figure 2.1: Assembly of KUCA reactor and the KURRI-FFAG accelerator complex. Reproduced from [28]

Beam power	$\leq$ 0.1 W
Beam current	$\leq$ 1 nA
Beam energy	$\leq$ 100-150 MeV
Reactor output power	$\sim$ 10 W
Neutron Multiplication factor	$\leq$ 100

Table 2.2: ADSR experiment - Basic parameters. Reproduced from [28]

decays exponentially and the slow component caused by delayed neutrons which is almost constant in time. The higher value of the response corresponds to higher K_{eff} indicating lower sub criticality of the fuel system. This very first ADSR experiment at KURRI successfully demonstrated the concept of a chain reaction induced by spallation neutrons that were produced by the high energy proton beam.

Large thorium reserves in India gives an added incentive to India's nuclear programme on nuclear energy generation. However, it requires the development of several related technologies on high power accelerator, removal of generated heat from spallation and material development. Development of simulation codes for ADSR are carried out to include fueling operation. Purnima lab, BARC is conducting experiments on ADSR. Advanced Heavy Water Reactor at BARC is the development in this area for thorium utilization [22].

The Belgian nuclear research Centre SCK·CEN at Mol [18] has designed a multipurpose reactor MYRRHA (Multipurpose hYbrid Research Reactor for High-tech Applications) to replace the old Belgian reactor 2 (BR2). This reactor is one of the

promising designs in the area of nuclear waste transmutation with fast neutrons. It is a flexible design which can run either in critical or subcritical mode. It consists of a proton accelerator delivering a proton beam (of 600 MeV in energy and about 4 mA beam current), molten lead bismuth eutectic (LBE) as coolant which also acts as a spallation target and a subcritical core fueled with mixed oxide (MOX). Figure 2.2 shows the overview of MYRRHA. The chosen fuel for MYRRHA is MOX with 33%

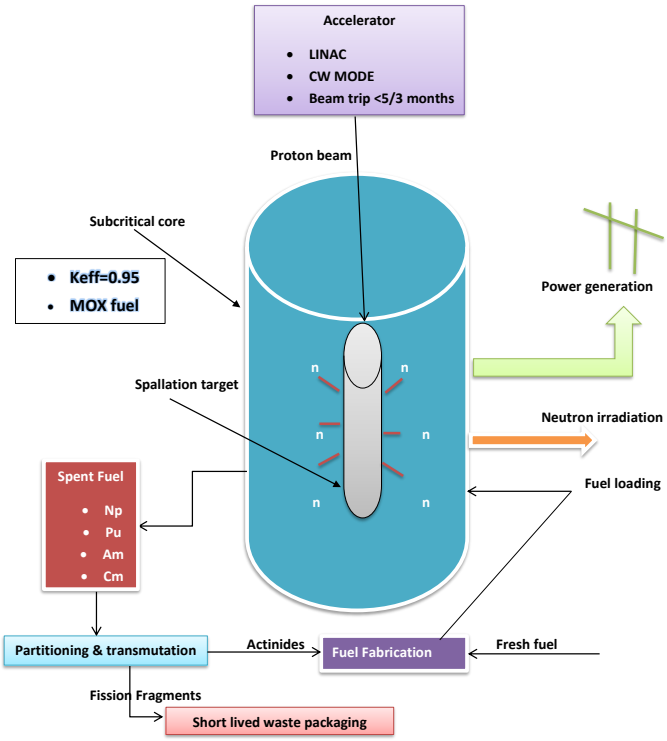

Figure 2.2: Schematic of MYRRHA

Plutonium enrichment. It contains Pu from the spent fuel of LWR which is recycled as PuO_2 and then combined with UO_2. Other transuranic elements (TRU) can also be there in the spent fuel. This ensures efficient extraction of energy from the spent fuel in addition to the recycling of the other toxic waste by fission preventing them from

going to the final repository.

The proton accelerator is one of the main components of an ADSR. Highly energetic protons from the accelerator hit the target creating spallation neutrons. These neutrons induce fission in the core so that the core can operate as a subcritical fission reactor.

The spallation target is an important interface between the accelerator and the sub critical reactor. Two design options were considered for MYRRHA: a window target and a windowless target design. The window target design physically separates the beam and the target unit. In the second configuration there is no window between the beam and the target and hence the beam impinges the target directly. The first configuration (Window target design) is preferred in MYRRHA [6]. MYRRHA is expected to be fully operational by 2023. The objectives of MYRRHA are [1]:

- Endeavour to demonstrate ADSR technology
- Efficient transmutation of high level waste (HLW) in the core
- To operate as a flexible irradiation facility allowing innovative fuel development, material studies for other types of reactor such as fusion reactors, radioisotope production for nuclear medicine and industry and industrial irradiation application

2.3 Fertile to fissile conversion and minor actinides production

Nuclear fission of uranium and plutonium atoms is the process used in the thermal reactors for the generation of heat and electricity. Fissioning of uranium atoms by the thermal neutrons limits the efficient use of raw uranium as only a small part of it can be used. Thermal neutrons can fission only ^{235}U which is 0.7% of natural uranium. ^{238}U as the major part of the core remains unusable. This may lead to the shortage of uranium resources that can adversely affect the nuclear power production in the future. Fast neutron spectrum reactors allow efficient use of uranium by transforming the remaining 99.3% of ^{238}U into ^{238}Pu [29]. Neutron capture on ^{238}U produces short lived isotope ^{239}U which quickly decays in two steps to ^{239}Pu. ^{239}Pu is a fissile isotope, so the process of conversion of fertile ^{238}U to fissile ^{239}Pu by neutron capture is called fertile to fissile conversion which is a very important process for nuclear reactors [11].

The fission products carry away the excess energy in the form of kinetic energy which is passed to the fuel as heat. Mostly fission products are radioactive with a half - lives of few seconds to millions of years. They represent the largest component of high

level radioactive waste.

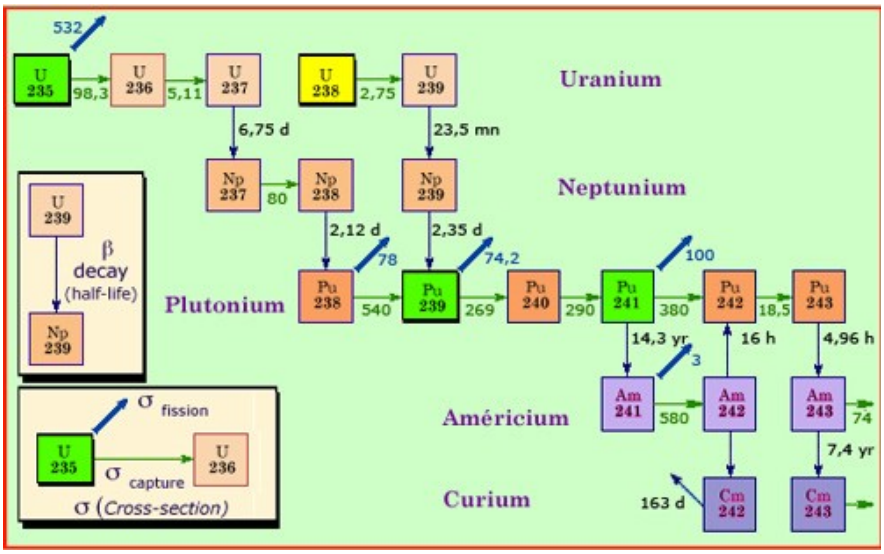

Figure 2.3: Actinide generation in a fission reactor. Reproduced from [5]

After the production of ^{239}Pu, further neutron interactions can lead to the production of following processes as shown in Figure 2.3 [30]:

1. Fission of ^{239}Pu
2. Higher plutonium isotopes (^{240}Pu, ^{241}Pu and ^{242}Pu)
3. Production of other nuclides (^{240}Np, ^{238}Pu, ^{241}Am, ^{242}Cm and ^{244}Cm)

Some fission products categorized as long lived fission products (LLFP) as well as transuranic elements pose significant storage issues due to their lifetimes of more than 10 years. Fission products are β emitters while transuranic elements decay essentially by α radiation. The radiotoxicity of α emitters is much more than that of β emitters for the same disintegration rate [3]. This is the reason that minor actinides are the main contributors to the radiotoxicity of the spent fuel.

Out of the other minor actinides produced in a nuclear reactor, americium, neptunium and curium are highly radioactive. Figure 2.3 shows the generation of actinides in a fission reactor. In spite the fact that these minor actinides are produced in small quantities, they are the major contributor of neutron emission, decay heat and radiotoxicity of the spent fuel and are considered as candidates for partitioning and transmutation. Transmutation of these three actinides has gained sustained international interest [30].

2.4 Partitioning and transmutation

Separating out (partitioning) the radiotoxic components (plutonium and minor actinides) from the spent fuel and recycling them (transmutation) minimizing their toxicity while recovering their contained energy is an increasingly attractive alternative to direct disposal, referred to as closed fuel cycle.

The actinides after separation from the spent fuel are exposed to fast neutron spectrum in a reactor. They are then transmuted through fission into short lived fission products. Efficient transmutation of actinides requires fast neutron spectrum systems for which both critical or sub critical reactors are potential candidates. However, in fast critical reactors the content of minor actinide has to be limited to avoid the deterioration of safety related parameters. So the fuel cycle needs to be extended for these minor actinides over a rather large ensemble of fast reactors rather than optimizing them for efficient power production as well as plutonium burning. On the other hand, the sub criticality of the ADSR allows its safe operation with fuel containing rather large amount of minor actinide resulting in maximum transmutation rates [1, 31]. Figure 2.4 presents the minor actinide transmutation scenarios.

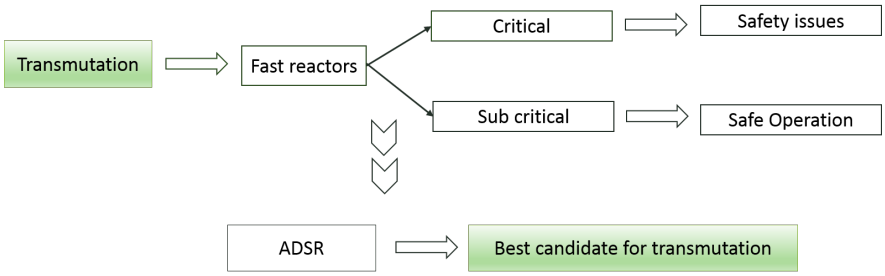

Figure 2.4: Transmutation scenarios

The radio toxicity of nuclear waste is contributed primarily by the actinides and the amount of actinides sent to the final repository is reduced by the factor of 10 if all the plutonium is recycled and fissioned and further by the factor of more than 100 if minor actinides are also burned by partitioning and transmutation [7]. This is illustrated in Figure 1.2, chapter 1. Comparing the fuel cycles; the toxic waste needs around 10^6 years to reach to the natural toxicity level while the time is reduced to few hundred years by the closure of fuel cycle by partitioning and transmutation [1].

2.4.1 Minor actinides for transmutation

Transmutation of minor actinide is the process of irradiating it in a high intensity neutron flux in order to decrease the long term radiotoxicity of the spent nuclear fuel. Factors responsible for the candidature for minor actinide transmutation are:

1. Very long life
2. Very high production level
3. Neutron emission and decay heat of final repository.

Very high neutron flux is needed for transmutation and it is most effective when all the minor actinides are fissioned either with a single neutron interaction (direct) or through neutron captures followed by fission (indirect). Since the reaction cross section for both direct and indirect fission tends to be very low, for high reaction rate the neutron flux should be high in addition to long irradiation times [30].

Neptunium: Neptunium (the predominant isotope is ^{237}Np) is considered as a secondary candidate for transmutation. It does not contribute to the decay heat output [30]]. ^{237}Np is a very long lived nuclide with a half - life of 2.144 million years. The production routes of ^{237}Np are:

a) Two steps neutron capture on ^{235}U whose products are ^{236}U and ^{237}U.^{237}U (half life = 6.75 days) finally decays to ^{237}Np. This reaction is preponderant in thermal reactors.

$^{235}\mathrm{U} + n \rightarrow {}^{236}\mathrm{U} + n \rightarrow {}^{237}\mathrm{U} \rightarrow {}^{237}\mathrm{Np}$

b) 90% of neptunium production in fast reactors is through (n,2n) reactions on ^{238}U.

$^{238}\mathrm{U} + n \rightarrow {}^{237}\mathrm{Np} + 2n$

During the irradiation process, neptunium either fissions or captures a neutron to become ^{238}Np which is short lived with a half life of 6.75 days. ^{238}Np decays to ^{238}Pu . The following reaction represents the transmutation steps of ^{237}Np:

$^{237}\mathrm{Np} + n \rightarrow {}^{238}\mathrm{Np} \rightarrow {}^{238}\mathrm{Pu}$

^{238}Pu being a strong alpha emitter is highly thermally active. Nevertheless, when mixed with existing plutonium it can be utilized as fuel since it is a neutron provider in a fast spectrum [29].

Americium: Due to its significant production level and gamma activity, Americium is considered as the prime candidate for transmutation. It has relatively short half - life and the dominant isotope in the irradiated nuclear fuel is ^{241}Am. Nevertheless,

smaller but significant quantities of ^{242}Am and ^{243}Am are also there. ^{241}Am is produced from the decay of ^{241}Pu which has a half-life of 14.4 years. ^{241}Am is consumed by absorption rather than fission, and the main product in the process is ^{238}Pu, from the successive decays of ^{242}Am and ^{242}Cm . Further isotopes are also produced in small quantities [29]. The transmutation of ^{241}Am involves following reactions:

$^{241}\text{Am} + n \rightarrow {}^{242}\text{Am}$

$^{242}\text{Am} \rightarrow {}^{242}\text{Cm} \rightarrow {}^{238}\text{Pu} \rightarrow {}^{239}\text{Pu}$ (82.7%)

$^{242}\text{Am} \rightarrow {}^{242}\text{Pu}$ (17.3%)

Curium: It is a major contributor to neutron emissions. It also significantly contributes to the gamma activity and radiotoxicity. However, its transmutation is generally ruled out due to low fission and capture cross sections of its principal isotopes i.e. ^{242}Cm and ^{244}Cm.

For the reasons given above, ^{241}Am is chosen for transmutation studies that will be covered in chapter 7.

2.5 Scope of the study

The study covering the important aspects of MYRRHA including the potential for MA burn up has been performed by M Sarotto et al. [31]. However, a fuel mixture based on thorium rather than uranium needs to be considered to see whether this replacement increases the potential of MYRRHA ADSR as an actinide-burner. Moreover, the geometry implementation of MYRRHA in Geant4 and the investigations for flux and burn up calculations will provide a novel contribution.

Before starting the investigations on the complicated geometry of MYRRHA, spallation target studies will be performed for the neutronics using GEANT4 simulation toolkit and the results will be evaluated with the experimental data as well as with another code MCNPX. The aim of these target studies is to provide a parametrized form for source neutrons that can be used for the neutronics studies in reactor cores. In addition, it is to investigate the level of agreement between the different simulation programs.

2.6 Objectives

Based on the aims presented in chapter 1 and after conducting the literature review, the following specific objectives are formulated to achieve the aims of this research:

- Simulation of spallation neutron target to predict the overall numbers, spatial distribution, neutron cross section in lead and energy spectra of the spallation neutrons.
- Spallation neutron distribution with target length variation.
- Parametrization of spallation neutron distribution.
- MYRRHA: Detailed geometry implementation of the reactor MYRRHA in Geant4.
- Energy distribution of the neutron flux in MYRRHA for different fuel mix.
- Fuel Evolution in the reactor.
- Minor actinide (MA) production.
- Prospect of MA burn up in MYRRHA with thorium fuel.

3

Numerical Methods

In this chapter, numerical methods are discussed for two topics: Monte Carlo Simulation and Solution of differential equations.
Although the need for experimental facilities cannot be neglected, advanced computer simulations provide a cheap and effective alternative to model even the complicated problems. The simulation technology in nuclear industry has gained increased interest for research on the design, utilization and safety of nuclear devices particularly for nuclear reactors. GEANT4([32], [33], [34]) is one such important tool for nuclear research. It is one of the largest open source codes in terms of its scope and size, developed by the GEANT4 consortium. GEANT4 simulates the passage of particles through matter. It is an object oriented code written in C++ that can adapt to a wide variety of problems. The toolkit is capable of simulating applications covering a wide range of problems from basic physics simulation to detector simulation for particle accelerators such as the Large Hadron Collider (LHC) [35]. The flexibility and functionality of this simulation code allows the user to create new simulation methods by providing a framework. In the present work GEANT4 particle transport simulation tool kit has been used to simulate an ADSR, in particular MYRRHA. As a benchmarking process, these results are compared with the corresponding MCNPX [36] predictions which is used 'out of the box' with default ENDF/B-V library.

GEANT4 is based on the Monte Carlo method. In the present study, neutrons are the particles of interest, particularly for the investigations on flux measurement and energy distribution. So, for the better understanding of Monte Carlo simulation of the interaction of neutrons with matter, it is important to develop an insight into the neutron transport theory. Figure 3.1 shows the basic concepts of Monte Carlo simulation.

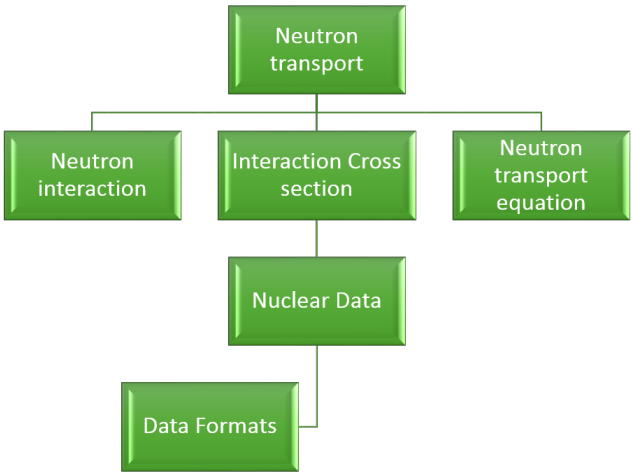

Figure 3.1: Monte Carlo Simulation (Underlying concepts)

3.1 Nuclear data

Nuclear data contains the parameters needed to model the neutron interactions. These interactions are indexed by the incoming energy of the particle initiating them. The Monte Carlo simulation of neutron interaction depends on evaluated nuclear data libraries as well as models. These evaluated libraries are the compilation of measured parameters such as cross section along with the predictions of nuclear model calculations adjusted to reproduce the experimental data. ENDF/B series, JEFF series and JENDL series are few popular evaluation series. The evaluated nuclear data file ENDF/B contains the recommended evaluation for each material. The data evaluations are stored in a computer readable ENDF-6 format. Similarly JEFF (Joint evaluated fission and fusion file) and JENDL (Japan evaluated nuclear data library) are the names of the data libraries written in ENDF-6 format. As the use of a single library does not guarantee the correctness of the results in diverse applications, it is good practice to run the simulations with different data libraries [37]. In the present investigations ENDF/B series is used which is the default series in GEANT4.

3.1.1 Data formats

A specialized format is used by most of the simulation codes. MCNP and GEANT4 use ENDF/B data but it is reformatted to be read directly by the simulation program without parsing the original file. While it reduces the compilation overhead, it also reduces the portability of datasets between the codes. For example, a dataset created

for MCNPX cannot be used directly in GEANT4.

The nuclear data in GEANT4 can be in various forms based on the implementation of a particular physics process. G4NeutronHP (High Precision) model is used for the simulation of neutron transport below 20 MeV. It relies on the GEANT4 neutron data library (G4NDL) which in turn relies on ENDF/B-VII.1 [37]. Data is separated into interaction cross section and final state data. Interactions are further divided into elastic scattering, radiative capture, fission and all other inelastic interactions. Final state data includes all the parameters for the interaction. These parameters include outgoing energy, angular distribution and secondary particle yields [35].

3.2 Neutron transport

Neutron transport is concerned with the transport of neutrons through various media. The motion of a neutron and its interaction with the material are studied in this theory. Neutron transport is described in the following sub sections: Neutron interaction, interaction cross section and neutron transport equation.

3.2.1 Neutron interaction

Scattering and absorption are the two main categories for neutron interactions. Scattering occurs when a neutron collides with a nucleus without being permanently absorbed. The momentum of the neutron changes based on the nature of the collision. Sometimes the neutron is temporarily absorbed by the nucleus forming an excited compound nucleus that decays and emits a neutron. These interactions can be elastic or inelastic.

- Elastic collisions: Energy is transferred between the neutron and the nucleus. Kinetic energy is conserved and additional particles are not created.
- Inelastic collisions: Kinetic energy is not conserved and some of it is released as radiation.

In absorption interactions the neutron is absorbed by the nucleus and an unstable compound nucleus is formed. Radiative capture and fission are the two main absorption interactions. In radiative capture the incident neutron remains and the nucleus decays by emitting gamma rays. Fission means that the compound nucleus is split into two smaller nuclei and fission neutrons are emitted. The fission products being unstable decay over time by particle emissions

3.2.2 Interaction cross section

The microscopic cross section of the neutron material pair is defined as "effective cross sectional area per nucleus seen by the neutron" [35]. It is not the actual cross section, rather it can be seen as the probability of a neutron to interact with the nucleus. This probability also depends upon the number density of the material. The macroscopic cross section (X) is defined as the interaction probability per unit length and is given as:

$$X_i(E) = N\sigma_i(E) = N_A\frac{\rho}{m}\sigma_i(E) \tag{3.1}$$

where

N is the atomic number density

N_A is Avogadro's number

ρ is the density

m is the molar mass

i is the type of interaction

E is the energy

Overall effect of multiple cross section is:

$$\sigma_t = \sigma_s + \sigma_a = \sigma_e + \sigma_{in} + \sigma_r + \sigma_f + ... \tag{3.2}$$

$$X_t = X_s + X_a = X_e + X_{in} + X_r + X_f + ... \tag{3.3}$$

where t stands for total and the type of interaction is: s for scattering, a for absorption, e for elastic, in for inelastic, r for radiative and f for fission.

The neutron cross sections are defined for a given particle, interaction and isotope. For materials having multiple isotopes

$$X_t = \sum_i \sum_j N_j \sigma_i^j \tag{3.4}$$

where t stands for total, j denotes the isotope and i is the type of interaction.

3.2.3 Neutron transport equation

Neutron can be defined completely by its energy E, location $\vec{r}$ and direction of travel $\vec{\Omega}$ at time t. Neutron angular density N ($\vec{r}$, $\vec{\Omega}$, E, t) can be defined as the density of neutron in volume ($\vec{dr}$) about $\vec{r}$, direction of travel as ($d\vec{\Omega}$) about $\vec{\Omega}$, with energy dE about E and time dt about t.

Angular flux (ψ) as the product of angular density and velocity $\vec{v}$ when integrated over the directions gives total or scalar flux (ϕ) [6].

$$\psi(\vec{r}, \vec{\Omega}, E, t) = N(\vec{r}, \vec{\Omega}, E, t)\vec{v} \tag{3.5}$$

$$\phi = \int_{4\pi} \psi(\vec{r}, \vec{\Omega}, E, t) d\vec{\Omega} \tag{3.6}$$

The scalar flux (ϕ) is proportional to the reaction rate (R) and the proportionality constant relating the flux to the reaction rate is the macroscopic cross section (X).

$$R = \phi X \tag{3.7}$$

The transport of a neutron through various media is explained by the neutron transport theory. Assuming no neutron-neutron collision due to sufficiently low neutron density, the neutron being a neutral particle travels in straight lines and deviates only when it is scattered or absorbed by an interaction with a nucleus. The neutron transport equation is organized with neutron sinks on the left and the neutron gain on the right. The net neutron gain equals the time dependent rate of change of the neutron flux. The neutron balanced can be expressed as:

$$\frac{dN}{dt} = Gain - Loss \tag{3.8}$$

So the neutron transport equation is formulated as:

$$\begin{aligned} &\frac{1}{\vec{v}}\frac{\partial \psi}{\partial t}(\vec{r}, \vec{\Omega}, E, t) + \vec{\Omega}.\nabla\psi(\vec{r}, \vec{\Omega}, E, t) + X_t(\vec{r}, E, t)\psi(\vec{r}, \vec{\Omega}, E, t) = \\ &\int_{4\pi} d\vec{\Omega}' \int_0^\infty dE' X_s(\vec{r}, E' \to E, \vec{\Omega}' \to \vec{\Omega}, t)\psi(\vec{r}, E', \vec{\Omega}', t) + S(\vec{r}, E, \vec{\Omega}, t) \end{aligned} \tag{3.9}$$

where

$\vec{v}$ = neutron velocity vector

$\vec{\Omega}$ = unit vector in direction of motion

E = energy

t = time

So, the neutron is initially at position r moving in direction $\vec{\Omega}$ with energy E

ψ ($\vec{r}$, $\vec{\Omega}$, E , t) = angular flux

X_t ($\vec{r}$, E, t) = total macroscopic cross section

X_s ($\vec{r}$, $E' \rightarrow$ E, $\vec{\Omega}' \rightarrow \vec{\Omega}$, t) = scattering in cross section from an incident energy E' to E and from direction $\vec{\Omega}'$ to Ω in dE and $d\vec{\Omega}$ respectively

S ($\vec{r}$, E, $\vec{\Omega}$, t) = source term

The description of the five terms used in equation 3.9 is as follows:

- First term - change rate in the number of neutrons
- Second term - Leakage rate
- Third term - detailed collision rate
- Fourth term - Neutron that scatter and enter the volume from all direction and energy
- Fifth term- Other sources

The solution of the neutron transport equation (equation 3.9) gives the scalar flux (from equation 3.5 and equation 3.6) that can be used for the calculation of measurable quantities such as reaction rates (from equation 3.7).

3.2.4 Monte Carlo

Monte Carlo simulations are used to solve neutron transport equation by converting the integrals for gain and loss of neutrons into probabilities and applying these probabilities to a neutron moving through a material [35].

This method uses the sequence of random numbers to obtain sample values for the problem. The particle flight path and interactions are imitated in this method. Defining a geometry in which neutron will be investigated along with the source term is the first and one of the most important parts of this method. The geometry description includes the size, shapes and location of the objects along with the description of their material.

The execution of the neutron flight path throughout the material is the next step after the geometry description. The simulation of the neutron flight path is called random walk. It creates a set of neutron collision points from information such as neutron energy and direction after the collisions [6].

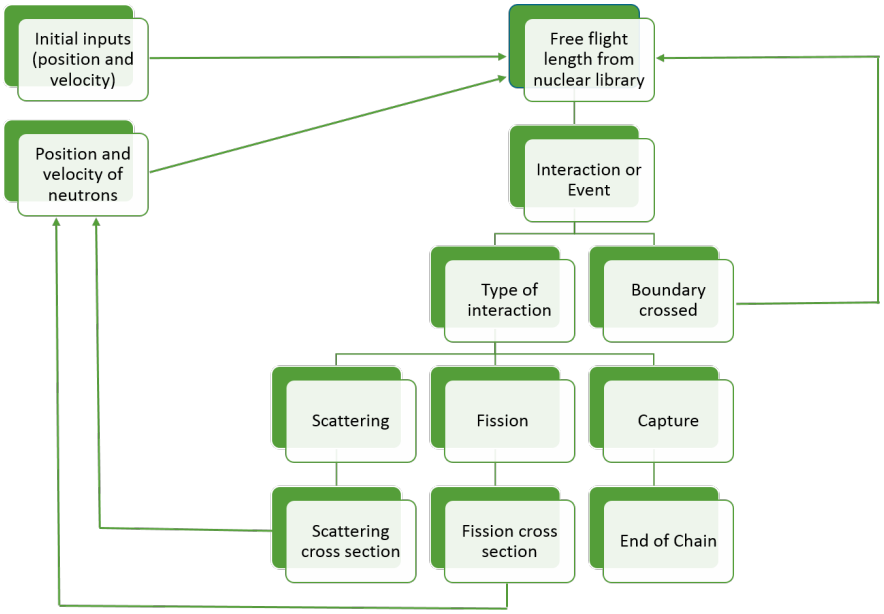

Figure 3.2: Steps in Monte Carlo approach [6]

Neutrons are followed in space from creation to loss. Creation refers to a neutron-producing interaction (example fission, source particle creation) and loss refers to a neutron- removing interaction (Absorption, capture). Neutron moves through a series of steps along this path, each step ends with an interaction [35].

Figure 3.2 presents the history of a neutron moving throug a material. To generate this, inputs such as position and velocity are initialized. Then the length of free flight is determined from the nuclear data library. Either neutron crosses one of the material boundaries or it collides resulting either in an event or an interaction. The type of interaction is calculated from the interaction cross section given by equation 3.1.

Event : When the neutron crosses the boundary and enters a new material, an event occurs. Then new flight paths are calculated from the material properties and the algorithm is executed all over again.

Interaction : Can be one of the three collision types: Scattering, fission or absorption. Chain is terminated in case of absorption. In collisions due to scattering the new velocity is determined from the previous velocity and scattering cross section from the data library. Then the neutron goes back to the algorithm with a new velocity. In the case of fission, the number and velocities of new neutrons are obtained from the fission cross section library. These neutrons will also follow the algorithm until all the neutrons are absorbed and the chain is terminated [6].

To summarize, starting with a single neutron the result of Monte Carlo simulation is the outcome of that neutron and all of its descendants [35].

3.3 GEANT4 modeling

The major domains for GEANT4 simulation can be identified as:

- Materials and geometry
- Particle interaction in matter
- Tracking management
- Digitization and hit management
- Event and track management
- Visualisation
- User interface

User interface domain is the medium by which the user interacts with GEANT4. It combines the features from the other six domains. Eight classes are provided by the basic user interface. The following three user interface classes are mandatory:

1. Detector Construction
2. Physics List
3. Primary Generator Action

The remaining five classes are optional and can be included depending on the requirements of the simulation problem [38].

In GEANT4 the Kernel is the fundamental structure for every simulation. It uses manager classes to handle every step in the tracking process. The manager classes in GEANT4 are:

- Event Manager
- Run Manager
- Tracking Manager
- Stepping Manager
- Process Manager

Only one instance of these classes is allowed. The user specifies a driver file that contains the main function. This driver file instantiates the kernel, the run manager and the user defined classes. After all the necessary classes and functions are defined,

the user generated source files are compiled and linked to GEANT4 libraries to build the simulation program [35].

Due to broad nature of hadronic physics, the only viable approach in GEANT4 is to use different models covering different region of interest based on incident particles, target material type and interaction energies. In GEANT4 scheme the calculation aspects include: Physics model (calculation of final stage of the reaction), Process and Physics list (List of processes for each particle). Process combines the cross section (when a reaction takes place) and model to create a description of how interaction of particle takes place with matter. So physics list is a place where the physical processes required by the simulation are specified [39].

As discussed in chapter 2, three stages are involved in the simulation of spallation reaction. These three stages are:

1. Intra-nuclear Cascade (INC)
2. Pre-equilibrium
3. Evaporation and fission model

In GEANT4, for each stage a special model is used. The two theoretical models used in the simulation are QGSP_ BERT_HP (Bertini cascade model) and QGSP_BIC_HP (binary cascade model). The data driven high precision neutron package (NeutronHP) is included in these models to transport neutrons below 20 MeV down to thermal energies.

The Bertini cascade (BERT) model includes INC. The particle-nucleus collision is approximated by particle-nucleon collision. Fast collisions such as spallation results in an excited nucleus solved by pre-equilibrium emissions while the slow collisions result in compound nucleus decaying by evaporation [38]. The binary cascade (BIC) model includes the time dependent development of INC [40] and the nucleus is considered as a collection of nucleons. So the particle-nucleon collisions take place that are modelled by the decay of resonances within the nucleus. It uses the native pre-equilibrium and de-excitation models of GEANT4. Comparing with the corresponding MCNPX predictions for low energy spectra BIC_HP gives better results than BERT_HP, so BIC_HP is used in the simulations as will be discussed in chapter 4.

3.4 Differential equation and its solution

For fuel evolution studies that will be covered in chapter 7, differential equations need to be solved. All the systems undergoing changes can be described by differential equa-

tions. When the system described by the differential equation are complex or very large then purely analytical solution is usually not tractable. Computer simulations and numerical methods are useful in such scenarios [41].
In numerical methods, algorithms are used to present approximate solution to mathematical problems while formulas from exact theorem are used to obtain analytical solutions. Analytical methods provide exact solution while numerical methods give approximate solution.
The nuclide concentration following the decay chain is governed by a set of equation, known as Bateman equations [42]. It is defined by a mathematical model which on the basis of decay rates and initial abundance, describes the abundances and activities in a decay chain as a function of time. Rather than a single equation it is of a set of equations, one for each isotope involved. For a radioactive n nuclide decay series, the Bateman equation can be written as follows:

$$\frac{dN_1}{dt} = -\lambda_1 N_1 \tag{3.10}$$

$$\frac{dN_\mathrm{i}}{dt} = \lambda_{\mathrm{i}\text{-}1} N_{\mathrm{i}\text{-}1} - \lambda_\mathrm{i} N_\mathrm{i} \tag{3.11}$$

where λ_i is decay constant of ith nuclide. At t = 0, concentration is assumed to be zero for all daughters. The first term (at right) in equation 3.11 corresponds to the growth of daughter from the decay of parent while the second term denotes the decay of daughter at time t. This is for a decay chain which is a simple single sequence. In more complicated decay chains more terms appear. For example, in the reactor, there are additional terms as expressed in equation 7.1, in chapter 7.

The solution of Bateman equations can be obtained either by stepwise integration or by algebraic approach.

3.4.1 Numerical method for the solution of differential equation

Euler's method is the simplest method of numerical approximation for solving differential equations. Using the numerical derivative form from equation 3.10 as $\frac{dN_1}{dt} = -\lambda_1 \mathrm{N}_1$ Eulers method uses the initial slope $\left.\frac{dN}{dt}\right|_{t=0}$ to extrapolate and predicts the future.
i. At initial time $t = 0$,

$$N = N_0 \tag{3.12}$$

ii. At a later time t_1, the value can be predicted using extrapolation as:

$$N_1 = N_0 + \left.\frac{dN}{dt}\right|_{t=0} (t_1 - t_0) \tag{3.13}$$

or

$$N_1 = N_0 - \lambda N_0 (t_1 - t_0) \tag{3.14}$$

This is valid if $t_1 - t_0$ is small.

iii. Getting the value of variable at time t_1, we can calculate N_2 as:

$$N_2 = N_1 + \left.\frac{dN_1}{dt}\right|_{t=t_1} (t_2 - t_1) \tag{3.15}$$

Substituting $\frac{dN_1}{dt}$ from equation 3.10, we get

$$N_2 = N_1 - \lambda_1 N_1 (t_2 - t_1) \tag{3.16}$$

The process repeats and the solution can be plotted with respect to time. For comparison, the analytical solution can also be plotted. For a larger time step, the trend is similar however the deviation of numerical solution from the analytical solution is larger. Numerical solution becomes closer to the true solution by making the time step as smaller. This is very easy to implement, which is why it is used even though it is not as accurate as the algebraic approach.

3.4.2 Algebraic approach

For a matrix $\mathbf{A}$, the equation for the eigenvalue and eigenvector is:

$$\mathbf{A}x = rx \tag{3.17}$$

Where $\mathbf{A}$= matrix, x= eigenvector and r= eigenvalues. We find eigenvalues by solving $|\mathbf{A} - rI| = 0$ and substitute the values of r in equation 3.17 to find eigenvector. Alternatively the solutions can be found by a matrix package such as in R, `eigen(A)` can be used to find the eigenvalues and eigenvectors of matrix $\mathbf{A}$. To show how this works, we will go through a simple case, the one already mentioned through the set of equations (equation 3.10 and equation 3.11) which can be written compactly using

matrices. So, the equation becomes

$$N' = \mathbf{A}N \tag{3.18}$$

where $\mathbf{A}$, in this simple case, can be expressed as:

$$\mathbf{A} = \begin{bmatrix} -\lambda_1 & 0 \\ \lambda_1 & -\lambda_2 \end{bmatrix} \tag{3.19}$$

Equation 3.18 is a first order linear differential equation, so if N is an eigenvector satisfying equation 3.17, the solution is:

$$N = Ke^{\mathrm{rt}} \tag{3.20}$$

Substituting equation 3.20 into equation 3.18 gives the equation 3.21 which is similar to matrix equation 3.17

$$\mathbf{A}K = rK \tag{3.21}$$

Where K is eigenvector and r is eigenvalue. In general, N will not be an eigenvector, but it can always be written as sum over eigenvectors, as they form a basis. So, the general solution for equation 3.21 is

$$N = C_1K_1e^{\mathrm{r_1t}} + C_2K_2e^{\mathrm{r_2t}} \tag{3.22}$$

Now the values of r_1, r_2 and K_1, K_2 need to be found. For a triangular or diagonal matrix the diagonal elements are eigen values. So from equation 3.19,

$r_1 = -\lambda_1$, $r_2 = -\lambda_2$

To find the eigen vectors, we solve

$(\mathbf{A} - r_1\mathbf{I})N = 0$ and $(\mathbf{A} - r_2\mathbf{I})N = 0$

Substituting the values of $\mathbf{A}$, $\mathbf{I}$, r_1 and r_2 in the above equations, we get

$$\mathbf{K}_1 = \begin{bmatrix} 1 \\ \dfrac{\lambda_1}{\lambda_2 - \lambda_1} \end{bmatrix} \text{ and } \mathbf{K}_2 = \begin{bmatrix} 0 \\ \lambda_1 - \lambda_2 \end{bmatrix}$$

To evaluate C_1 and C_2, we use the following initial condition at $t = 0$:

$$\mathbf{N}(0) = \begin{bmatrix} N_{1,0} \\ N_{2,0} \end{bmatrix} = \begin{bmatrix} 1 \\ 0 \end{bmatrix}$$

Substituting K_1, K_2 and the above initial condition in equation 3.22, we get

$$\begin{bmatrix} 1 \\ 0 \end{bmatrix} = \begin{bmatrix} C_1 \\ \dfrac{C_1\lambda_1}{\lambda_2 - \lambda_1} \end{bmatrix} + \begin{bmatrix} 0 \\ (\lambda_1 - \lambda_2)C_2 \end{bmatrix}$$

$$= \begin{bmatrix} C_1 \\ \dfrac{C_1\lambda_1}{\lambda_2 - \lambda_1} - (\lambda_2 - \lambda_1)C_2 \end{bmatrix}$$

which gives,

$$C_1 = 1 \text{ and } C_2 = \frac{\lambda_1}{(\lambda_2 - \lambda_1)^2}$$

Substituting r_1, r_2, K_1, K_2, C_1 and C_2 in equation 3.22, we get

$$\begin{bmatrix} N_1 \\ N_2 \end{bmatrix} = \begin{bmatrix} e^{-\lambda_1 t} \\ \dfrac{\lambda_1}{\lambda_2 - \lambda_1}(e^{-\lambda_1 t} - e^{-\lambda_2 t}) \end{bmatrix} \tag{3.23}$$

From equation 3.23, we get

$$N_1 = e^{-\lambda_1 t} \tag{3.24}$$

$$N_2 = \frac{\lambda_1}{\lambda_2 - \lambda_1}(e^{-\lambda_1 t} - e^{-\lambda_2 t}) \tag{3.25}$$

which are by inspection, correct solutions. The same principle can be applied (and will be later) to larger matrices with more terms.

4

Characteristics Of Spallation Neutrons

Spallation process being an established technique for the production of high intensity neutron flux, the design of target and neutronic studies is an area of growing interest. The present chapter covers some detailed investigations performed for the neutron distribution for ADSR. This was also performed as a way of gaining experience with GEANT4 and neutron fluxes in a simple geometry before moving on to the more complicated MYRRHA geometry. To provide a spallation neutron source, a proton beam with energy ranging from 100 MeV to 1.4 GeV is incident on a lead target that is a cylinder with typical dimensions as 30 cm in radius and 30 cm in length.The proton beam is taken as monochromatic, parallel and incident at the centre of the circular face. Notional detectors are placed at various locations around the target to record the neutron distributions from near end (where the proton beam enters), far end (opposite to near face) and the sides of the cylindrical target as shown in Figure 4.1.

Investigations are performed to determine the overall number of neutrons produced, their longitudinal distribution, radial distribution and their energy spectra. In the present study, computations are performed using GEANT4.10.1 [44] simulation code. As a benchmarking process, these results are compared with the corresponding MCNPX predictions produced with the default ENDF/B-V library. In the preliminary studies ([45],[46]) GEANT4 simulations are performed initially with the Bertini model and then with its high precision version but both of these show serious discrepancies with MCNPX predictions. The Binary cascade model with high precision BIC_HP gives good agreement with the MCNPX results [43] and this model is used for the results

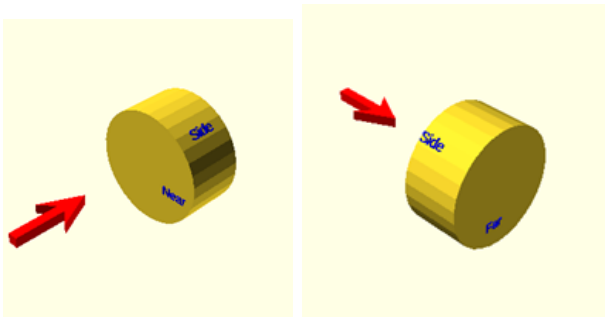

Figure 4.1: Schematic view of target. Reproduced from [43]

presented here.

It is found that the properties of spallation neutrons can be parametrized by simple forms which can then be used as a source term for neutronics simulations for ADSR reactors [47].

4.1 Neutron numbers

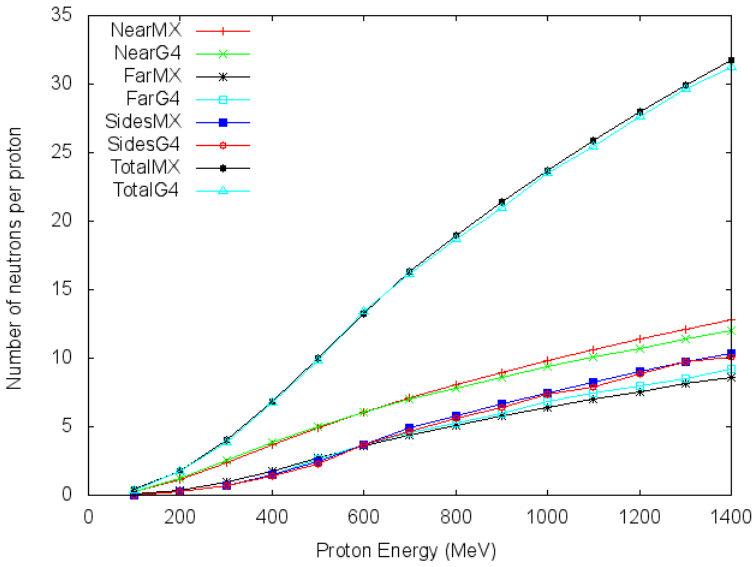

Figure 4.2: Number of neutrons from lead target for MCNPX and GEANT4

Overall numbers of spallation neutrons using Geant4 (G4) and MCNPX (MX) are shown in Figure 4.2. They are in good agreement for the total numbers as well as for

the number of neutrons obtained from the sides and ends. Both the codes predict that more neutrons are available at near face where the proton beam falls. This is somewhat counter-intuitive, but can be explained as the neutrons undergo many collisions in lead and 'forget their original direction, and the near face receives the full energy of the proton beam. As the proton energy increases, the number of neutron also increase. At 1 GeV approximately 30 neutrons are available per proton. The shape is very roughly linear and above 600 MeV the concave becomes convex. So it can be nicely fitted through two parabolas above and below 600 MeV. The parameterization of this curve is shown in Figure 4.3. The curve can be described by the equation

$$N = aE^2 + bE + c \tag{4.1}$$

where N is the total number of neutrons and E is the energy of proton beam. The values of fitting parameters a, b and c satisfying equation 4.1 are presented in Table 4.1.

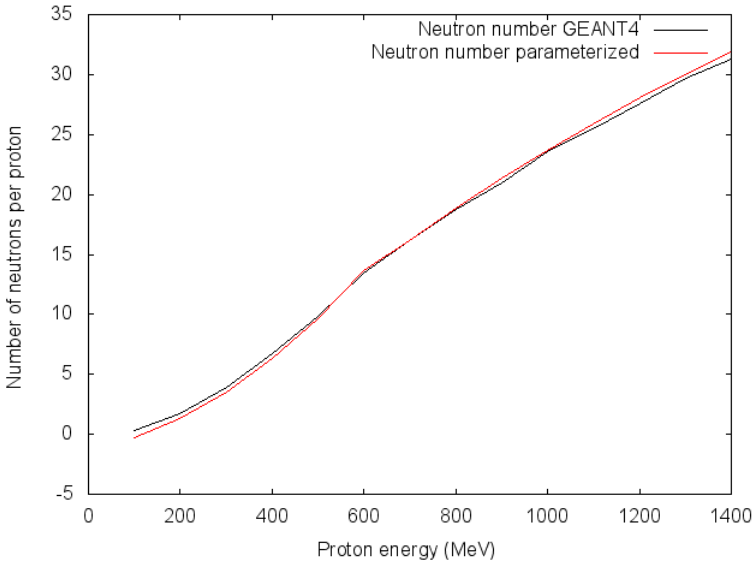

Figure 4.3: Overall number parameterization

For the purpose of validation with the data from the real experiment, the simulations are performed further for a cylindrical target with 10 cm radius and 60 cm length. The results from GEANT4 are compared with the real data [48] as shown in Table 4.2. The experiment was conducted on a lead target of radius 10 cm and length 60 cm, placed at the Joint Institute for Nuclear Research (JINR), Dubna. For neutrons with

Fitted Parameter	a	b	c
Below 600 MeV	2.9E-5	0.00749	-1.312
Above 600 MeV	-5.9E-6	0.0357	-5.9037

Table 4.1: Fitted parameters satisfying equation 4.1

Proton energy (GeV)	Number of neutrons/proton		
	Experimental		GEANT4
	Moderation technique	Threshold technique	
0.99	21.3 ± 0.6	25.1 ± 3.0	22.8
1.47	31.4 ± 0.8	Not available	33.8
2	40.2 ± 1.1	44.2 ± 3.1	44.3
2.56	51.3 ± 1.5	63.5 ± 7.6	54

Table 4.2: Number of neutrons from lead target as reported in [48] and by GEANT4 simulation

energy $\leq$ 15 MeV, neutron moderation technique was used while for higher energy neutrons, solid-state nuclear track detectors (SSNTD) were used (threshold technique). GEANT4 simulation satisfactorily reproduces the experimental data, more accurately the data obtained from the moderation techniques. However it underestimates the data produced by threshold technique which itself is not agreeing well with the moderation experimental technique. This indicates the need to further validate the data with another simulation code MCNPX as well.

4.2 Target length variation

The influence of the target length on the neutron production is shown in Fig 4.3. The beam energy is taken as 1000 MeV and the simulations are run to record the contribution of ends and sides as a function of target length. The predictions of GEANT4 (G4) and MCNPX (MX) agree well for neutrons from the near end, far end and the sides of the cylindrical target. It can be concluded from the graph that as the length of the target increases:

1. The number of neutrons coming out of the near end is almost the same for all target lengths above 30 cm. It means what happens further down the target does not affect what comes out of the near end.

2. The curve for far face gets smaller indicating fewer numbers of neutrons from face

for longer target. The maximum number of neutrons is recorded at 30 cm.

3. The curve for sides gets bigger as we increase the length, and thus the area of the side face, the number of neutrons continues to increase.

It can be fairly interpreted from the graph that the total number of neutrons from the cylindrical lead target increases up to 60 cm target length and there is no benefit of increasing it beyond 60 cm.

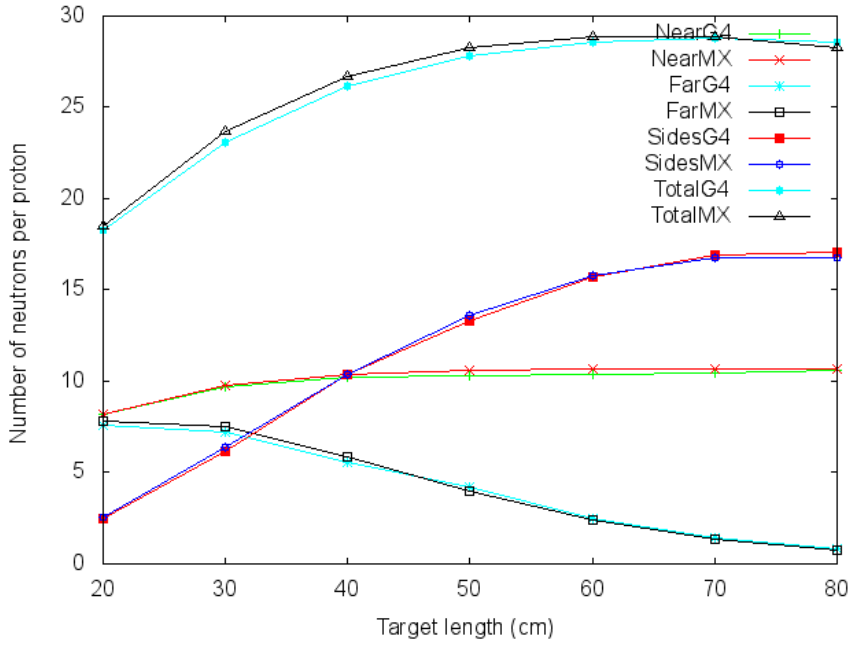

Figure 4.4: Number of neutrons for variable target length of lead at 1 GeV proton energy using MCNPX and GEANT4

4.3 ENERGY DISTRIBUTIONS

The neutron energy spectra can be categorized as high energy spectra, low energy spectra and intermediate energy spectra showing different characteristics.

4.3.1 High energy neutrons

In the high energy spectrum, the effects of spallation appear in a tail of neutrons which falls roughly exponentially with energy, with an additional cutoff as the energy of the

original proton is reached. The predictions of energy spectra for these two categories by Geant4 and MCNPX are shown in Figure 4.5. Spectra are plotted for 1000 MeV beam energy. These high energy neutrons emerge overwhelmingly from the far face. Both the codes predict that the high energy component of spectra are dependent on proton energy and the contribution from different faces are also different.

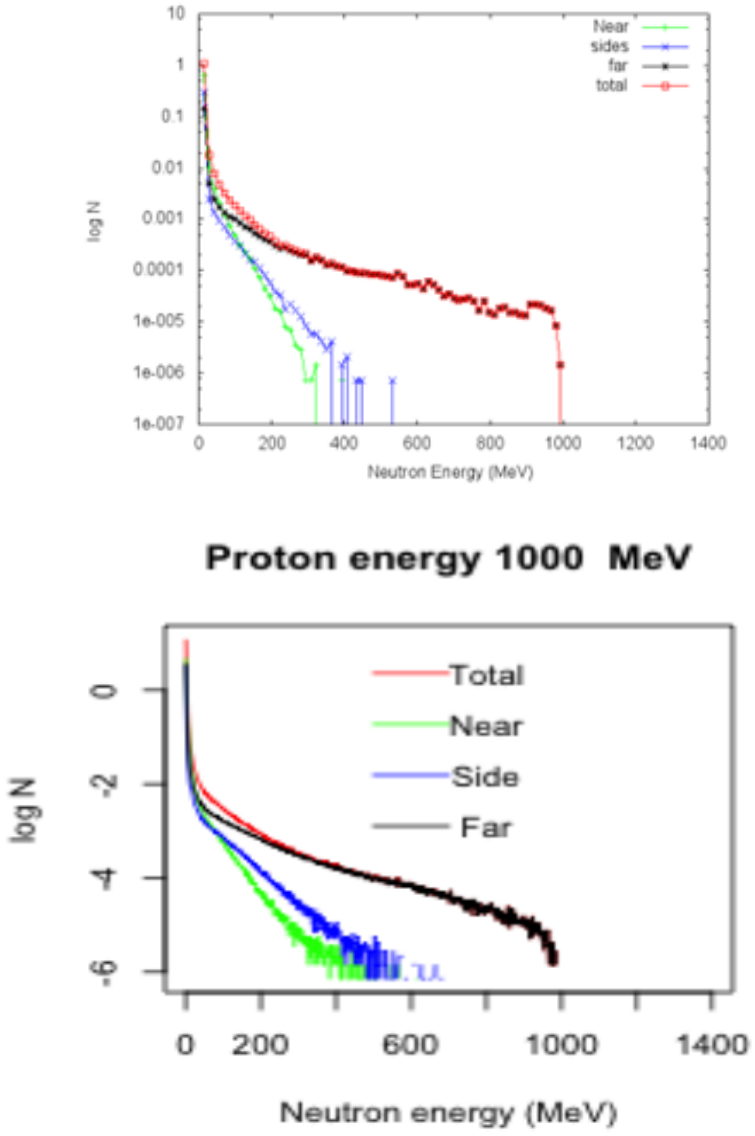

Figure 4.5: High energy spectra (Top: GEANT4, Bottom: MCNPX)

4.3.2 Low energy neutrons

At low energies (below 1 MeV) the neutron spectrum is fairly flat, with an intricate shape which is similar from each face (Figure 4.6). The curves show the number of neutrons from near end (green), far end (black), sides (blue) and total (red). The low energy neutron could have suffered a number of elastic scatters off the moderator and 'forgotten' their origin. The shape of neutron spectrum at low energies is dominated by cross sections in lead. It can be seen from the figure that the spectra from the different faces are identical which is in contrast to the high energy spectra of Figure 4.5.

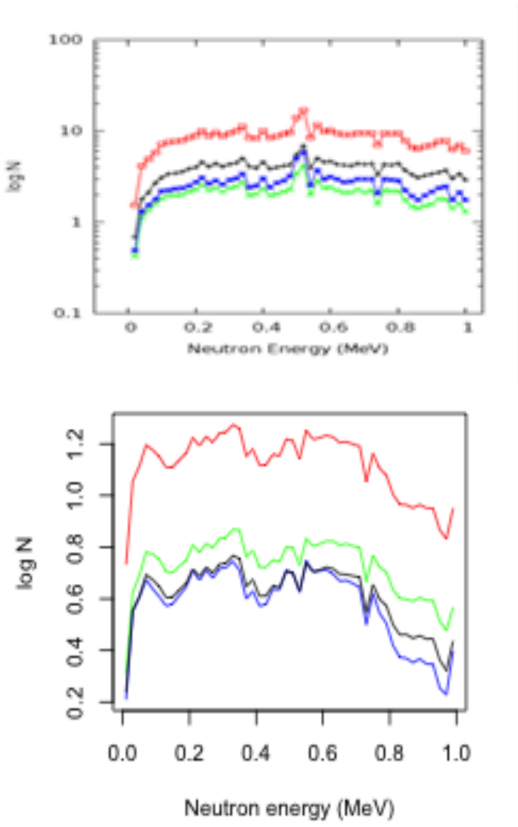

Figure 4.6: Low energy spectra (Top: GEANT4, Bottom: MCNPX)

4.3.3 Intermediate energy neutrons

From the above discussion we can say that at low neutron energies the shape of spectrum is independent of faces and only the size changes and is complicated to parameterize.

At high neutron energies the shape of spectrum depends on faces and is simple i.e. exponential with cutoff. The question arises "What is high and low?" It is a relative term and it can be defined by looking at the spectra of intermediate energy neutrons (Figure 4.7) and the plots says that $\sim$ 2 MeV is the limit above which the shapes of the spectra are different for different faces. It means that below 2 MeV the spectra is categorized as low (independent of the face) and above 2 MeV (dependent on the face) as high for face dependence. In Figure 4.7, the colour codes for the curves are same as before i.e. red for near end, green for far end, blue for sides and black for total number of neutrons.

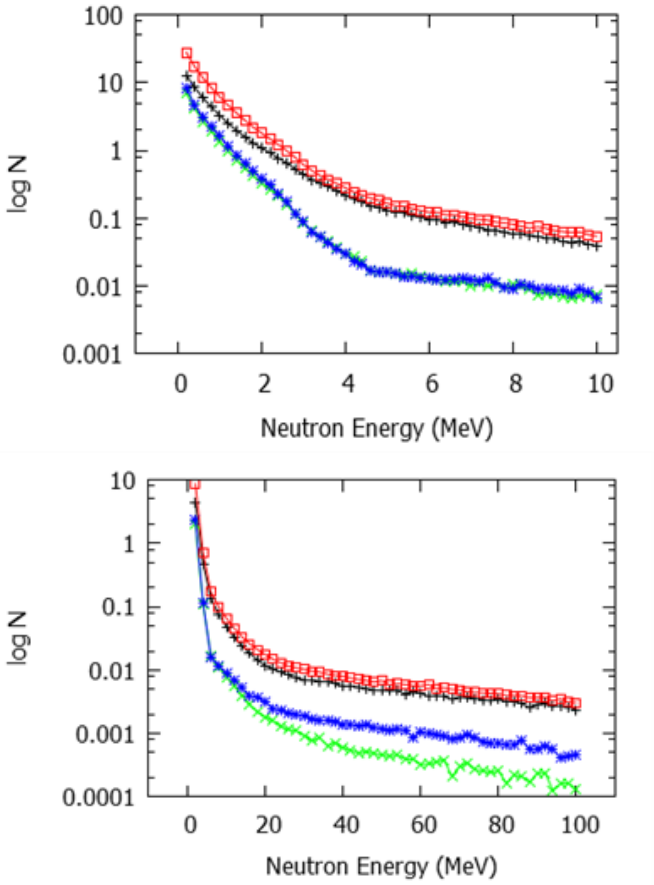

Figure 4.7: Intermediate energy spectra (GEANT4)

4.4 SPATIAL DISTRIBUTIONS

In addition to counting the number of neutrons emerging from each face, it is interesting to study the spatial distribution of the point at which they emerge.

4.4.1 Longitudinal distributions

Neutrons emerging from the sides are simulated. They emerge uniformly around the circumference because of the axial symmetry, however the distributions along the length of the target will be discussed.

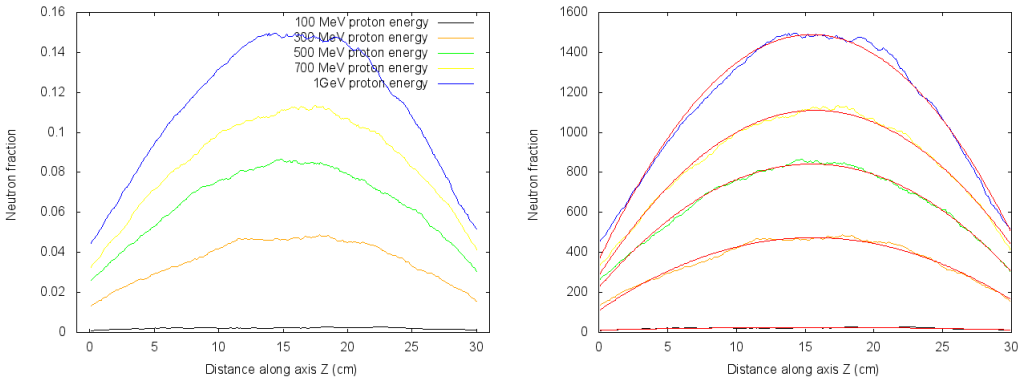

Figure 4.8: a) z-distribution in GEANT4 b) Its parameterization

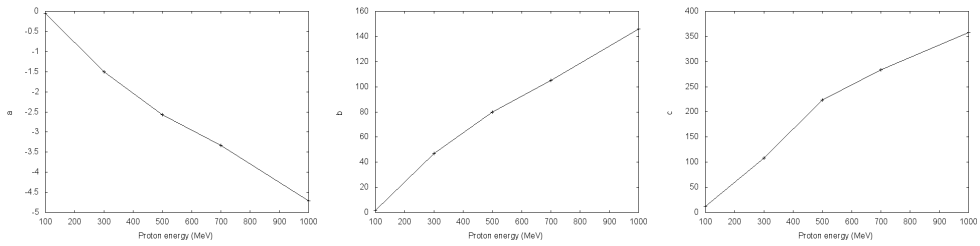

Figure 4.9: Coefficient a, b and c from left to right, as in equation 4.2

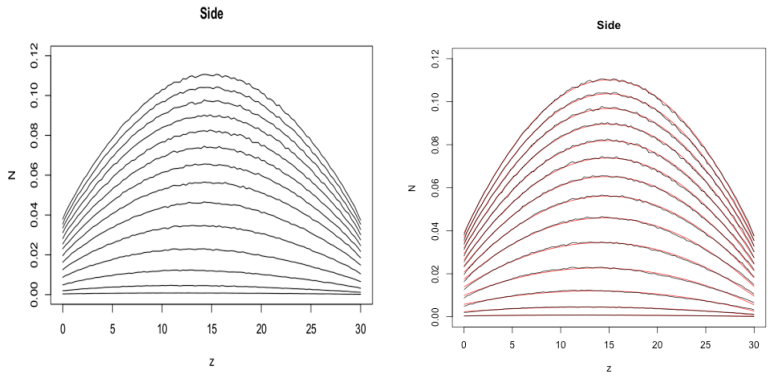

Figure 4.10: a) z-distribution in MCNPX b) Its parameterization. [43]

The neutrons obtained from the longitudinal distribution shows similar behavior for GEANT4 and MCNPX. Figure 4.8 shows the z-distribution for different proton energies using GEANT4 and Figure 4.10 shows its MCNPX equivalent. The shape is similar for all proton energies, almost symmetric about mid plane. The plots are normalized to show the number of neutrons/proton/cm.
For the neutrons emitted along the side, the longitudinal distribution varies remarkably little with energy. It is well described by a parabola. The center of the parabolas increases only very slowly with proton energy. The parameterization of z-distribution is shown in Figure 4.8 b. It can be described by the equation

$$N = az^2 + bz + c \tag{4.2}$$

where N is the total number of neutrons and z is the distance along Z axis. The parameters a, b and c satisfying equation 4.2, vary with the proton energy as shown in Figure 4.9.

4.4.2 Radial distributions

The r-distribution of neutrons coming out of the two ends is similar at large 'r' but interestingly different at r = 0. For the far face the distribution falls to zero at small r while for near it does not. The radial distribution for the two ends obtained by GEANT4 are shown in Figure 4.11 and Figure 4.14. The corresponding MCNPX results for the two ends are shown in Figure 4.13 and Figure 4.16. The prediction of the two programs agrees well for the two faces. The plots are normalized to show the number of neutrons/proton/ cm.

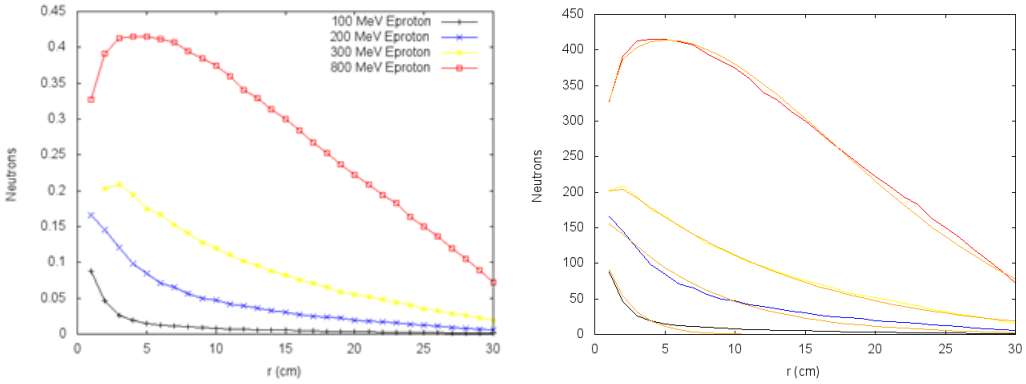

Figure 4.11: a) Radial distribution in GEANT4 (for near end) b) Its parameterization

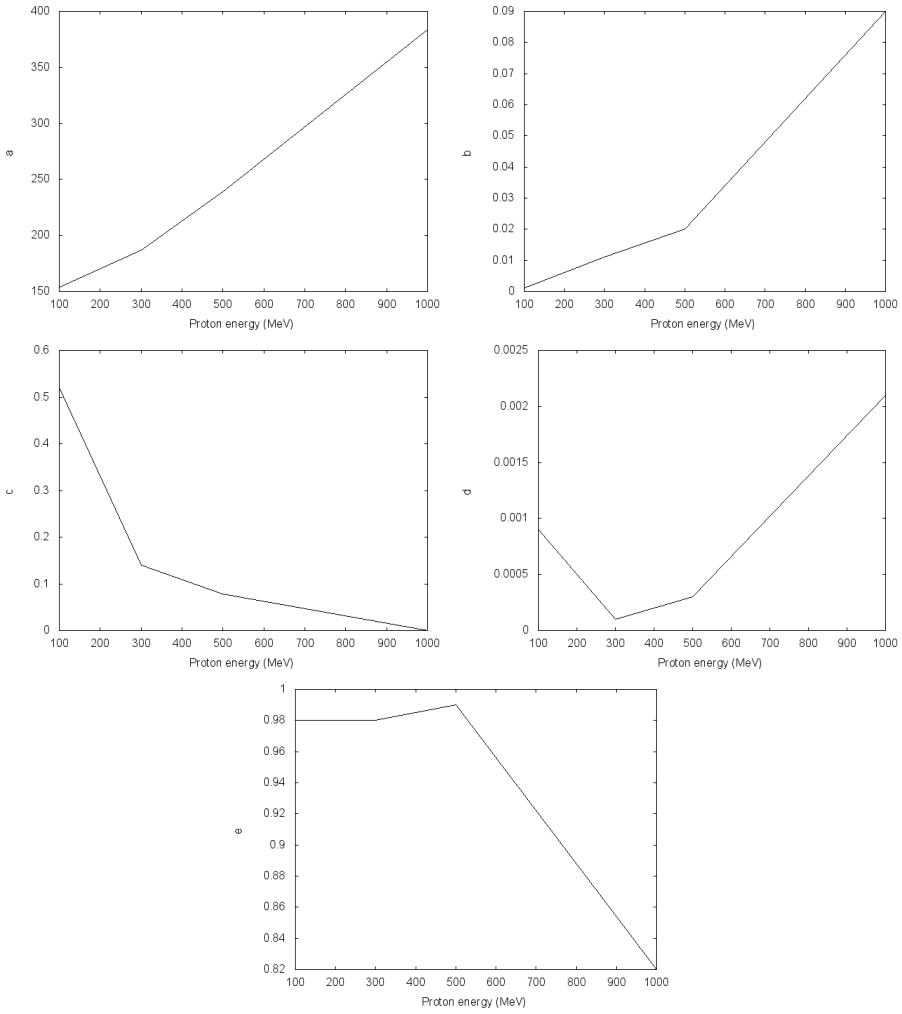

Figure 4.12: Coefficient a, b, c, d and e (from left to right), as in equation 4.3, for near end

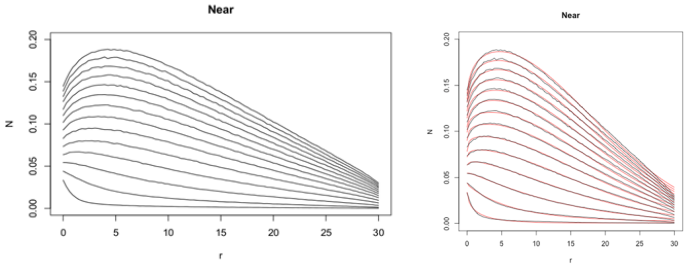

Figure 4.13: a) Radial distribution in MCNPX (for near end) b) Its parameterization. [43]

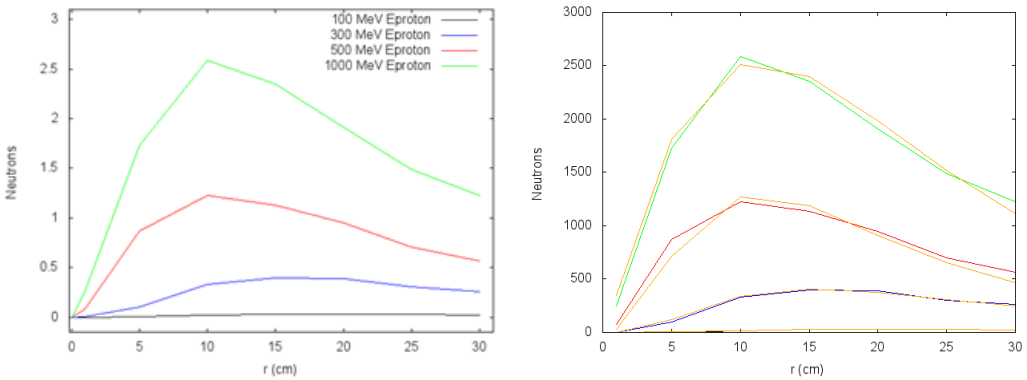

Figure 4.14: a) Radial distribution in GEANT4 (for far end) b) Its parameterization

The parameterization of the radial distribution for near and far end are shown in Figure 4.11 b and Figure 4.14 b respectively. These curves can be described by the following equations

Far face:

$$N = ar^b \exp(-cr - dr^2) \tag{4.3}$$

Near Face:

$$N = a(r - e)^b \exp(-cr - dr^2) \tag{4.4}$$

where N is the total number of neutrons and r is the radial distance. The parameters a, b, c, d and e satisfying equation 4.3, vary with the proton energy as shown in Figure 4.12 and the parameters a, b, c, and d satisfying equation 4.4, vary with the proton energy as shown in Figure 4.12.

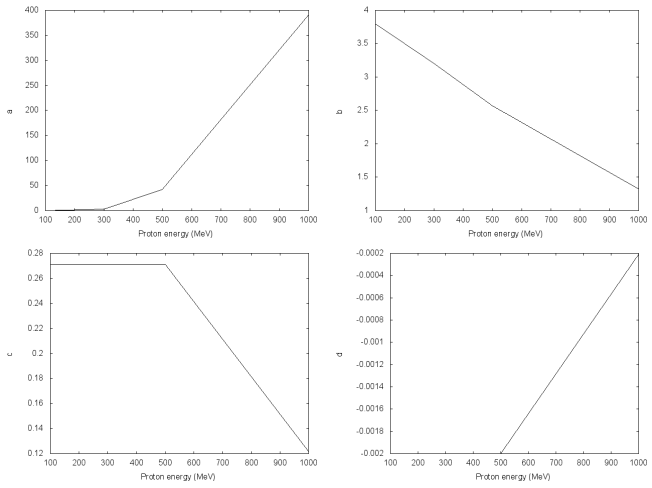

Figure 4.15: a, b, c and d (from left to right), as in equation 4.4, for far end

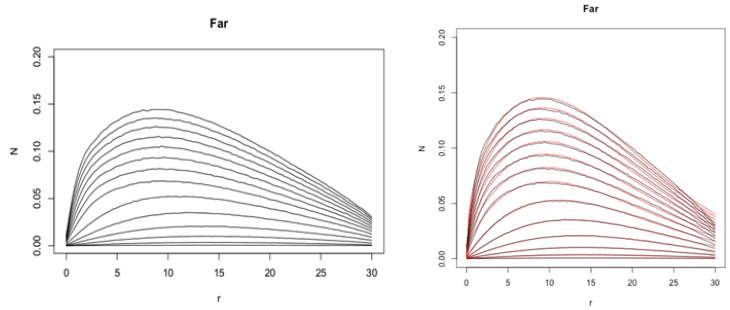

Figure 4.16: a) Radial distribution in MCNPX (for far end) b) Its parameterization. [43]

4.5 MODEL DEPENDENCE AND CROSS SECTIONS

Using GEANT4 'out of the box' gave results considerably different from MCNPX: the default option to use models for cross sections is inapplicable for low energy neutrons, where resonances dominate. Hence a High Precision model, using a cross section library, had to be used.

The two theoretical models used in the simulation are QGSP_BERT_HP and QGSP_BIC_HP. The data driven high precision neutron package (NeutronHP) is included in these models to transport neutrons below 20 MeV down to thermal energies. The energy spectra of neutrons using Bertini high precision model are shown in Figure 4.17. The high energy spectra show good agreement while the low energy spectra show agreement

to some extent with MCNPX predictions shown in Figure 4.18. The results obtained using Binary cascade with high precision model as shown in Figure 4.19 show good agreement at high as well as low energy spectra with the corresponding MCNPX predictions.

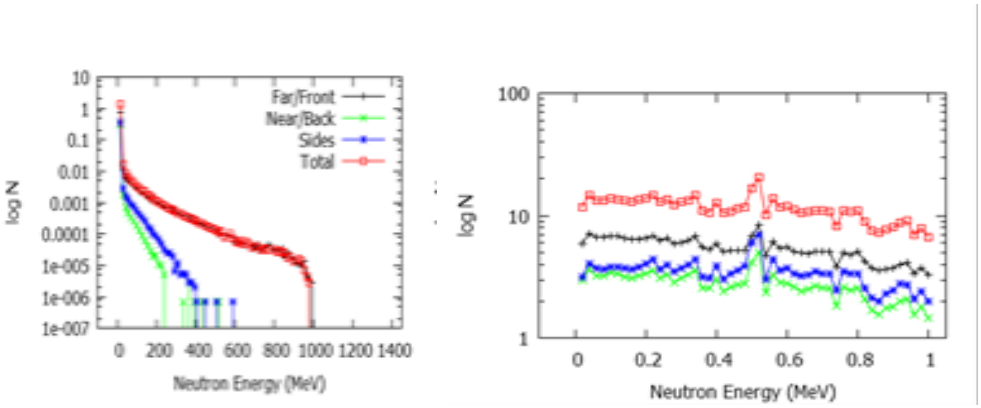

Figure 4.17: Energy spectra using BERT_HP (Left: High energy spectra, Right: Low energy spectra)

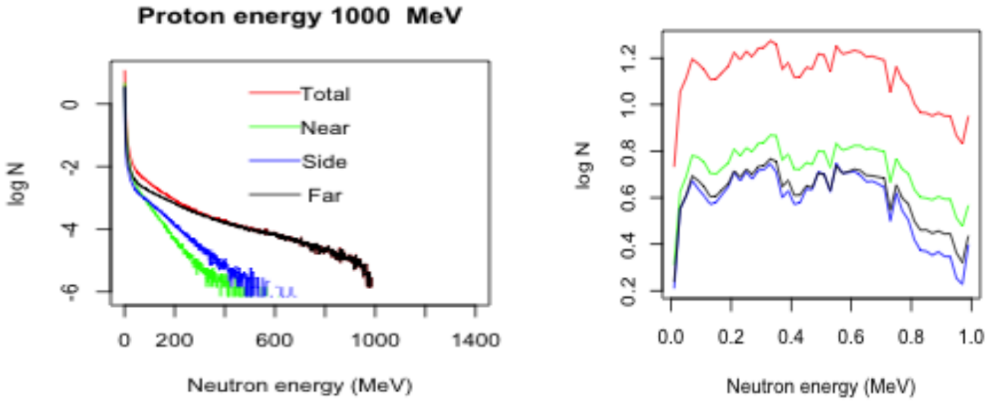

Figure 4.18: Energy spectra using MCNPX (Left: High energy spectra, Right: Low energy spectra)

So, binary cascade BIC_HP model is used in the investigations. For MCNPX ENDF/B-V library [49] is used.

The energy spectrum of spallation neutrons depends on the energy dependence of the cross sections in [43]. The shape of low energy spectrum is driven by the neutron

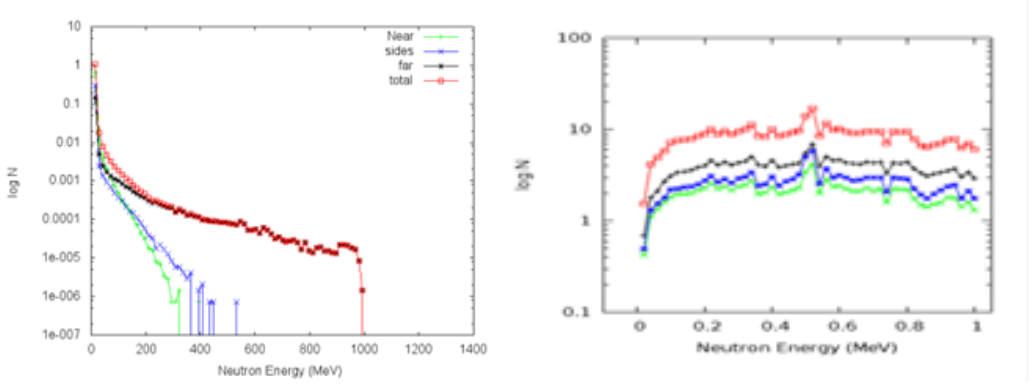

Figure 4.19: Energy spectra using BIC_HP (Left: High energy spectra, Right: Low energy spectra)

cross section in lead, which has many resonances. Figure 4.20 shows the energy dependence of the cross section for GEANT4. As clear from the figure, peak in the spectrum matches the dips in the cross section. In Figure 4.20, there is a peak in the neutron spectrum around 475 KeV which corresponds to a minimum of the cross section. This highlights the sensitivity of low energy spectrum to the cross section library used.

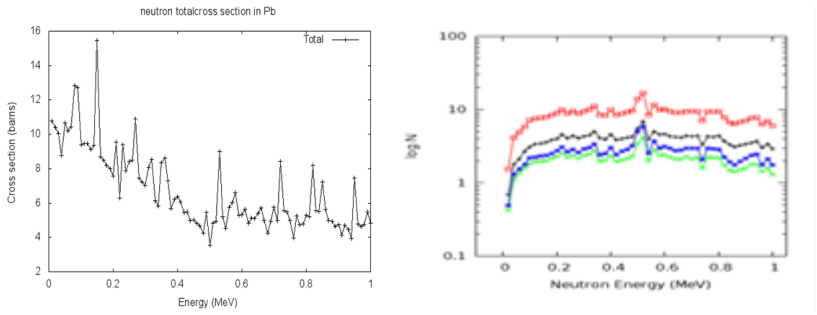

Figure 4.20: Correlation between cross section (left) and energy spectra (right) for GEANT4

4.6 Chapter summary

The spallation neutron distributions are investigated using GEANT4 and its comparison with MCNPX shows a good agreement for the overall numbers, spatial distribution, radial distribution, energy spectra and neutron cross section in lead.

Further, the analysis shows that the neutron spectra and properties produced by spallation are parameterisable by simple forms, with the exception of the low energy spectrum which is, nevertheless of the same shape, independent of proton energy. However, in subsequent work, to avoid biases from these parameterisations, neutrons were generated from protons and the parameterisations were not used.

5

Implementing the MYRRHA reactor in GEANT4

The reactor MYRRHA is modelled in GEANT4. This chapter includes the details of geometry construction, material composition and scoring. Cross sections for transuranic elements in GEANT4 are discussed and JEFF 3.1 library is installed to run the simulations for Z >92.

5.1 The geometry of MYRRHA

The MCNPX file is provided by MYRRHA team [15] for the geometry and material composition. MCNPX visualization of the full reactor is shown in Figure 5.1 [12, 50]. The cells shown in the above geometry are hexagonal cells with 10.45 cm as the distance between the opposite faces. In longitudinal dimensions, the rods are divided into three parts, with the height of central active part as 65 cm. It is helpful to divide the cells as:

1. Inner cells, also known as core which comprises of fuel cells (black), spallation target (deep blue) and In Pile Section (IPS) cells (turquoise). The inner cells include total 54 fuel assemblies and six IPS cells constituting the reactor core. Six fuel assemblies are there around the spallation target. The next ring contains 12 cells, half of which are fuel assemblies and half are IPS cells for material testing. Fuel assemblies in the next two annuli make total 54 fuel assemblies [50].

2. Outer cells - Outer cells contain lead bismuth eutectic (LBE) filled cells (brown), control rods (yellow-green), Molybdenum cells (light brown), Actinium cells (green),

Figure 5.1: MCNPX visualization of the full reactor. Reproduced from [12, 50]

Beryllium loaded reflectors (light blue) and stainless steel shielding (green). LBE filled cells and four control rods are there in the next annulus after the core. Similar LBE cells make the next annulus except six cells for radioisotope production; two for Molybdenum and four for Actinium. Reflectors and shieldings are included in the later annuli. Controls rods are not used but space is there to enable MYRRHA to be used in critical mode.

5.2 Implementation of MYRRHA geometry in GEANT4

The complex geometry is divided into smaller parts and then level by level these parts are combined together to shape up the whole geometry. To implement the complicated reactor geometry in GEANT4, initially, the bottom-up approach is followed in which fuel pin is considered as the smallest unit. Pins are constructed with their gaps and cladding. In the next step, fuel assemblies are created by arranging the pins in a hexagonal lattice. Different types of cells are created: In Pile Section (IPS) cells and spallation target as the central cell. These cells are then arranged in another lattice to build up the whole core. After the core, 5 outer rings are constructed including Lead bismuth eutectic (LBE) cells, Mo Ac cells, control rods, reflectors and steel shieldings. GEANT4, being a simulation toolkit has a variety of visualization drivers offering specific features to meet different demands of its users. In the present simulations, OpenGL

driver is used due to its fast visualization feature for demonstrating geometries, trajectories and hits [51]. The driver is developed by John Allison and Andrew Walkden [52].
OpenGL offers interactive features: zoom, rotate and translate. However, for the complicated dimensions (Radial dimensions in millimeters and vertical dimensions in centimeters) of the reactor, 'zoom' did not work and temporarily dimensions are enlarged with respect to radii for the purpose of better visualization (later on reverted to the original dimensions). This proved to be quite helpful in designing and debugging.

5.2.1 Geometry in GEANT4

As discussed in subsection 3.2.4, the geometry description is very important for every Monte Carlo simulation application. For the geometry description, the geometrical structures and properties of all the components need to be specified such as the shape, type, position and material of the components. Geometry and material composition [15] are implemented in detail in GEANT4.
GEANT4 geometry description starts with an initial world volume that contains all the other volumes. Each volume must be contained within its mother volume and there should be no overlap of volumes. The volume should be positioned in such a way that the coordinates of the volume's central point must be taken with respect to the central point of its mother's volume. For a volume with multiple sections (subvolumes) having different properties, each section must be contained within its mother volume and should be positioned such as the edges of the two sections are adjacent [38].
As highlighted in subsection 3.3, `Detector construction` is the first mandatory class to create the geometry of the model. It defines a detector volume in the following three stages:

1. Solid: Shape and dimensions of the volume are specified here. An example of GEANT4 code to create a cylindrical volume is given below:

```
G4double containerR = 4.75 *cm;
G4double HalfheightOfUpperFA = 153*cm;
G4double spanningAngleOfMother = 360.*deg;
G4Tubs* solidScorerUpperFA
= new G4Tubs("Upper_FA",
0.,
containerR,
```

```
HalfheightOfUpperFA,
0.,
spanningAngleOfMother);
```

2. Logical volume: A material is added through logical volume. Materials can be defined either at the beginning of the source file or in a separate file from where it can be called into the source file. In the following code snippet, material `LeadBismuth` is added to the solid `solidScorerUpperFA`:

```
G4LogicalVolume*  fLogicScorerUpperFA
= new G4LogicalVolume( solidScorerUpperFA, LeadBismuth, "Upper_FALog");
```

3. Physical volume: After the construction of geometrical shapes and setting their properties, the next important step is their placement. By defining the mother volume, central coordinates, rotation etc., the physical volume is responsible to place the logical volume into the geometry. Below is a sample piece of code to place a logical volume:

```
G4double ScorerPosUpper_x = 0.0*mm;
G4double ScorerPosUpper_y = 0.0*mm;
G4double ScorerPosUpper_z = 81*mm;
G4VPhysicalVolume* Scorer_physUpper
= new G4PVPlacement(0, // no rotation
G4ThreeVector(ScorerPosUpper_x,ScorerPosUpper_y,ScorerPosUpper_z),
fLogicScorerUpperFA,
"Upper_FA",
nn_FAmother_log,
false,
0,
checkOverlaps);
```

Placement of repeated volumes was a particular concern in the implementation of MYRRHA geometry because of repetition of volumes. The "Parameterisation" feature in GEANT4 helped with this repetitive positioning.

5.2.1.1 Parameterisation

The reactor contains several types of repeated volumes: 91 fuel pins in a fuel assembly, 54 fuel assemblies, 6 IPS cells, Mo-Ac cells, reflectors and shieldings. Detailed calculations are performed to place the components at their correct locations.

In order to place the repeated volumes in GEANT4, `G4VPVParameterisation` class is used and that parameterises a volume by copy number. The volumes to be parameterised must be either identical in size and shape or must not have further daughter volumes. `G4VPVParameterisation` is an example of Object oriented programming (OOP) approach in Geant4. It offers the concept of data abstraction which reduces the programming complexity. G4VPVParameterisation also reduces memory consumption. However, the limitation with its use is reduced simulation speed. Alternatively, several 'for loops' can be used for the placement of repeated volumes in Detector Construction class.

Four parameterisation classes are used for the following types of repeated volumes as mentioned above:

1. FuelPinParameterisation - For the placement of fuel pins in a fuel rod.
2. FuelAssemblyParameterisation - For the placement of fuel assemblies.
3. IPSParameterisation - For the placement of IPS assemblies.
4. OtherParameterisation - For the placement of outer cells: LBE cells, Mo-Ac cells, control rods, reflectors and shielding assemblies.

The hexagonal structure makes the layout complicated and for partial illustration, a calculation is performed. The pitch (p, taken from [23]) is considered for the calculation of the diameter of the reactor. Pitch is the distance between the centers of the neighboring assemblies. Then the whole reactor is considered to have several annuli and the cells are divided horizontally. Referring Figure 5.1, the target is at the central cell, and the horizontal row including the target is central row. The above row is first row above central and similarly the row below is the first row below central cell. For position vector calculation, the reactor is envisaged to be divided into 4 quadrants. For each quadrant, depending on the annulus, position vector (x,y,z) is calculated.
Parameterisation is the 3rd of the steps mentioned in section 5.2.1. A sample code snippet in GEANT4 for the placement of cells in the first row, above and below the central cell is as follows:

```
# 1st row above central cell:
if(copyNo > 7 && copyNo <= 11)
{
  x = 0.5*p + (copyNo-8)*p;
  y = y1;
G4ThreeVector origin(x,y,0);
physVol -> SetTranslation(origin);
}
else if (copyNo > 11 && copyNo <= 15)
{
x = -(0.5*p + (copyNo-12)*p);
y = y1;
G4ThreeVector origin(x,y,0);
physVol -> SetTranslation(origin);
}
# 1st row below central cell:
if(copyNo > 15 && copyNo <= 19)\\
{
  x = -(0.5*p + (copyNo-16)*p);
  y = -y1;
G4ThreeVector origin(x,y,0);
physVol -> SetTranslation(origin);
}
else if (copyNo > 19 && copyNo <= 23)
{
x = (0.5*p + (copyNo-20)*p);
y = -y1;
G4ThreeVector origin(x,y,0);
physVol -> SetTranslation(origin);
}
# End of sample code
```

In the above code, copyNo = 0 to (N-1), where N is the number of cells to be placed. For example, N = 54 for fuel assemblies and N = 6 for IPS cells.

5.2.2 Fuel pin

Fuel pin is basically a rod with cylindrical cladding loaded with cylindrical fuel pellets. It consists of three regions with 65 cm as length of the central active region (red). Fuel is loaded as fuel pellets in the central active region. Fuel pellets are not simulated, the fuel is taken as being continuous in the rod. The fuel composition is described in the next chapter (section 6.1). The upper and lower regions include insulator segments and gas plenum chamber. Figure 5.2 shows the prototype of the fuel pin [53] and Figure 5.3 shows the implementation of fuel pin in GEANT4 with the specifications provided by [15]. The prototype is slightly different than the actual specifications used. A single mother volume holds different sections of the fuel pin. The dimensions for the placement of each section is calculated with respect to the mother volume such as they are placed adjacent to make one whole fuel pin volume as shown in the enlarged picture (Figure 5.4).

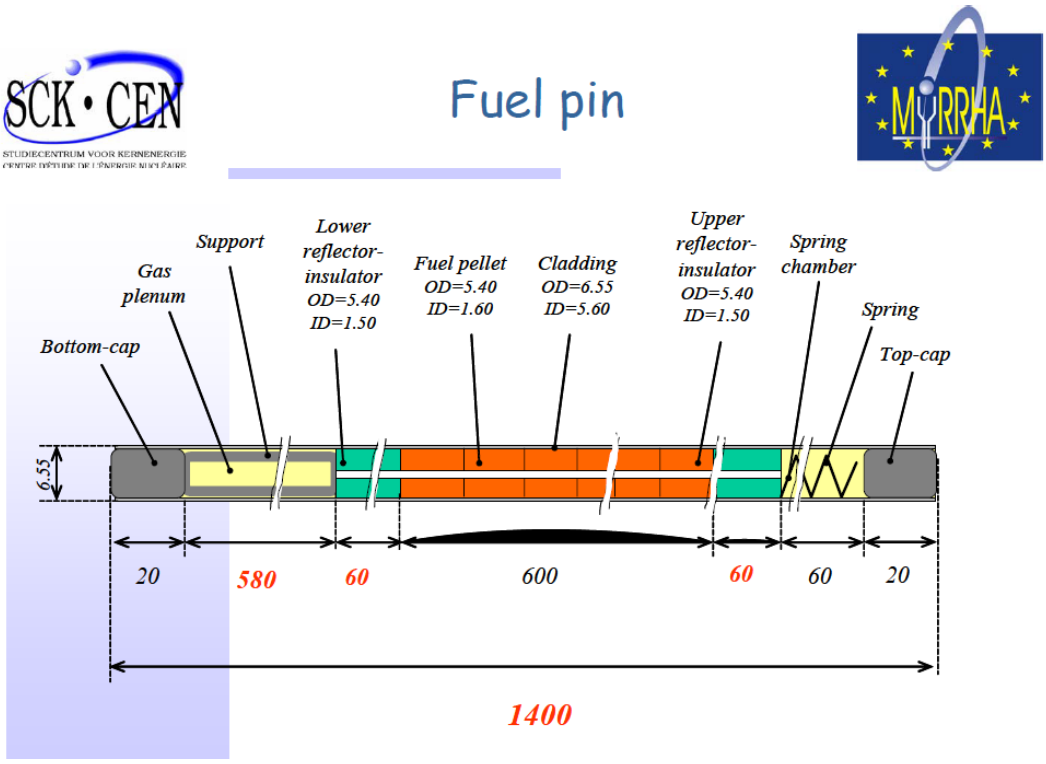

Figure 5.2: Fuel pin prototype. Reproduced from [53]

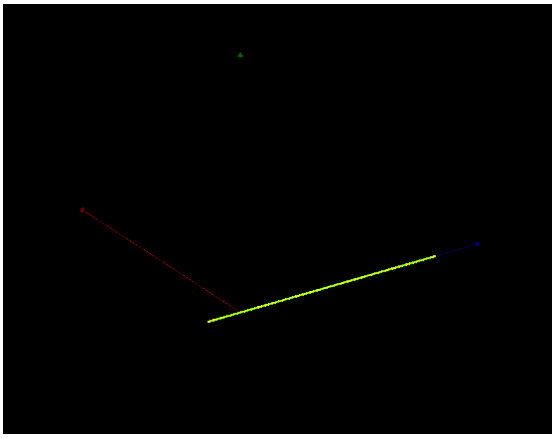

Figure 5.3: GEANT4 visualization of fuel pin: Original dimensions

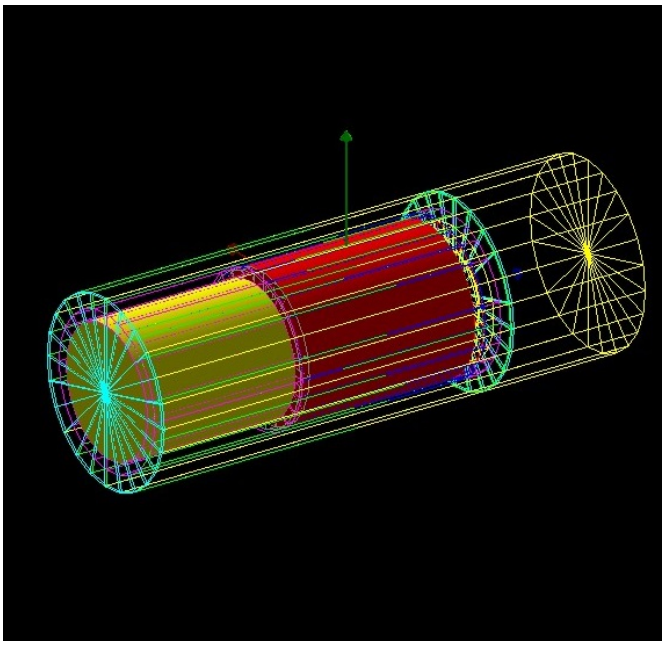

Figure 5.4: GEANT4 visualization of fuel pin: Enlarged dimensions

5.2.3 Fuel assembly

Fuel assembly is the collection of 91 fuel pins that are arranged in a hexagonal bundle. `FuelPinParameterisation` class is used to place 91 fuel pins in a fuel assembly. The prototype of the fuel assembly is shown in Figure 5.5 [53]. Figure 5.6 shows the steps in the creation of the fuel assembly from the fuel pin. In the enlarged picture (Complete

FA), the blue and red cylindrical shape shows the upper and lower part of the fuel assembly respectively and the central region is the active part of the fuel assembly.

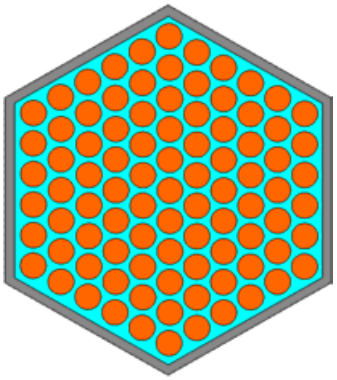

Figure 5.5: Fuel assembly prototype. Reproduced from [53]

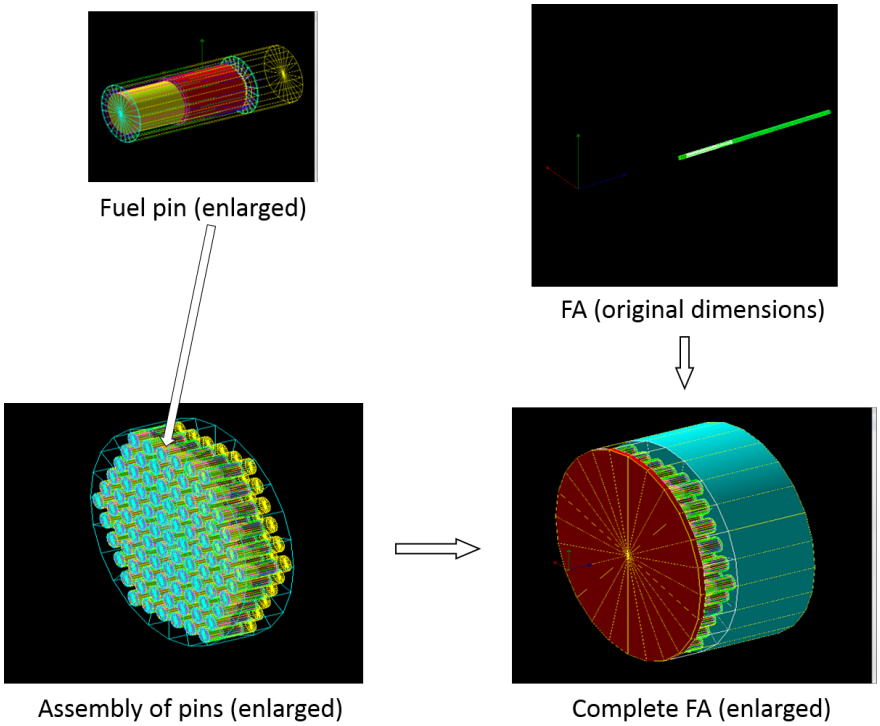

Figure 5.6: GEANT4 visualization of fuel assembly (FA)

5.2.4 IPS cells

Six IPS cells are created and placed in the reactor core as shown in the Figure 5.7 using `IPSParameterisation` class. Initially, in the development of the program, the reactor core was created with all the fuel assemblies, then the designated locations are made empty as shown in the Figure 5.8 and IPS cells are placed at these locations.

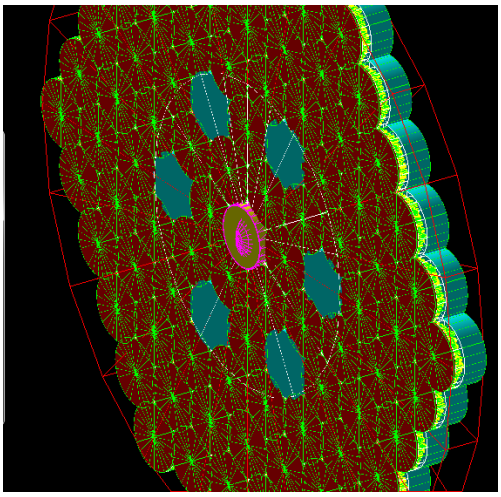

Figure 5.7: IPS assemblies: IPS placed in the core

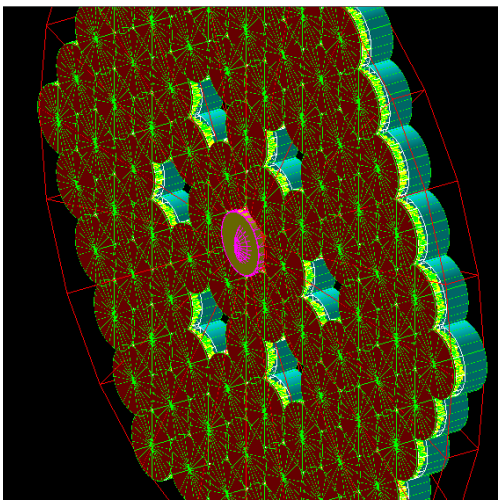

Figure 5.8: IPS assemblies: Emptied locations for IPS

5.2.5 Central cell - Spallation target

Spallation target is one of the key component of the ADSR. The beam tube ends on a hemispheric window as shown in the enlarged picture (Figure 5.9). The target is constructed using `G4Tub` shape for the beam tube and `G4Sphere` for the hemispherical end with appropriate coordinates for the adjacent placement of these two sections of the target. Spallation target cell is then placed with the hemispheric end located at the center of the core. Spallation target with the original dimension is shown in Figure 5.10.

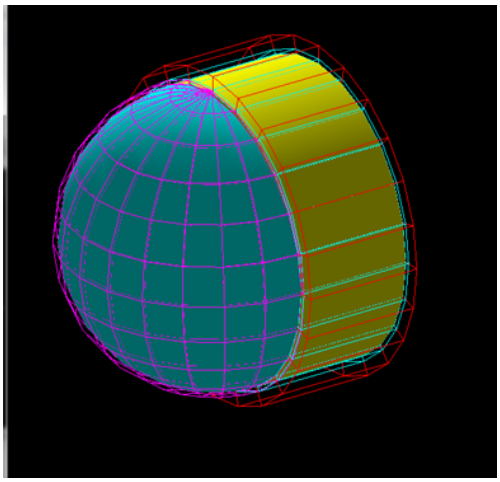

Figure 5.9: GEANT4 visualization of spallation target: Enlarged dimensions

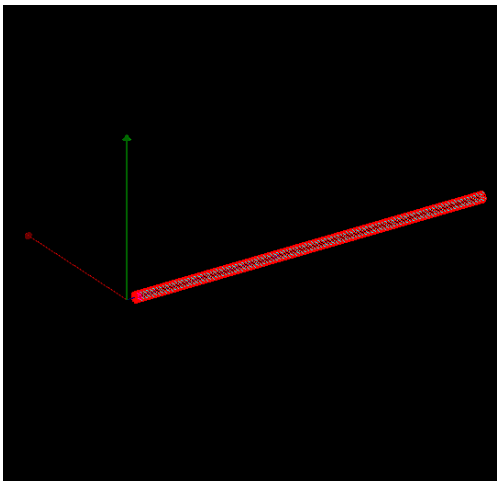

Figure 5.10: GEANT4 visualization of spallation target: Original dimensions

5.2.6 Inner cells - Reactor core

The inner cells include a total of 54 fuel assemblies and six IPS cells constituting the reactor core. Six fuel assemblies are there around the spallation target. The next ring contains 12 cells, half of which are fuel assemblies and half are IPS cells for material testing. Fuel assemblies in the next two annuli make total 54 fuel assemblies [50].
`FuelAssemblyParameterisation` and `IPSParameterisation` classes are used for the

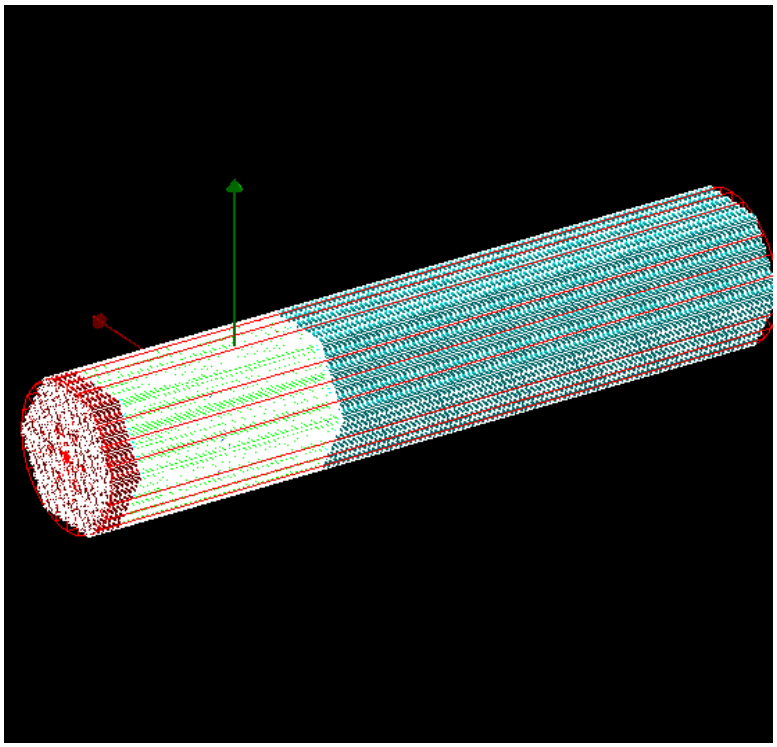

Figure 5.11: GEANT4 visualization of reactor core: Original dimensions

placement of fuel assemblies and IPS cells in the reactor core. Figure 5.11 shows the visualization of reactor core with fuel assemblies and IPS cells. IPS cells are shown by blue colour in the enlarged picture (Figure 5.12).

5.2.7 Outer cells

Outer cells are all similar, filled with different materials for LBE cells, Mo-Ac cells, reflectors and shieldings. `OuterParameterisation` class is used for the placement of these cells in the reactor.

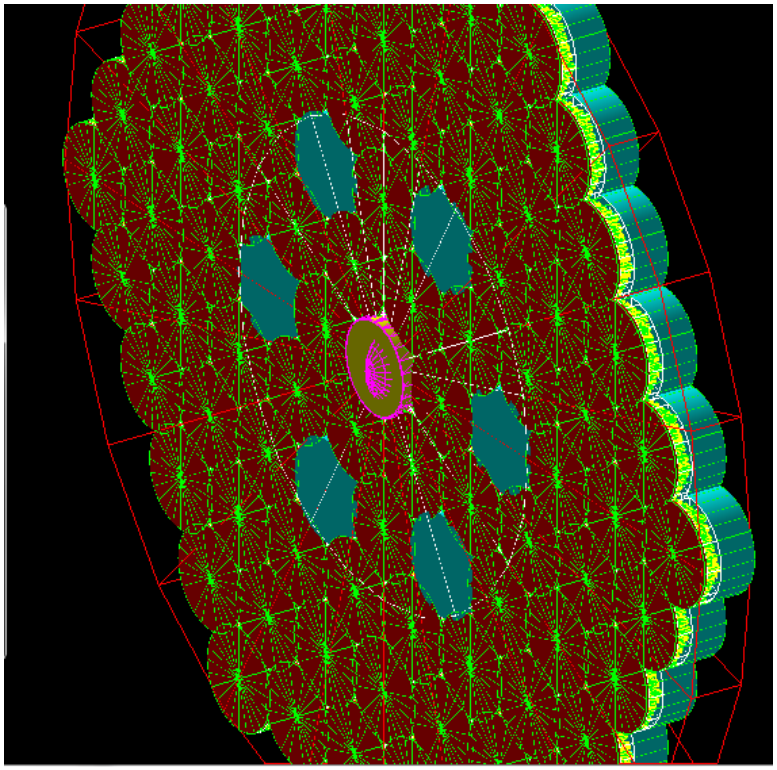

Figure 5.12: Geant4 visualization of reactor core: Enlarged dimensions

5.2.8 Reactor modelled in GEANT4

The complete picture of the reactor as modelled in GEANT4 with all the cells placed, is presented in Figure 5.13. Figure 5.14 shows the enlarged picture of the reactor. As we can see from the enlarged picture, the spallation target (Magenta) is shown at the centre of the reactor. The fuel assemblies shown in brown-green colour along with six IPS cells (brown) make the core. After the core, there are four control rods shown in yellow colour. Molybdenum cells are black and Actinium cells are magenta coloured. Mostly LBE filled cells (red) are there in the outer configuration. Reflectors are shown in deep blue colour and the outermost configuration involves shielding (green). Figure 5.14 is functionally identical with Figure 5.1, proving that MCNPX geometry has been successfully and correctly incorporated in GEANT4.

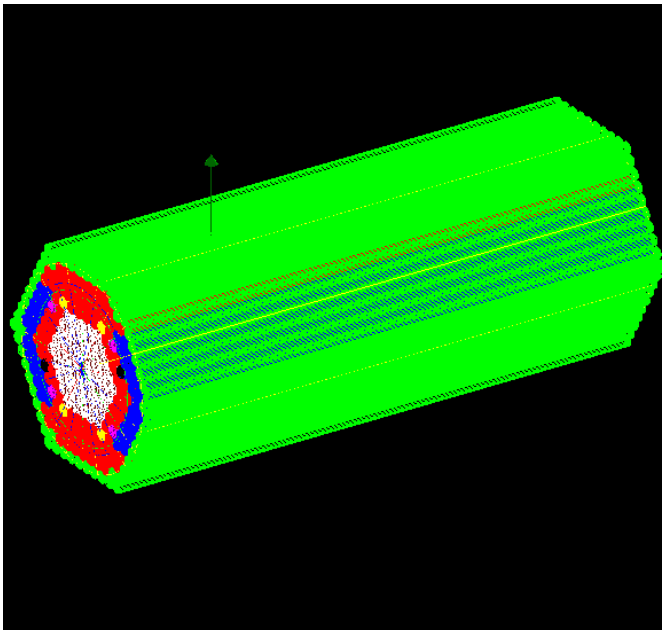

Figure 5.13: GEANT4 visualization of the reactor: Original dimensions

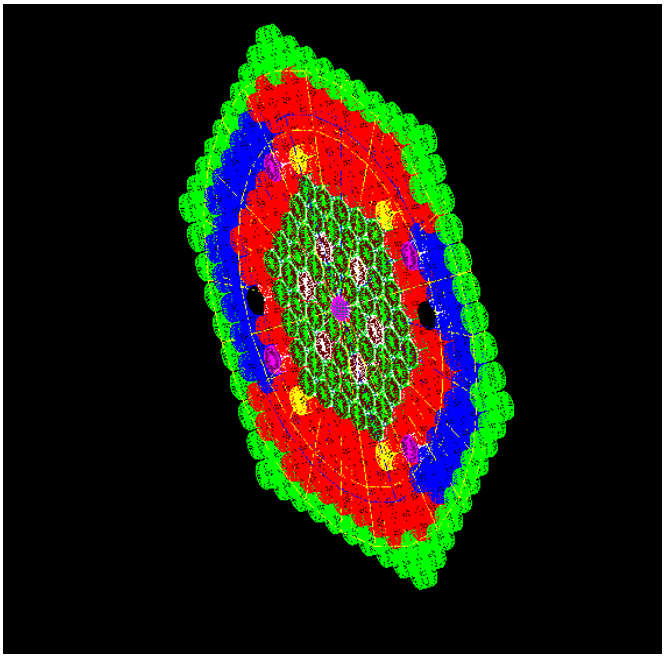

Figure 5.14: GEANT4 visualization of the reactor: Enlarged dimensions

5.3 Scoring

To extract the required information from the simulation, "Sensitive Detector" functionality of GEANT4 is used. `G4VSensitiveDetector` is assigned to the logical volume for which information needs to be recorded. Once Sensitive Detector is assigned to a volume, it becomes Sensitive [54].

For scoring the flux, `G4PSPassageCellFlux` and `G4PSCellFlux` sensitive detectors are available. Both are similar and the only difference is that `G4PSPassageCellFlux` ignores the generated or stopped tracks in the volume whereas `G4PSCellFlux` scores all flux. In order to consider the neutrons from spallation only, `G4PSPassageCellFlux` is chosen. This will slightly underestimate the flux in case a track is stopped inside the volume. `G4PSPassageCellFlux` is the sensitive detector used to score the particle flux at different locations of the reactor. Multiple filters of type `G4SDParticleWithEnergyFilter` were attached to the sensitive detectors, defining neutrons as particles with a particular energy range to be filtered [55].

Hit that corresponds to a snapshot of the physical interaction of a track is collected from a step. A hit may store position, energy deposit etc. At the end of each run, `HitsCollectionOfThisEvent` is accessed in the `Run` class. `G4SDManager`, that manages the operation of sensitive detectors, returns a hit collection id (`GetCollectionId`). `G4HitsMap` corresponding to a particular hit collection id is accessed. The relevant information (neutron flux and neutron energy) is then retrieved from the hits map and is written to an output file which is used for plotting. The resulting plots are shown in chapter 6.

5.4 Materials

Materials can be either elements or compounds. For defining the compounds, the elements are first described and then added to the material. Rather than taking materials from a built-in GEANT4 library, materials defined in MYRRHA specification [15] are taken to make a meaningful comparison with MCNPX predictions of MYRRHA. An example of LBE material defined in GEANT4 is given below:

```
// --------------------------------------------------------------------
// Elements
// --------------------------------------------------------------------
G4Element* element3006 = new G4Element("3006", "Li", 1);
```

```
element3006->AddIsotope(new G4Isotope("3006", 3, 6), 1);

G4Element* element3007 = new G4Element("3007", "Li", 1);
element3007->AddIsotope(new G4Isotope("3007",  3, 7), 1);

G4Element* element5010 = new G4Element("5010", "B", 1);
element5010->AddIsotope(new G4Isotope("5010", 5, 10), 1);

G4Element* element5011 = new G4Element("5011", "B", 1);
element5011->AddIsotope(new G4Isotope("5011", 5, 11), 1);

G4Element* element47107 = new G4Element("47107", "Ag", 1);
element47107->AddIsotope(new G4Isotope("47107", 47, 107), 1);
G4Element* element47109 = new G4Element("47109", "Ag", 1);
element47109->AddIsotope(new G4Isotope("47109", 47, 109), 1);

G4Element* element82204 = new G4Element("82204", "Pb", 1);
element82204->AddIsotope(new G4Isotope("82204", 82, 204), 1);
G4Element* element82206 = new G4Element("82206", "Pb", 1);
element82206->AddIsotope(new G4Isotope("82206", 82, 206), 1);
G4Element* element82207 = new G4Element("82207", "Pb", 1);
element82207->AddIsotope(new G4Isotope("82207", 82, 207), 1);
G4Element* element82208 = new G4Element("82208", "Pb", 1);
element82208->AddIsotope(new G4Isotope("82208", 82, 208), 1);

G4Element* element83209 = new G4Element("83209", "Bi", 1);
element83209->AddIsotope(new G4Isotope("83209", 83, 209), 1);
// ------------------------------------------------------------------------
// leadBismuth (Material)
// ------------------------------------------------------------------------
G4Material* leadBismuth = new G4Material("leadBismuth",10500*kg/m3,11);
//Placeholder density

leadBismuth->AddElement(G4Element::GetElement("3006"), 2.28*pow(10,-8));
leadBismuth->AddElement(G4Element::GetElement("3007"), 2.77*pow(10,-7));
```

```
leadBismuth->AddElement(G4Element::GetElement("5010"), 5.97*pow(10,-7));
leadBismuth->AddElement(G4Element::GetElement("5011"), 2.40*pow(10,-6));

leadBismuth->AddElement(G4Element::GetElement("47107"), 1.07*pow(10,-5));
leadBismuth->AddElement(G4Element::GetElement("47109"), 9.92*pow(10,-6));

leadBismuth->AddElement(G4Element::GetElement("82204"), 6.23*pow(10,-3));
leadBismuth->AddElement(G4Element::GetElement("82206"), 1.07*pow(10,-1));
leadBismuth->AddElement(G4Element::GetElement("82207"), 9.83*pow(10,-2));
leadBismuth->AddElement(G4Element::GetElement("82208"), 2.33*pow(10,-1));

leadBismuth->AddElement(G4Element::GetElement("83209"), 5.55*pow(10,-1));
```

Materials defined in MCNPX are converted into GEANT4 format by writing an R script. A sample R script for importing the data for LBE material is:

```
df=read.table("m3.dat")
col1<- df$V1
col2<-df$V2
T1<- 'leadBismuth->AddElement(G4Element::GetElement('
T2<-')'
B<-data.frame(T1,col1,T2,col2,T2,';')
write.table(B,"m3G4.dat",row.names=F)
```

In the above script, "m3.dat" is a file for LBE material in MCNPX and "m3G4.dat" is the corresponding material file in GEANT4.

In the LBE material described above, there is 44.4% lead, 55.5% bismuth and only trace amount of lithium, boron and silver. Lead involved in LBE is slightly different to G4_Pb. The GEANT4 material database does not provides lead bismuth material.

Similarly, reflectors are made up of material Yttrium Zirconium Oxide (YZrO) which consists of isotopes: oxygen (26%), yittrium (4%) and zirconium (70%). Ferritic martensitic steel (FMS) is used for shielding, consisting of isotopes: carbon, nitrogen, aluminum, silicon, phosphorus, sulphur, vanadium, chromium, manganese, iron, nickel, copper, niobium and molybdenum with a high percentage of iron and copper and smaller percentage of other isotopes. In GEANT4, G4_STAINLESS _STEEL material is available that is composed of chromium, iron and nickel [56].

5.5 Cross sections

GEANT4 was developed initially for detectors in particle physics and people do not make detectors out of transuranic elements. The use of GEANT4 has been extended to a wide variety of applications but still it could not be envisaged to be used for Z>92. In the present study, simulations for the reactor are performed and transuranic elements are studied. Although the performance of the G4NDL library has been improved over time, still there are some limitations. It does not provide data for isotopes having atomic number Z>92 on web. This apparently limits the investigations particularly on transuranic (TRU) elements for complex simulations. To address this problem a software tool was developed [37] that provides flexibility and control of the nuclear data used in GEANT4 simulations. It transforms any evaluated cross section library (ENDF/B, JEFF, JENDL, CENDL, BROND...) in the ENDF-6 format into G4NDL format. Hence it provides access to the complete list of standard evaluated data libraries to the GEANT4 users.
Based on the tool described above for importing the data library for Z>92, JEFF 3.1 library (chosen arbitrarily out of the evaluated cross section libraries, mentioned above) is installed by following the procedure mentioned in [57]. The following environmental variables are set:
a) G4NEUTRONHP_SKIP_MISSING_ISOTOPES=1
b) G4NEUTRONHP_DO_NOT_ADJUST_FINAL_STATE=1
c) AllowForHeavyElements=1
However, some unhandled exception rose while running the simulations for Z>92 for large numbers of beam particles (protons). The following messages are prompted before the program crashes:

- "Called G4PiNuclearCrossSection outside parametrization"
- ***G4ElectroNuclearCrossSection::GetFunctions: A="<<244.064<<"(?). No CS returned!"

These messages are generated from the code related to pion cross section and since pions decay into muons, hence also related to muon cross section. The threshold energy for pions is 289 MeV, so at 600 MeV beam energy, pions and consequently muons are generated. Presumably, other people might have run the simulation for Z>92, they might have run for beam energy <289 MeV.
There was also a warning produced - "### G4SeltzerBergerModel Warning: Majoranta exceeded! ", but it does not cause the program to crash. After carefully checking

for the related functions in the source file of GEANT4, it is found that the following files need to be altered as exceptions are thrown from these files for Z>92 which causes the program crash:

- G4KokoulinMuonNuclearXS.cc
- G4KokoulinMuonNuclearXS.hh
- G4PiNuclearCrossSection.cc

There are some code snippets in the above files that assume Z<92. As per the suggestion from Alberto Ribon [58] for this version of GEANT (Version 4.10.1), Z>92 elements are treated as Uranium (Z=92). Changes are made in these files to make Z = 92 in such cases. This solved the problem of program crash. For 600 MeV protons, few pions/muons are produced, and the fraction of transuranics is small. The program could run for hundreds of events before a crash. Each event involves many particle collisions. MCNPX studies show that with 10000 protons fired, 9830554 neutrons and 438 charged pions are produced. The number of pions is tiny compared to the number of neutrons (only 0.04 pions per event, compared to 983 neutrons). Hence, the change (Z>92 treated as Z=92) will only have a small effect on the accuracy of the simulation which arises only in a small fraction of interactions and the overall effect on the results will be negligible.

5.6 Running the program

Simulations were performed on Windows 8, 64 bit operating system. It took around 10 hours to run the program with 10^5 protons. To reduce the time taken for the simulation, if the number of protons were decreased, it resulted in statistical fluctuations. So there is a trade off between statistical fluctuation and running time. As a solution to this, the program was run on three systems in parallel, using 10^5 protons.
Program can be made faster by using simpler geometry, different physics list or in-built material composition provided by GEANT4. However, it may result in compromised accuracy. 10 hours is a reasonable time to run a program, hence it is decided not to compromise the accuracy by looking for short running time.

6

Neutron Flux And Energy Spectrum

The energy distribution of the neutron flux is one of the most important properties for reactor core investigations [59]. In this chapter, the neutron flux spectrum obtained through GEANT4 simulations is presented for the reactor MYRRHA. Some particular relevant locations of the reactor are chosen, such as fuel cells, IPS cells and isotope production cells (Mo and Ac cells), to record the neutron flux. To ensure the reliability of the results, the outcomes of GEANT4 simulations are compared with those of MCNPX.

6.1 Fuel Mix

To know whether the standard uranium mix can be replaced by thorium based fuel mix, the following three fuel mixtures are taken into consideration:

1. U/Pu mixture (Mix 1): Standard MYRRHA MOX fuel. It consists of ^{234}U, ^{235}U and ^{238}U (natural isotopes), Pu isotopes (^{238}Pu, ^{239}Pu, ^{240}Pu, ^{241}Pu and ^{242}Pu) and ^{241}Am. Oxygen is also included, as the fuel is used in this form rather than the pure metal.

2. Th/Pu mixture (Mix 2): All the uranium in Mix1 is replaced by ^{232}Th.

3. Th/U mixture (Mix 3): All the Pu and Am in Mix2 is replaced by ^{233}U.

For all the above three fuel mix, the isotope concentrations are adjusted to maintain k_{eff} close to 0.95 as provided by MYRRHA team [15]. The composition of these three

fuel mix are shown in Table 6.1.

Geant 4.10.1 with physics list QGSP_BIC_HP is used for the simulations. After solving

Fuel mix	Element	Percentage
Mix 1	^{16}O	11.6718
	^{234}U	0.0033
	^{235}U	0.4395
	^{238}U	61.3717
	^{238}Pu	0.6083
	^{239}Pu	14.8343
	^{240}Pu	7.0417
	^{241}Pu	1.5924
	^{242}Pu	2.0066
	^{241}Am	0.4304
Mix 2	^{16}O	11.6718
	^{232}Th	52
	^{238}Pu	0.6083
	^{239}Pu	14.8343
	^{240}Pu	7.0417
	^{241}Pu	1.5924
	^{242}Pu	2.0066
	^{241}Am	0.4304
Mix 3	^{16}O	11.6718
	^{232}Th	59.82
	^{233}U	16.0

Table 6.1: Element's composition for different fuel mix

the program crash issue as discussed in subsection 5.5, 10^5 beam protons were used for the simulations. These protons are sufficient to provide statistically reliable results that can be compared with the results predicted by earlier studies [12, 31, 50].

6.2 Neutron flux and spectra at various locations of the reactor

The neutron fluxes and spectra averaged over the fuel assemblies, IPS and isotope production cells are examined for 1 mA proton current. At different currents, the fluxes just scale and the spectra are unchanged. These fluxes will be appropriate to carry out the fuel evolution studies at the fuel cells and incineration studies at IPS and Mo/Ac cells.

6.2.1 Neutron flux

The average flux for different fuel mixes at various location of the reactor is quantified and values are presented in Table 6.2. Statistical errors are of order 5%. To calculate this, same job was run twice and the percentage difference between the two flux values were calculated. Neutrons of energy range 10^{-8} MeV to 100 MeV are considered. The Table shows that GEANT4 and MCNPX results are in fair agreement for the flux values at designated locations of the reactor. Comparable flux values can be noted for fuel cells and IPS cells while the flux values are relatively lower at Mo and Ac cells. Different fuel mix yield very similar flux values. The differences between fuel mixtures are largely due to the value of k_{eff} not matching exactly.

Location	Mix1		Mix2		Mix3	
	G4	MX	G4	MX	G4	MX
Fuel	6.28E+14	7.08E+14	6.37E+14	5.8E+14	8.62E+14	8.41E+14
IPS	5.19E+14	8.48E+14	8.76E+14	6.98E+14	8.34E+14	9.95E+14
Mo cell	2.8E+14	4.8E+14	5.07E+14	3.91E+14	6.94E+14	6.04E+14
Ac cell	1.17E+14	1.09E+14	9.31E+13	8.98E+13	1.98E+14	1.37E+14

Table 6.2: Average flux values (Neutrons/cm^2/MeV/s) for a 1 mA proton beam

6.2.2 Neutron energy spectra

Energy distribution of the neutron flux can be divided into the following three regions [59]:

1. Thermal region: It is the region with Neutrons energy in the range of 5×10^{-11} MeV to 5×10^{-7} MeV.
2. Epithermal region: Neutron energy in this region is 5×10^{-7} MeV to 0.5 MeV.
3. Fast region: The neutron energy is 0.5 MeV to 20 MeV.

As proposed by F. Molina, the neutrons in these three regions are described by the following distributions:
Thermal neutron distribution - described by Maxwell-Boltzmann distribution [60]. The equation can be written as:

$$\phi_{\text{th}}(E) = aE \exp(-bE) \tag{6.1}$$

where ϕ_{th} is the thermal neutron flux and E is the neutron energy.

Epithermal neutron distribution - described by power distribution. The equation can be written as:

$$\phi_{\text{epi}}(E) = a/E^{\text{b}} \tag{6.2}$$

where ϕ_{epi} is the epithermal neutron flux.

Fast neutron distribution - described by Watt distribution. The equation can be written as:

$$\phi_{\text{fst}}(E) = a\exp(-bE)\sinh((cE)^{0.5}) \tag{6.3}$$

where ϕ_{fst} is the fast neutron flux.

6.2.2.1 Fuel cell

Neutron flux for the three fuel mix as obtained by GEANT4 and MCNPX is presented in Figure 6.1 and Figure 6.2 respectively. For convenience spectra are plotted per unit energy (Figure 6.1) and per unit lethargy (Figure 6.2), both are the standard ways of plotting. Lethargy can be defined as the natural logarithm of the ratio of maximum energy that a neutron might have in a reactor to the neutron energy. Although these two curves look different, they are the same.
The fuel cell spectra show a hard component all the way up to the proton energy - though energies go all the way down to thermal energy. The spectra and the overall numbers agree well for GEANT4 and MCNPX. This is true for all the three fuel mixtures. Nevertheless they differ in detail. As discussed in the subsection 4.5, the fluctuations in the spectrum do not stem from low simulation statistics rather due to the energy dependence of the cross section. For comparison, fuel cell spectra obtained by M.Sarotto et al. is shown in Figure 6.3 [31]. The spectra are plotted for MYRRHA - FASTEF (FAst Spectrum Transmutation Experimental Facility) in sub-critical mode. The spectra in the fissile zone and in the spallation target are shown in red and black colour respectively in Figure 6.3. A good agreement is observed between the fuel cell spectra produced by GEANT4, MCNPX and the spectra reported in literature (Figure 6.3) with different design versions. They agree both in the shape and the overall size.

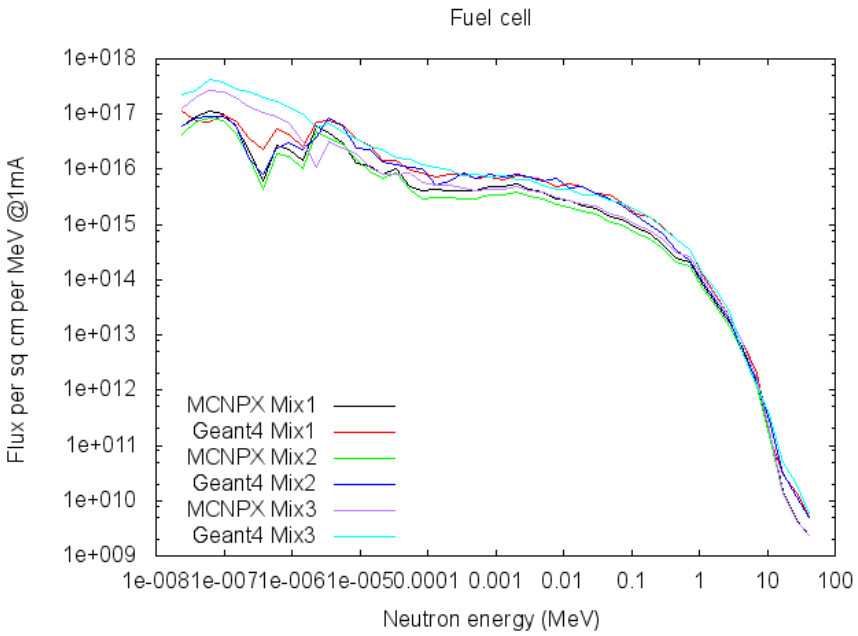

Figure 6.1: Neutron flux averaged over the fuel cells per unit energy

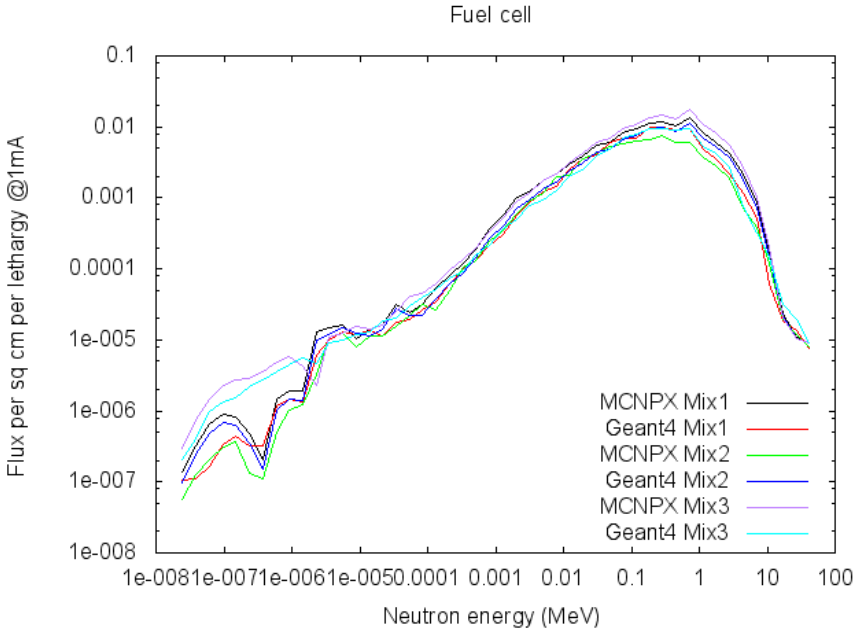

Figure 6.2: Neutron flux averaged over the fuel cells per unit lethargy

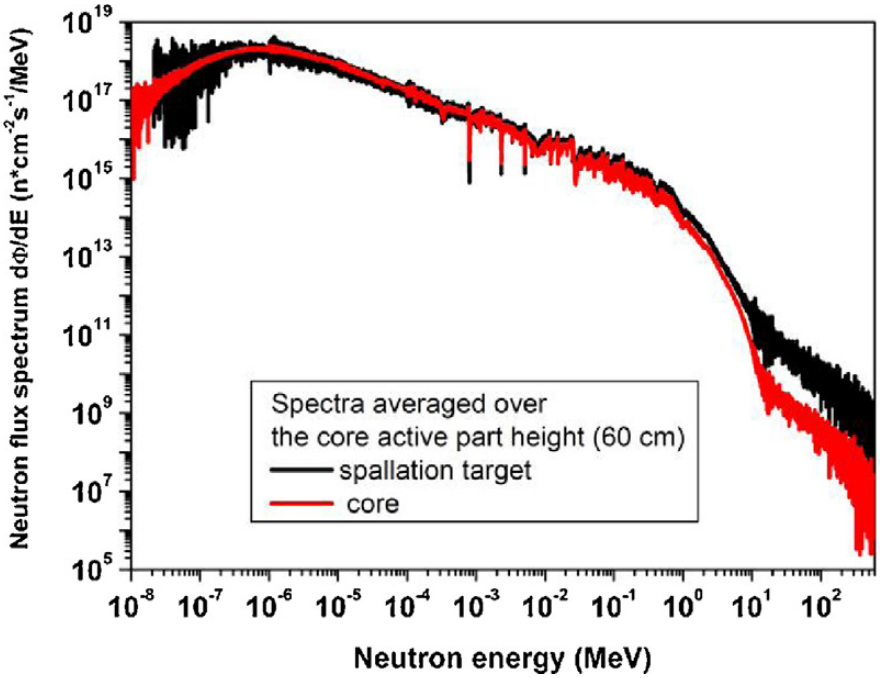

Figure 6.3: Neutron flux spectra as reported in [31]

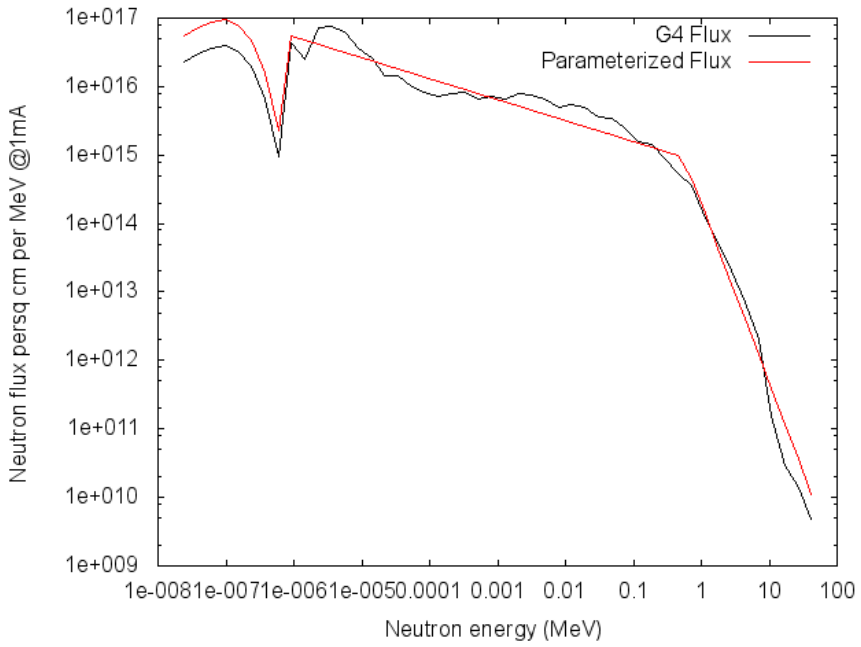

Figure 6.4: Parameterisation of neutron flux

Figure 6.4 shows the parametrization of the fuel cell spectra. To fit the estimated data with the GEANT4 values, Excel solver add-in is used to minimize the sum of the squares of the normalized error. As discussed in subsection 6.2.2, different distributions are considered to parameterize different regions of neutron spectra. While thermal and epithermal neutrons are well described according to equation 6.1 and equation 6.2 respectively, fast neutrons when parameterized according to equation 6.3 gave the red curve in Figure 6.5, which is not a good fit for high energy neutrons. This is because the Watt spectrum is for fast neutrons from fissions and does not include anything that would describe spallation neutrons. Nevertheless, fast neutrons when fitted with a power distribution, gave good fit as shown by green curve in Figure 6.5.

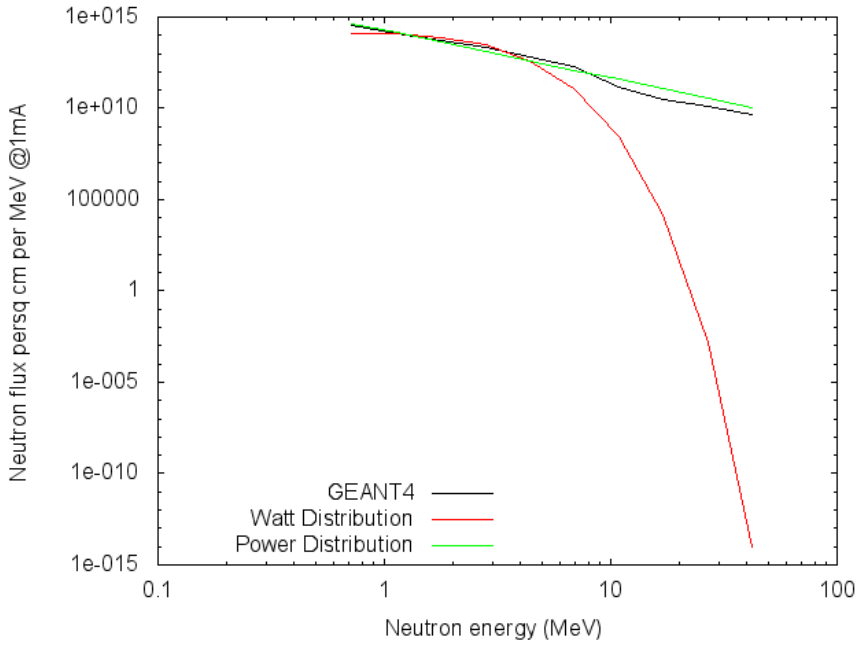

Figure 6.5: Parameterization of fast neutron flux

The describing equation for fast neutrons is found to be:

$$\phi_{\text{fst}}(E) = aE^{-\text{b}} \tag{6.4}$$

6.2.2.2 Neutron energy spectra in other reactors

In addition to the validation with MCNPX predictions, the neutron spectra by GEANT4 for MYRRHA reactor are also compared with those of the Chilean experimental nuclear

reactor RECH-1 [59] and the Gamma-3 assembly located at JINR, Dubna, Russia [61].

RECH-1 is a 5 MW reactor operated by the Chilean Nuclear Energy Commission at La Reina Nuclear Center, Chile [59]. Direct flux measurement of neutron flux spectra are challenging due to several reasons. Some of them are the broad neutron energy range, difficulties in placing the neutron detector near the core and neutron inelastic cross section resonances. So, different methods are adopted by F. Molina et al. for neutron flux and the results from different algorithms (EM - Expectation Maximization unfolding algorithm, GRAVEL) as well as MCNPX are presented as shown in Figure 6.6. Comparing these plots with Geant4 predictions for MYRRHA (Figure 6.1), if we look at the thermal region, more neutrons are available in the Chilean reactor which is because of it being a thermal reactor, whereas MYRRHA is a fast reactor. However, the spectra are broadly similar above 1 eV. For comparison, scaling is needed to convert neutron energy from 'eV' to 'MeV' in Figure 6.6.

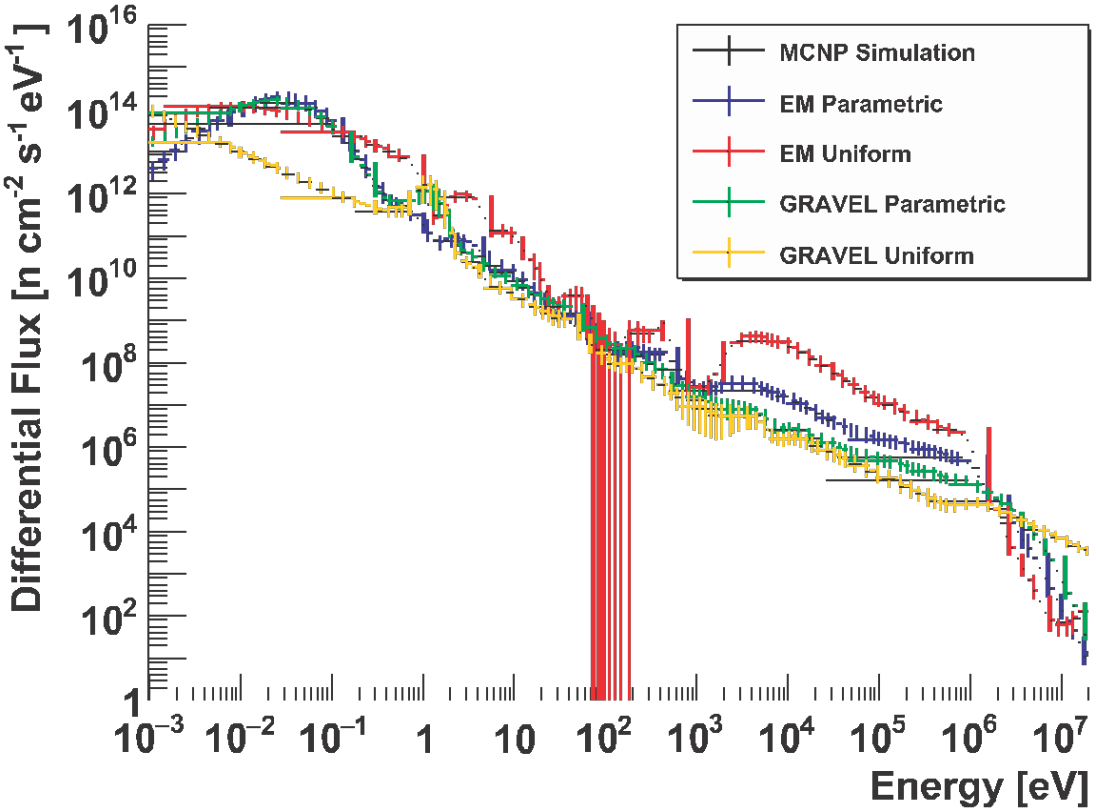

Figure 6.6: Differential neutron flux using different methods. Reproduced from [59]

An experiment was conducted at the Gamma-3 assembly to measure the track

densities [61]. The assembly was irradiated with 1.6 GeV deuteron beam. MCNPX code was used to simulate the irradiation of the assembly and the neutron spectra at two chosen locations A and B are shown in Figure 6.7. To compare this figure with Figure 6.1 for MYRRHA flux by Geant4, Figure 6.7 needs to be normalized by a factor of 10^{15} to give the flux in cm^2 per MeV per deuteron per second.

From the comparison of the GEANT4 spectra for MYRRHA reactor with those of the

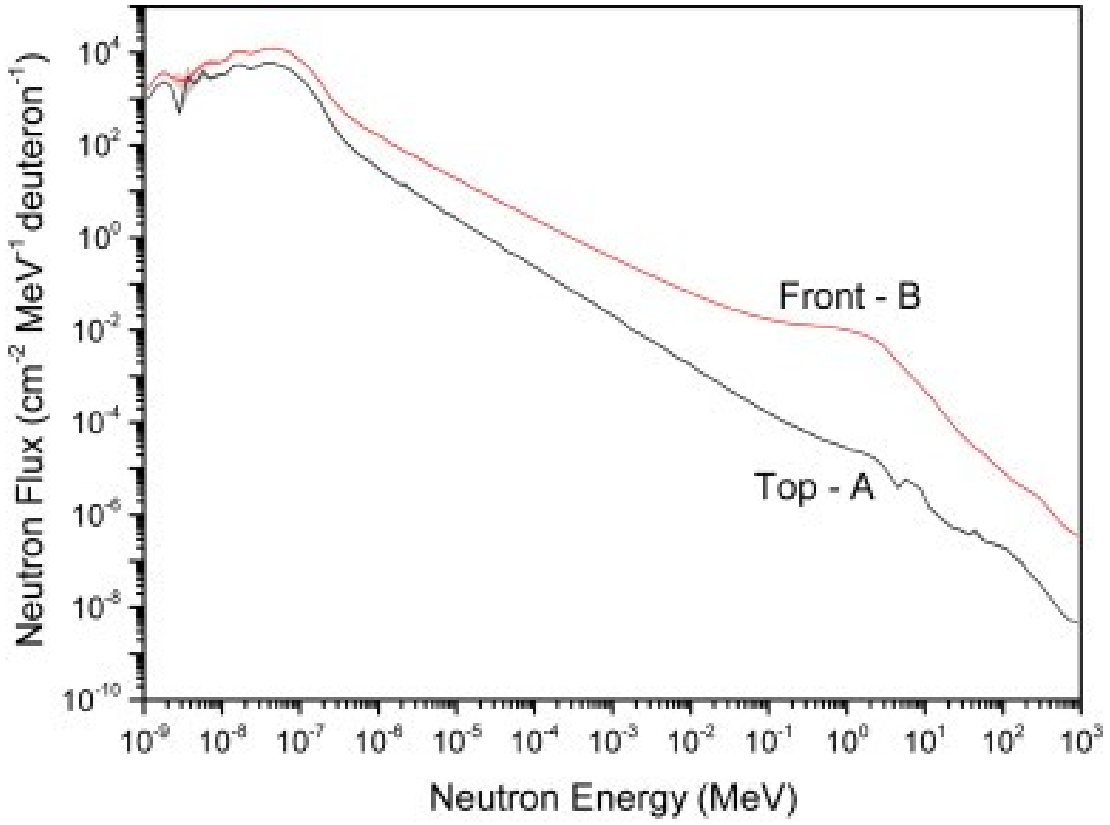

Figure 6.7: Neutron spectra in Gamma-3 assembly. Reproduced from [61]

above mentioned reactors, we observe that the shape is much similar, though they differ in size which is logical because of the different designs and operating parameters. An interesting similarity is the noticeable dip in the thermal region which can be ascribed to the dependency of low energy spectrum on absorption cross sections in the material as discussed in section 4.5.

6.2.2.3 IPS cell

IPS cells are available for the purpose of doing high-flux fast neutron irradiation. Spectra of IPS regions (Figure 6.8) are taken as the average of 6 IPS cells spectra. Being 'in pile' they have neutron fluxes very similar to those in the fuel cells that surround them. However, as noted from the figure fewer thermal neutrons are noted in the IPS spectrum.

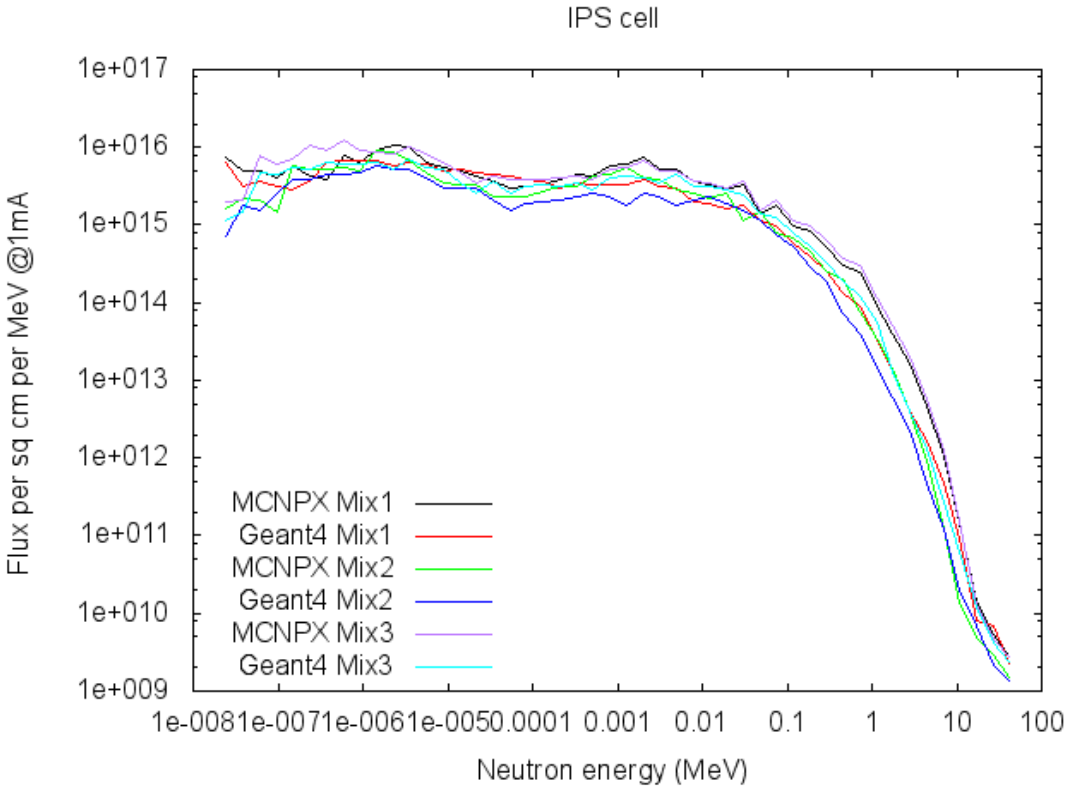

Figure 6.8: Neutron flux averaged over the IPS cells

6.2.2.4 Mo Ac cell

Mo and Ac production cells are farther away from the centre and the spectra in these regions are found to be softer as shown in Figure 6.9 and Figure 6.10 respectively. The reason could be, the neutrons reaching the outer cells have travelled further and undergone more collisions [50].

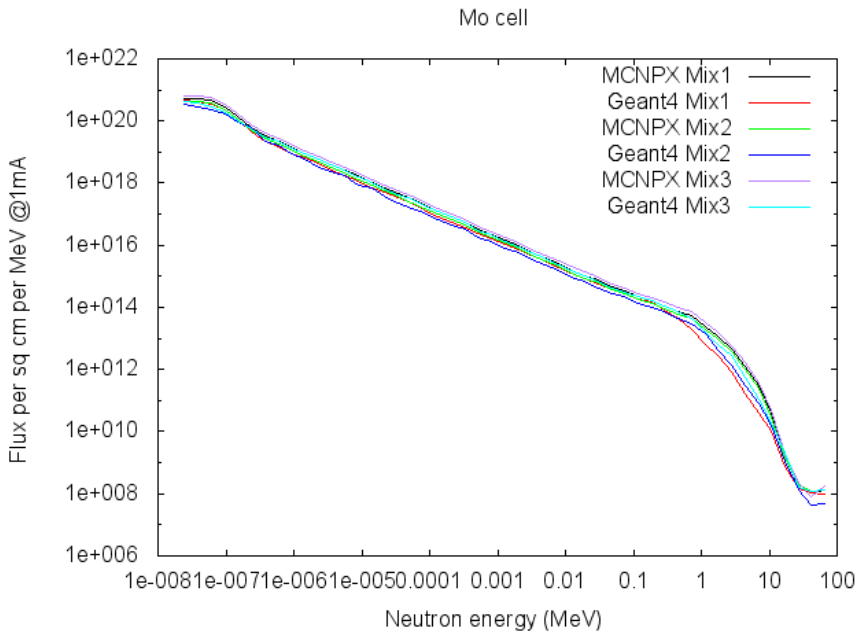

Figure 6.9: Neutron flux averaged over the Mo cells

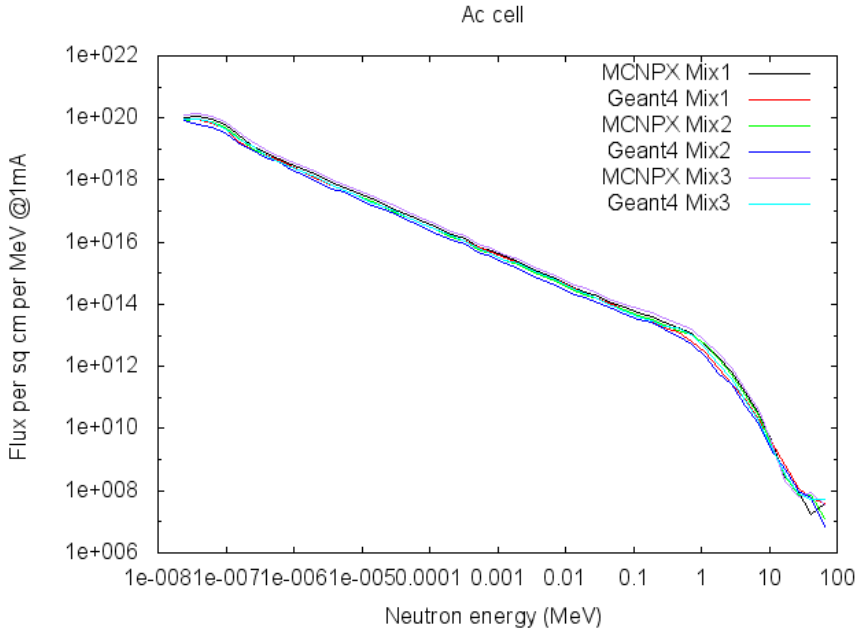

Figure 6.10: Neutron flux averaged over the Ac cells

6.3 Chapter summary

Based on the results obtained from this study, following conclusions are drawn for reactor MYRRHA with three different fuel mix:

1. The neutron flux spectra obtained by different simulation programs GEANT4 and MCNPX are benchmarked against each other and show good agreement for neutron flux spectra at various location of the reactor. The fuel spectra by these two programs also agree with other studies ([31]).

2. Broad features of neutron spectra are same for the three fuel mix at all the chosen locations of the reactor. This indicates that provided the reactivity remains the same (in this case $K_{\text{eff}} = 0.95$), the spectra is insensitive to different fuel composition. Nevertheless they differ in detail which could be due to different absorption cross section of the isotopes.

3. It can be fairly concluded that spectrum is harder and greater near the centre of the reactor. While the fuel cells are full (with fuel) there is space in the IPS that can be used for incineration studies.

7

Fuel Evolution And Minor Actinide Incineration

Fuel evolution takes place during irradiation due to following four main processes [47]:

1. Fission.
2. α or β decay.
3. Neutron capture that can transform nuclei from fertile to fissile, followed by radioactive decay.
4. Production of fission fragments.

So, the number of atoms of some isotope X in an element of a nuclear reactor can change with time due to 4 processes: it is formed by reactions on other isotopes like $Y(\mathrm{n},\gamma)X$ and by decays of other isotopes, and it is lost by reactions like $X(\mathrm{n},\gamma)Z$ and decays of X. The corresponding equation is:

$$\frac{dX}{dt} = Q_1 Y + \lambda_2 P - Q_3 X - \lambda_4 X \tag{7.1}$$

where X, Y , Z and P are the numbers of atoms of isotope X, of the isotope which produces X in a reaction, and of the parent which decays to X by alpha or beta decay. Q_1 is the creation reaction probability $\int \sigma_1(E)\phi(E)dE$ and Q_3 is the destruction probability $\int \sigma_2(E)\phi(E)dE$, σ_1 and σ_2 are the cross sections and ϕ is the flux; it should

be noted that these involve different cross sections but the same neutron flux. For a particular isotope not all of the terms in equation 7.1 may be relevant, however these four are the maximum. λ_2 and λ_4 are the decay rates (reciprocal of the lifetime) for the decays into X and from X. This is a differential equation involving three unknowns: X, Y and P. Y and P will have similar equations of their own, and these may involve further species. To predict what will happen, a complete set of equations needs to be written, one for each isotope involved. This set is called the Bateman Equations.

Dropping the different names and calling the isotopes X_1 , X_2 ...X_{n}, or just $\vec{X}$ there are n equations for the n isotopes. The equations have the simple form:

$$\frac{d\vec{X}}{dt} = M\vec{X} \tag{7.2}$$

where M is a matrix, of which the elements are decay rates λ or reaction probabilities ($\int \sigma(E)\phi(E)dE$). Initial composition $\vec{X}$ $(t = 0)$ needs to be supplied. The solution to these equations can be obtained either by stepwise integration or by algebraic approach as discussed in section 3.4. The results following are by algebraic approach of solving the equations by programming them in the R computer language.

When the evolution $\vec{X}$(t) is plotted then typically the decay $e^{-\lambda t}$ is observed: one sees the $e^{-\lambda t}$ decay of the components one starts with, and the rise and then fall , $e^{-\lambda t}$ $(1 - e^{-\lambda' t})$ of the daughter products.

7.1 Incineration of minor actinides

Based on the investigations performed for the neutron flux in chapter 6, the actinide burning rate in the reactor can be calculated. The absorption and fission cross sections taken from JEFF 3.1 library [13] for different minor actinides are illustrated in Figure 7.1 to Figure 7.5.

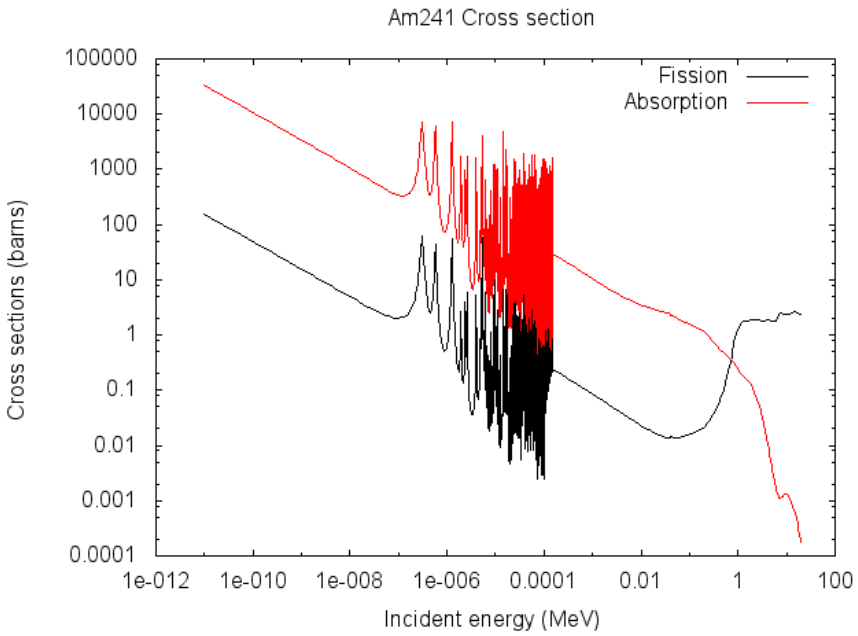

Figure 7.1: Fission and absorption cross sections for ^{241}Am

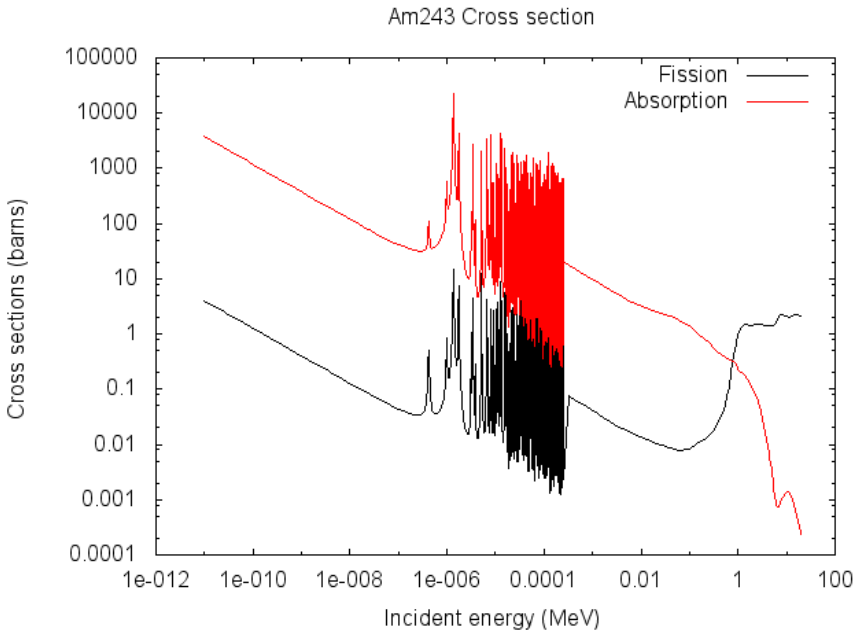

Figure 7.2: Fission and absorption cross sections for ^{243}Am

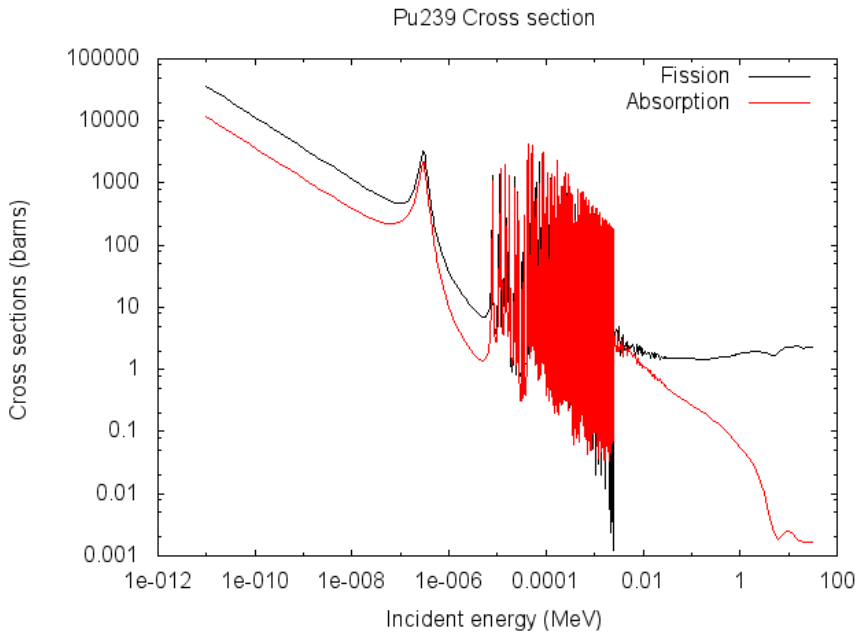

Figure 7.3: Fission and absorption cross sections for ^{239}Pu

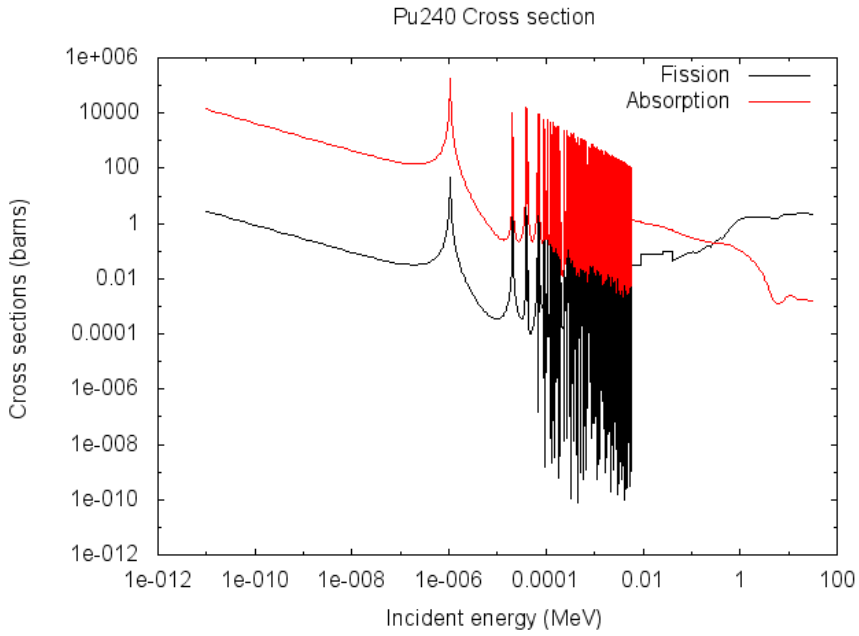

Figure 7.4: Fission and absorption cross sections for ^{240}Pu

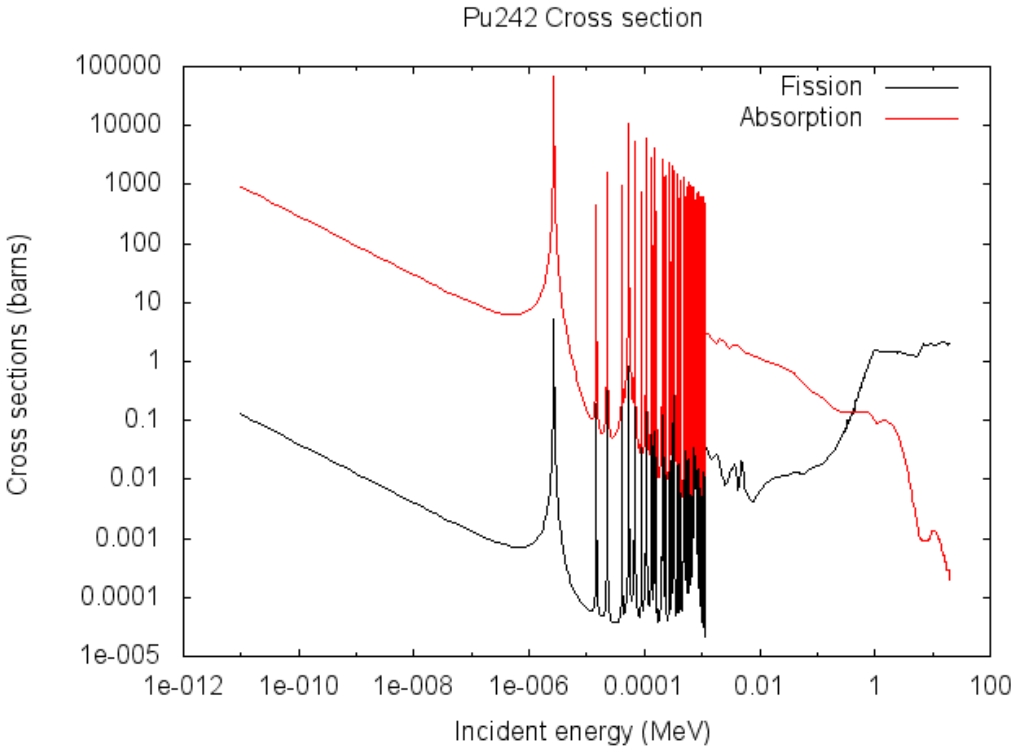

Figure 7.5: Fission and absorption cross sections for ^{242}Pu

From these figures (Figure 7.1 - Figure 7.5), it is clear that the fission cross section dominates over the absorption cross section above 1 MeV. This indicates the need of fast neutrons for burn up. As follows from chapter 6, a hard neutron spectrum can be observed in the fuel cell, IPS cell and also up to some extent in Mo, Ac cells. The spectrum in the Mo, Ac cells are not as hard as in IPS and fuel cells but since these cells are available for irradiation, so it is worth considering these locations for burn up studies.

7.1.1 Burn up rate calculation

The weighted flux is calculated for a number of significant actinide species: ^{241}Am, ^{243}Am, ^{237}Np, ^{239}Pu, ^{240}Pu and ^{242}Pu for both the inner IPS cells and the outer cells used for Mo and Ac production. Three fuel mixtures described earlier are considered for these calculations and the cross sections are taken from JEFF 3.1 library [13].

By including the energy dependence of the cross section, the normalized integrated weighted flux F can be written as the fluence of neutrons per cm^2 [50]:

$$F = \frac{1}{V} \int_0^{E\max} \phi(E)\sigma(E)dE \tag{7.3}$$

where V is the volume in cm^3, ϕ(E) is the neutron flux per cm^2, σ(E) is the reaction cross section in barn.
The fluence of neutrons is produced by the spallation and fission process. If σ is the reaction cross section, then the probability of a minor actinide nucleus in a volume V to be hit by a neutron is Fσ (flux convolved with cross section) multiplied by 10^{-24}. The factor 10^{-24} is included to convert barn to cm^2. The burn up rate is then calculated as the probability of a MA nucleus to be transformed per second. The minor actinide burnup rate is the inverse of the mean life time of the MA in the reactor. To calculate this, the accelerator beam current can be included in equation 7.3 to find the probability per second of a minor actinide being converted in a way corresponding to the cross section.
The weighted flux calculated by GEANT4 and MCNPX for various minor actinides in the IPS and Mo-Ac cells are shown in Table 7.1 and Table 7.2 respectively. The ratio in 7^{th} and 8^{th} column corresponds to the ratio of fission to absorption. It tells whether fission or absorption is dominating. The higher the ratio, more will be the incineration. The results of the two programs agree well.

The results on burn up probabilities of actinides can be summarized as:

1. Slightly higher burn up rate is observed for Mix 3 by MCNPX predictions.

2. ^{239}Pu being important as a fuel rather than a waste product, is a special case. Its fission probability is higher than absorption, in the inner cells where the spectra are harder, as well as in the outer cells.

3. For the other isotopes in the table, the ratio of fission to absorption is respectable in the IPS cells but it is negligible in the outer cells. Further, the spectra in IPS is harder, so the ratio is also higher in IPS cells. Exposing such isotopes in the inner IPS cell will either transmute them to short lived fission products and/or to some higher atomic weight nuclei through neutron absorption. Further alpha and beta decay possibilities are there for the fission or absorption of these daughter products. The ratio in outer cells suggest limited use of these cells for

incineration.

Isotope	Fuel	Inner IPS					
		Fission MX	Fission G4	Absorption MX	Absorption G4	Ratio MX	Ratio G4
^{239}Pu	U/Pu	0.23	0.12	0.04	0.02	5.57	4.92
	Th/Pu	0.19	0.24	0.03	0.04	5.82	5.64
	Th/U	0.27	0.16	0.05	0.03	6.09	4.73
^{240}Pu	U/Pu	0.06	0.02	0.04	0.02	1.49	1.00
	Th/Pu	0.06	0.07	0.03	0.05	1.62	1.43
	Th/U	0.06	0.04	0.05	0.03	1.15	1.19
^{242}Pu	U/Pu	0.05	0.02	0.05	0.03	0.98	0.62
	Th/Pu	0.04	0.05	0.04	0.05	1.02	1.02
	Th/U	0.06	0.02	0.06	0.04	1.15	0.59
^{241}Am	U/Pu	0.05	0.02	0.21	0.12	0.24	0.15
	Th/Pu	0.04	0.05	0.16	0.19	0.26	0.23
	Th/U	0.06	0.02	0.23	0.16	0.28	0.14
^{243}Am	U/Pu	0.04	0.01	0.20	0.12	0.18	0.11
	Th/Pu	0.03	0.03	0.15	0.18	0.20	0.17
	Th/U	0.05	0.02	0.21	0.15	0.21	0.10

Table 7.1: Neutron absorption rates for isotopes in the inner IPS cells using GEANT4 and MCNPX for 1 mA beam

Isotope	Fuel	Outer Mo Ac cells					
		Fission MX	Fission G4	Absorption MX	Absorption G4	Ratio MX	Ratio G4
^{239}Pu	U/Pu	5.78	4.43	2.91	2.22	1.98	2.00
	Th/Pu	4.70	3.51	2.37	1.89	1.99	1.85
	Th/U	6.50	4.10	3.37	2.15	1.93	1.91
^{240}Pu	U/Pu	0.01	0.00	3.80	2.77	0.00	0.00
	Th/Pu	0.01	0.01	3.08	2.36	0.00	0.00
	Th/U	0.01	0.01	4.67	3.22	0.00	0.00
^{242}Pu	U/Pu	0.01	0.00	0.26	0.19	0.03	0.01
	Th/Pu	0.01	0.00	0.21	0.15	0.03	0.02
	Th/U	0.01	0.01	0.32	0.23	0.03	0.02
^{241}Am	U/Pu	0.06	0.04	7.86	5.77	0.01	0.01
	Th/Pu	0.05	0.04	6.36	5.43	0.01	0.01
	Th/U	0.07	0.05	9.18	6.57	0.01	0.01
^{243}Am	U/Pu	0.01	0.00	2.04	1.50	0.00	0.00
	Th/Pu	0.01	0.00	1.66	1.26	0.00	0.00
	Th/U	0.01	0.01	2.51	1.86	0.00	0.00

Table 7.2: Neutron absorption rates for isotopes in the outer Mo Ac cells using Geant4 and MCNPX for 1 mA beam

7.1.2 ^{241}Am incineration

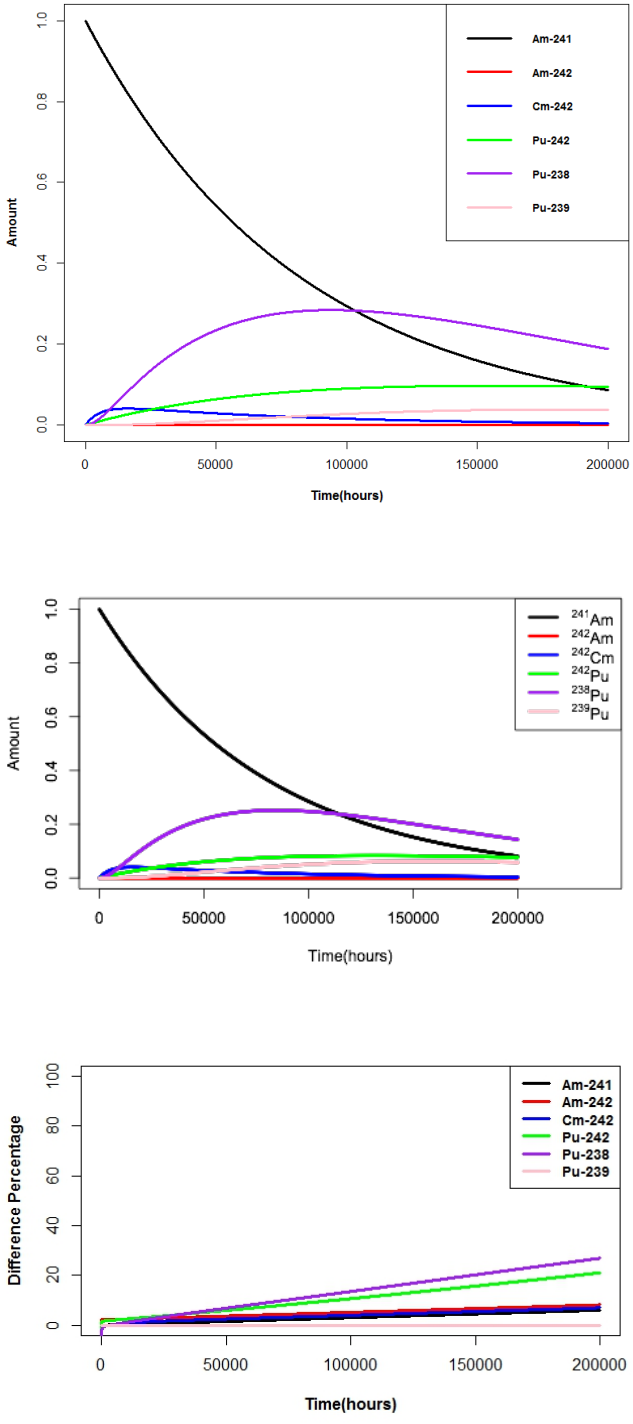

Figure 7.6: Evolution of ^{241}Am and its products: GEANT4 (Top), MCNPX (Centre) and percent difference between GEANT4 and MCNPX (Bottom)

The incineration of ^{241}Am in the IPS cell with Mix2 using GEANT4 and MCNPX is shown in Figure 7.6. The percent difference between GEANT4 and MCNPX results is shown in the third plot of Figure 7.6. The deviations are typically a few percent. Predictions of the two programs agree well as shown in these figures. The Bateman equation is solved over the period of 23 years by eigenvalue method described in section 3.4. The reaction rates, the Q factors in equation 7.1, are obtained from the tables and the decay rates, the lamda factors, are the inverse of the lifetimes of the isotopes. Single absorption and subsequent decays are considered. As discussed in subsection 2.4.1, ^{241}Am is consumed by absorption rather than fission. ^{238}Pu is the main product in this process which is produced from the successive decays of ^{242}Am and ^{242}Cm. Other isotopes are also produced in smaller quantities.

These solutions are indicative in that they assume continuous operation of the reactor, and they ignore changes in the composition of the fuel (including the accumulation of fission products). To include such efforts would require many assumptions about the duty cycle and fuel processing strategy, and would not effect the overall conclusions. This shows that ^{241}Am, taken as a typical minor actinide, would be incinerated in MYRRHA. There would be small quantities of other isotopes produced but they present less of a problem as regards storage. However the process would be slow. An economically effective ^{241}Am burner would need to operate at much higher currents. However, the MYRRHA reactor would be a useful prototype.

7.2 Fuel evolution: Thorium as fuel

It is important to consider the conversion of fertile isotopes to the intermediate nuclei through neutron capture events. For mix 1, it is the conversion of ^{238}U to ^{239}U while for mix 2 and mix 3 it is ^{232}Th to ^{233}Th. Rapid beta decay in both these cases leads to the formation of ^{239}Np and ^{233}Pa respectively. The half-life of ^{239}Np is 23 minutes and that of ^{233}Pa is 21 minutes, so these can be considered as instantaneous. Second beta decay transforms ^{239}Np to ^{239}Pu which is still rapid with a half-life of 2.4 days whereas for mix 2 and mix 3, conversion of ^{233}Pa to ^{233}U is relatively slower with a half-life of 27 days. Further, if ^{233}Pa absorbs a neutron in an intense neutron flux, it could lead to the process diverting in unwanted directions. This is an issue well known for thorium reactors [50].

GEANT4 and MCNPX calculated neutron flux convolved with the cross section (as per equation 7.3) for the three relevant isotopes are presented in Table 7.3. As per the relative values in the table, the two programs GEANT4 and MCNPX agree that

the conversion rates differ for the three fuel mixtures. As the composition changes, the probability of fertile to fissile thorium conversion increases. It is worth noting that protactinium absorption probabilities (indicating the loss of ^{233}Pa from the chain) are larger than the probabilities of thorium nuclei entering the chain. It should be balanced by the fact that the amount of ^{233}Pa in the fuel at any time is very small. The ^{233}Pa effect (neutron absoption in the intermediate state) can be evaluated by solving the Bateman equation over 230 days for 2.5 mA beam current. This is plotted in Figure 7.7. The Pa effect is observed to be very small as ^{233}Pa stabilizes soon.

Fuel	U238		Th232		Pa233	
	G4	MX	G4	MX	G4	MX
U/Pu (Mix1)	0.026	0.028	0.034	0.045	0.075	0.18
Th/Pu (Mix2)	0.032	0.036	0.028	0.028	0.061	0.15
Th/U (Mix3)	0.035	0.046	0.035	0.039	0.076	0.19

Table 7.3: Neutron absorption rates for isotopes in the fuel cells for 1 mA beam

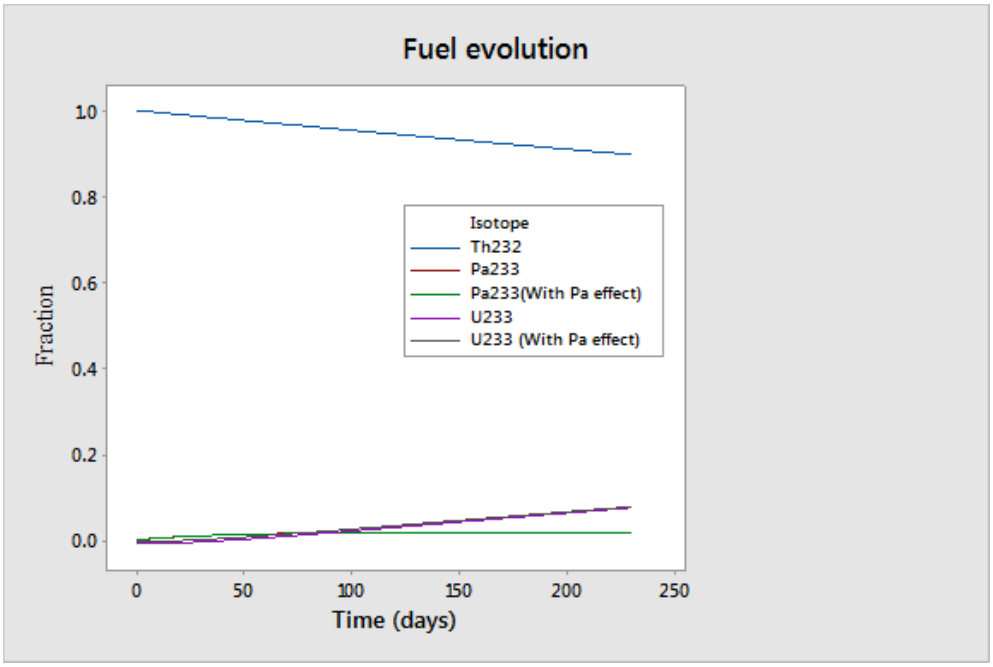

Figure 7.7: Thorium fuel evolution with and without ^{233}Pa neutron absorption effect

7.3 Minor actinide production and net incineration

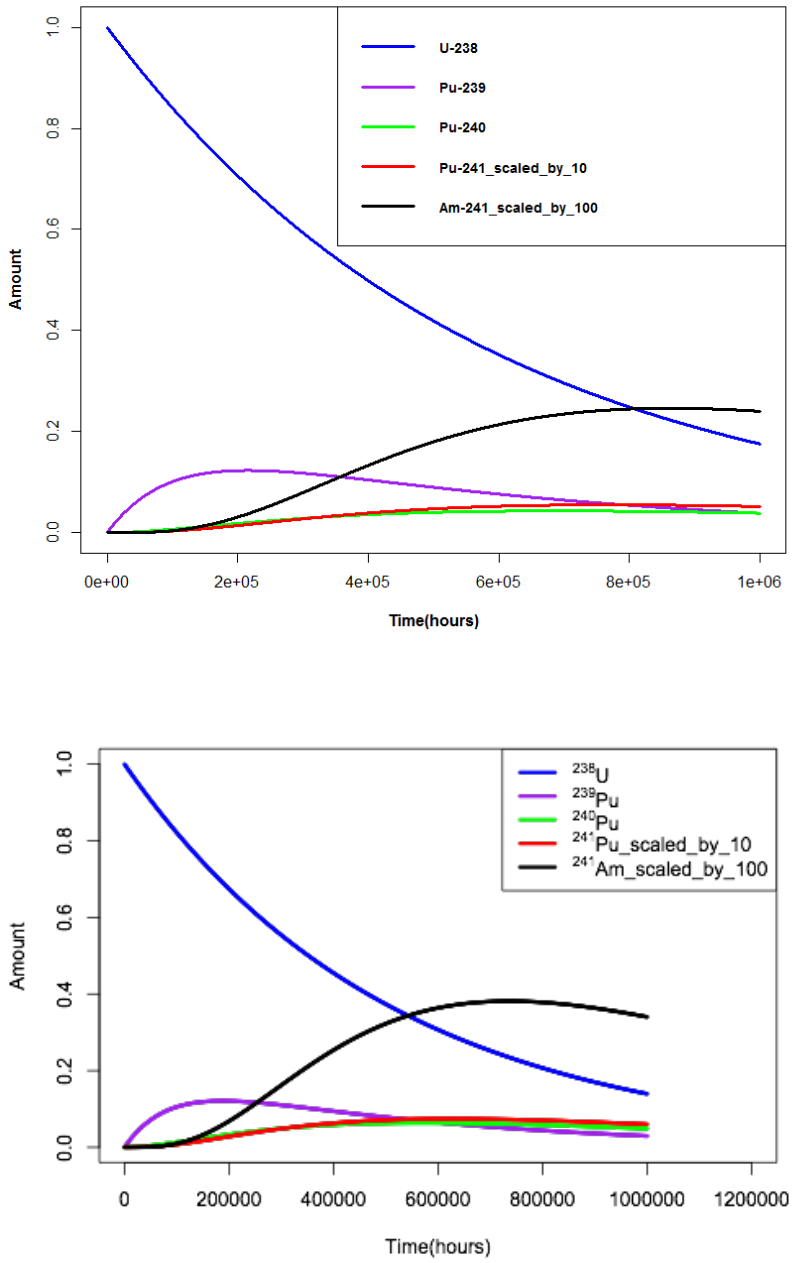

Figure 7.8: Evolution for ^{238}U and its products, Geant4 (Top) and MCNPX (Bottom)

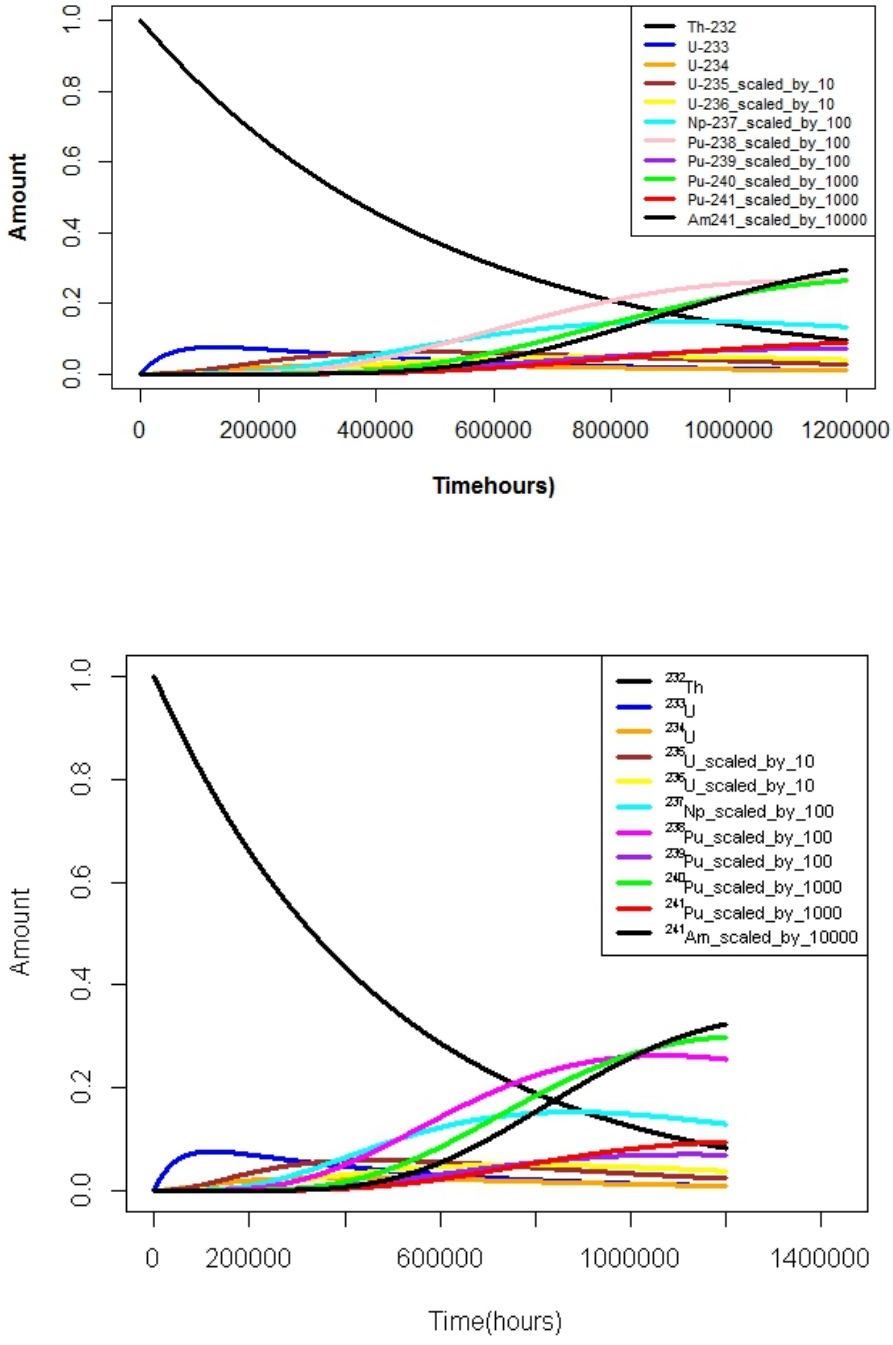

Figure 7.9: Evolution for ^{232}Th and its products, GEANT4 (Top) and MCNPX (Bottom)

In order to compare the incineration capability of uranium and thorium based fuel, it is important to investigate the net incineration in the two fuel cycles. The amount of minor actinide produced is compared with that incinerated.In subsection 7.1.2 a ^{241}Am incineration study is performed. In the same model the formation of ^{241}Am starting from uranium or thorium is considered using GEANT4 and MCNPX programs. Assumptions in this model are [50]:

1. Short life time decays are considered spontaneous.
2. Accelerator operation at 2.5 mA is continuous.
3. Entire fuel is treated as a single lumped object.
4. Variation in the neutron spectrum during fuel evolution is neglected.
5. Timescale is 100 years.

Results of GEANT4 and MCNPX for uranium and thorium fuel cycles are shown in Figure 7.8 and Figure 7.9 respectively. From the figures, it is clear that both the codes agree well for the trends in the two fuel cycles. It can be noted from Figure 7.8 that the amount of ^{241}Am produced in Uranium base needs to be scaled by a factor of ~ 100 to be visible. So ~ 0.4 % of ^{238}U transforms into ^{241}Am and although this is a small fraction, given the large amount of ^{238}U in the fuel, it is producing a significant amount of ^{241}Am. On the other hand, ^{241}Am production from thorium (Figure 7.9) needs scaling by a factor of 10000 to be visible. This indicates that minor actinide production is decreased by a factor of ~ 100 when using thorium based in place of uranium based fuels.

7.4 Chapter summary

1. The slow timescale in the study shows that long term waste problem is not going to be solved by MYRRHA itself, however it can be utilized as a demonstrator and a prototype for large scale systems that operate at much higher currents.

2. GEANT4 and MCNPX results presented in Table 7.1 and Table 7.2 depict that MYRRHA can convert measurable amount of minor actinide waste hereby proving the concept of industrial transmutation system.

3. Net incineration in case of ^{241}Am is improved with thorium fuels as the amount of ^{241}Am produced is much smaller than the amount incinerated.

8

Conclusions

The properties of spallation neutrons from a simple lead target were studied in detail and the comparison of Geant4 results with the experimental data for spallation neutron production served as a good validation for the MYRRHA simulation studies. The results on spallation neutron study revealed that along with the agreement between Geant4 and MCNPX for numbers, positions and spectra, they also agreed well for the relative contribution of sides and ends of the target for neutrons. This included the interesting fact that the neutrons came out predominantly backwards from the target. The properties of the spallation neutrons were parameterized by simple forms that can be used for neutronic studies of ADSR and other systems. The high energy neutron spectrum was dominated by the energy of the proton beam while the low energy spectrum was dominated by the absorption cross section in lead. Variation of the spallation neutron properties with target length was also investigated. This showed that neutron production varies slowly with length and radius of the target.

The design of the reactor MYRRHA was implemented in detail in Geant4 and its neutronic analysis was performed. The neutron fluxes were calculated at various locations of the reactor: fuel assemblies, IPS assemblies and Mo-Ac assemblies. These fluxes were used for the nuclear waste transmutation studies for MYRRHA. The validation of Geant4 simulation with MCNPX as well as with other predictions of MYRRHA provided reliable results that can be utilized for future studies on flux distribution and minor actinide incineration studies using the MYRRHA design.

A novel contribution of the thesis is considering thorium based fuel as an alternative to uranium fuels. Similar neutron flux distribution for the three different fuel mix showed that thorium based fuels can be used as a replacement of uranium fuels.A case study is performed for ^{241}Am incineration. A comparison is made between uranium and

thorium based fuels for their capability of net incineration. The potential of thorium based fuel for better minor actinide incineration is demonstrated as the amount of minor actinide produced is much smaller than the amount incinerated. Hence, MYRRHA with thorium fuel can be envisaged as an efficient transmutation system in addition to demonstrating the ADS concept. MYRRHA project is now approved and under construction in SCK-CEN, Belgium. Before implementing the actual design of the reactor, it is of immense importance to perform simulation based studies. The work presented in the thesis is entirely based on simulation. Although validation studies are performed for the investigations carried out in the thesis, it would be worth considering other codes to benchmark the results using the same model and fuel specifications.

8.1 Suggestion for future work

Although the potential of thorium filled ADSRs for better minor actinide incineration is well known in principle, it is shown here for a realistic ADSR design. However, thorium filled ADSRs tend to have reactivity variation due to the longer life of the intermediate protactinium isotope. Reactivity variation takes place due to the changes in the nuclide population with time. ^{232}Th to ^{233}U breeding chain can bring flux dependent changes in the nuclide population, particularly ^{233}Pa and ^{233}U. This causes two main effects:
1. At start up - ^{233}Pa when captures neutron rather than conversion to ^{233}U through decay, ^{233}U population becomes low and reactivity falls.
2. After shut down - ^{233}U should be produced before shut down, but if ^{233}Pa decays after shut down, reactivity will increase due to increase in population of ^{233}U.
A more detailed modelling of the neutronics should be done taking into account changes in the fuel composition, and build-up of fission fragments. These were beyond the scope of this work as they involve detailed assumptions about the operational cycle and refuelling.

References

[1] Alex C Mueller. Transmutation of nuclear waste and the future MYRRHA demonstrator. In *Journal of Physics: Conference Series*, volume 420, page 012059. IOP Publishing, 2013. 17, 33, 35

[2] Ciprian Zahan. Thorium nuclear reactors: Spallation target optimization using geant4 and fluka. *Intel Talent Search competition*, 2011. 17

[3] H Nifenecker, S David, JM Loiseaux, and O Meplan. Basics of accelerator driven subcritical reactors. *Nuclear Instruments and Methods in Physics Research Section A: Accelerators, Spectrometers, Detectors and Associated Equipment*, 463(3):428–467, 2001. 12, 18, 19, 20, 21, 22, 34

[4] Cristian Bungau, Adriana Bungau, Roger Barlow, and Robert Cywinski. Neutron spallation studies for an accelerator driven subcritical reactor. 2010. 18

[5] Minor actinides. `http://www.radioactivity.eu.com/site/pages/Minor_Actinides.htm`. Accessed: 1.12.2018. 12, 19, 34

[6] Sara Changizi. Neutronic analysis of the multipurpose hybrid research reactor for high-tech applications (MYRRHA) with a monte carlo code serpent, 2012. 12, 19, 30, 33, 43, 44, 45

[7] Kazuo Furukawa, Yoshio Kato, Toshihiko Ohmichi, and Hideo Ohno. Combined system of accelerator molten-salt breeder (AMSB) apd molten-salt converter reactor (MSCR). *Atomnaya Tekhnika za Rubezhom*, pages 23–29, 1983. 19, 35

[8] CD Bowman, ED Arthur, PW Lisowski, GP Lawrence, RJ Jensen, JL Anderson, B Blind, M Cappiello, JW Davidson, TR England, et al. Nuclear energy generation and waste transmutation using an accelerator-driven intense thermal neutron

source. *Nuclear Instruments and Methods in Physics Research Section A: Accelerators, Spectrometers, Detectors and Associated Equipment*, 320(1-2):336–367, 1992. 19

[9] F Carminati et al. Report cern-at-93-47 (et). Technical report, CERN/LHC/96-01 (EET), 1993. 19

[10] Thorium fuel cycle - potential benefits and challenges. `https://www-pub.iaea.org/mtcd/publications/pdf/te_1450_web.pdf`. Accessed 18.12.2018. 19, 21

[11] Comparison of thorium and uranium fuel cycles. `https://assets.publishing.service.gov.uk/government/uploads/system/uploads/attachment_data/file/65504/6300-comparison-fuel-cycles.pdf`. Accessed 18.12.2018. 22, 33

[12] Roger Barlow and Asiya Rummana. Actinide incineration with thorium fuel: A STUDY USING THE MYRRHA DESIGN. In *Proceedings of International Meeting on Nuclear Applications for Accelerators (AccApp'17). July 31-August4, 2017 (pp. 268-278). Quebec, Canada*, 2017. 12, 13, 22, 69, 70, 90

[13] Geant4 library. `https://www-nds.iaea.org/geant4/libraries/JEFF31N/`. Accessed 18.12.2018. 23, 102, 105

[14] Stephen Peggs, W Horak, Thomas Roser, VB Ashley, RF Ashworth, Roger Barlow, R Cywinski, Rebecca Seviour, J-L Biarrotte, S Henderson, et al. Thorium energy futures. JACoW, 2012. 23

[15] Edouard Malambou and Stankovskiy A. Description based on MYRRHA rev 1.6, 2014. 25, 69, 71, 75, 83, 89

[16] Adriana Bungau, Robert Cywinski, and Cristian Bungau. Target Optimisation Studies for the European Spallation Source. IPAC 10 OC/ACFA, 2010. 27

[17] Hamid Aït Abderrahim, Didier De Bruyn, Gert Van den Eynde, and Sidney Michiels. Transmutation of high-level nuclear waste by means of accelerator driven system. *Wiley Interdisciplinary Reviews: Energy and Environment*, 3(1):60–69, 2014. 27

[18] MYRRHA: An innovative research installation. `http://sckcen.be/en/Technology_future/MYRRHA`. Accessed 18.12.2018. 28, 31

[19] Tim Broome. High power targets for spallation sources. In *Proc. EPAC96 (Sitges, Spain, 1996)*, page 267, 1996. 28

[20] MNH Comsan. Spallation neutron sources for science and technology. 2011. 29

[21] Steve Peggs et al. The european spallation source. *Proceedings of PAC11 (New York)*, 2011. 29

[22] Advanced heavy water reactor (AWHR). `http://www.barc.gov.in/publications/eb/golden/reactor/reactor.pdf`. Accessed 18.12.2018. 29, 31

[23] H Ait Abderrahim, V Sobolev, E Malambu, et al. Fuel design for the experimental ADS MYRRHA. In *Technical Meeting on use of LEU in ADS. IAEA,(Viena, Austria, 2005)*, pages 1–13, 2005. 29, 73

[24] A Billebaud, R Brissot, D Heuer, C Le Brun, E Liatard, JM Loiseaux, O Meplan, E Merle-Lucotte, F Perdu, J Vollaire, et al. The MUSE-4 experiment: Prompt reactivity and delayed neutron measurements. In *GLOBAL 2003-Nuclear Science and Technology: Meeting the Global Industrial and R&D Challenges of the 21st Century*, pages 840–845. American Nuclear Society, 2003. 30

[25] GENEPI-3C accelerator for the GUINEVERE program. `http://lpsc.in2p3.fr/index.php/en/home/36-poles-plates-formes-technologiques/serviceaccelerateurs/153-laccelerateur-genepi-3c-pour-le-programme-guinevere`. Accessed 11.06.2019. 30

[26] Yousry Gohar, Donald L Smith, et al. Yalina facility a sub-critical accelerator-driven system (ads) for nuclear energy research facility description and an overview of the research program (1997-2008). Technical report, Argonne National Lab.(ANL), Argonne, IL (United States), 2010. 30

[27] TY Song, NI Tak, WS Park, JS Cho, YS Lee, JH Choi, and MK Song. Thermal and stress analysis of hyper target system. In *6th Information Exchange Meeting on Actinide and Fission Product Partitioning and Transmutation, Madrid, Spain*, 2000. 30

[28] Yoshihiro Ishi, M Inoue, Y Kuriyama, Y Mori, T Uesugi, JB Lagrange, T Planche, M Takashima, E Yamakawa, H Imazu, et al. Present status and future of FFAGs at KURRI and the first ADSR experiment. *Proc. of IPAC10, Kyoto*, page 1323, 2010. 12, 14, 30, 31

[29] Timothee Kooyman, Laurent Buiron, and Gerald Rimpault. A comparison of curium, neptunium and americium transmutation feasibility. *Annals of Nuclear Energy*, 112:748–758, 2018. 33, 36, 37

[30] Minor Actinide. Transmutation position paper. 34, 36

[31] Massimo Sarotto, Diego Castelliti, Rafael Fernandez, Damien Lamberts, Edouard Malambu, Alexey Stankovskiy, Wadim Jaeger, Marco Ottolini, Francisco Martin-Fuertes, Laurent Sabathé, et al. The MYRRHA-FASTEF cores design for critical and sub-critical operational modes (eu fp7 central design team project). *Nuclear Engineering and Design*, 265:184–200, 2013. 13, 35, 37, 90, 92, 94, 100

[32] J Allison, Katsuya Amako, J Apostolakis, Pedro Arce, M Asai, T Aso, E Bagli, A Bagulya, S Banerjee, G Barrand, et al. Recent developments in Geant4. *Nuclear Instruments and Methods in Physics Research Section A: Accelerators, Spectrometers, Detectors and Associated Equipment*, 835:186–225, 2016. 39

[33] John Allison, Katsuya Amako, JEA Apostolakis, HAAH Araujo, P Arce Dubois, MAAM Asai, GABG Barrand, RACR Capra, SACS Chauvie, RACR Chytracek, et al. Geant4 developments and applications. *IEEE Transactions on nuclear science*, 53(1):270–278, 2006. 39

[34] Sea Agostinelli, John Allison, K al Amako, John Apostolakis, H Araujo, P Arce, M Asai, D Axen, S Banerjee, G 2 Barrand, et al. Geant4 - a simulation toolkit. *Nuclear instruments and methods in physics research section A: Accelerators, Spectrometers, Detectors and Associated Equipment*, 506(3):250–303, 2003. 39

[35] Liam F Russell. *Simulation of time-dependent neutron populations for reactor physics applications using the geant4 monte carlo toolkit.* PhD thesis, 2012. 39, 41, 42, 44, 45, 46, 47

[36] Denise B Pelowitz et al. MCNPXTM users manual. *Los Alamos National Laboratory, Los Alamos*, 2008. 39

[37] Emilio Mendoza, Daniel Cano-Ott, Tatsumi Koi, and Carlos Guerrero. New standard evaluated neutron cross section libraries for the GEANT4 code and first verification. *IEEE Transactions on Nuclear Science*, 61(4):2357–2364, 2014. 40, 41, 86

[38] Naomi Ratcliffe. *Potential of a compact low energy proton accelertor for medical applications.* PhD thesis, University of Huddersfield, 2014. 46, 47, 71

[39] A Heikkinen, A Boudard, P Kaitaniemi, and G Folger. A geant4 physics list for spallation and related nuclear physics applications based on INCL and ABLA models. In *Journal of Physics: Conference Series*, volume 219, page 032043. IOP Publishing, 2010. 47

[40] Yury Malyshkin, Igor Pshenichnov, Igor Mishustin, and Walter Greiner. Modeling spallation reactions in tungsten and uranium targets with the Geant4 toolkit. In *EPJ Web of Conferences*, volume 21, page 10006. EDP Sciences, 2012. 47

[41] Numerical methods for differential equations. `http://faculty.olin.edu/bstorey/Notes/DiffEq.pdf`. Accessed 18.12.2018. 48

[42] Jerzy Cetnar. General solution of Bateman equations for nuclear transmutations. *Annals of Nuclear Energy*, 33(7):640–645, 2006. 48

[43] Asiya Rummana and R Barlow. Simulation and parameterisation of spallation neutron distributions. In *Proceedings of the 4th Workshop on ADS and thorium (ADST2016). 31 August-2 September 2016. University of Huddersfield, England. Online at http://pos. sissa. it/cgi-bin/reader/conf. cgi? confid= 279, id. 23*, 2016. 12, 13, 53, 54, 62, 64, 65, 66

[44] J Allison and K APOSTOLAKIS. Nuclear Science. *IEEE Transactions*, 53:270–278, 2006. 53

[45] Roger Barlow and Asiya Rummana. Simulations of spallation neutron distributions. In *Proceedings of International Meeting on Nuclear Applications for Accelerators (AccApp'15). November 10-13, 2015 (pp. 312-317). Washington, DC*, 2015. 53

[46] Roger Barlow, Asiya Rummana, and Rebecca Seviour. Characterisation of the spectra of spallation neutron sources through modelling. In *Proceedings of International particle accelerator conference (IPAC'16). May 8-13, 2016 (pp. 1950-1952). JACOW, Geneva, Switzerland*, 2016. 53

[47] Hervé Nifenecker, Olivier Meplan, and Sylvain David. *Accelerator driven subcritical reactors*. CRC Press, 2003. 54, 101

[48] RG Vassil'kov and VI Yurevich. Neutron emission from an extended lead target under the action of light ions in the Gev region. Technical report, 1991. 14, 55, 56

[49] BA Magurno, RR Kinsey, and FM Scheffel. Guidebook for the ENDF/BV nuclear data files. Technical report, National Nuclear Data Center, 1982. 66

[50] Roger Barlow, James Burlison, Tristan Edwards, Alisa Healy, Alex Masterson, Hamid Aït Abderrahim, Edouard Malambu, and Gert van den Eynde. Studies of MYRRHA using thorium fuel. *International Journal of Hydrogen Energy*, 41(17): 7175–7180, 2016. 13, 69, 70, 80, 90, 98, 106, 109, 113

[51] Detector Simulation Visualisation. `https://indico.cern.ch/event/294651/sessions/55918/attachments/552022/760637/Visualisation.pdf`. Accessed 25.12.2018. 71

[52] John Allison, Laurent Garnier, Akinori Kimura, and Joseph Perl. The Geant4 Visualization System - A Multi-Driver Graphics System. *International Journal of Modeling, Simulation, and Scientific Computing*, 4(supp01):1340001, 2013. 71

[53] G Van den Eynde, V Sobolev, E Malambu, D Maes, D Lamberts, H Aït Abderrahim, L Mansani, B Giraud, A Hogenbirk, P Vaz, et al. NEUTRONIC DESIGN OF THE XT-ADS CORE WITH IN-PILE-SECTIONS. *Fuel*, 501:1–50, 2007. 13, 75, 76, 77

[54] Sensitive detector and hits. `http://www-geant4.kek.jp/g4users/g4tut07/docs/SensitiveDetector.pdf`. Accessed 25.12.2018. 83

[55] G4MultiFunctionalDetector, G4VPrimitiveSensitivity, G4VSDFilter and G4THitsMap. `http://geant4.in2p3.fr/2005/Workshop/Wednesday/M.Asai.pdf`. Accessed 25.12.2018. 83

[56] Geant4 material database. `http://www.sixiangguo.net/code/geant4/AppDevelop/apas06.html`. Accessed 25.12.2018. 85

[57] E Mendoza, D Cano-Ott, C Guerrero, and R Capote. New evaluated neutron cross section libraries for the Geant4 code. Technical report, International Atomic Energy Agency, 2012. 86

[58] Alberto Ribon. Private communication, 2018. 87

[59] F Molina, P Aguilera, J Romero-Barrientos, HF Arellano, J Agramunt, J Medel, JR Morales, and M Zambra. Energy distribution of the neutron flux measurements at the chilean reactor rech-1 using multi-foil neutron activation and the expectation

maximization unfolding algorithm. *Applied Radiation and Isotopes*, 129:28–34, 2017. 14, 89, 91, 96

[60] Carl H Westcott. The specification of neutron flux and nuclear cross-sections in reactor calculations. *Journal of Nuclear Energy (1954)*, 2(1-2):59–75, 1955. 91

[61] NL Asquith, SR Hashemi-Nezhad, W Westmeier, I Zhuk, and S Tyutyunnikov. The spatial distribution of thermal and epithermal neutrons in a graphite moderated spallation neutron field. *Radiation Measurements*, 67:15–23, 2014. 14, 96, 97